DETERMINATION OF FRACTURE PARAMETERS OF HIGH STRENGTH CONCRETE DERIVED FROM RICE HUSK ASH CEMENT BLENDS

By

Anthony Olusegun BUCKNOR
(SI:85401)
B.SC. M. Sc. (U.1)

A Thesis in the Department of Civil Engineering
Faculty of Technology
In partial fulfilment of the Degree of

DOCTOR OF PHILOSOPHY
of the
UNIVERSITY OF IBADAN

SEPTEMBER, 2023

CERTIFICATION

I certify that this thesis was carried out by Anthony Olusegun **Bucknor** (Matric No.:85401) in the Department of Civil Engineering, Faculty of Technology, University of Ibadan, Ibadan, Nigeria.

……

Supervisor
W. O. Ajagbe
HND (Ibadan), B.Sc., M.Sc., Ph.D. (Ibadan), MNSCE,
Reg. Engr. (COREN)
Reader, Department of Civil Engineering
Faculty of Technology
University of Ibadan, Nigeria

……

CO-Supervisor
B. I. O. Dahunsi

B.Sc (Ife), M.Sc., Ph.D (Ibadan), MNSE, MASCE,
Reg. Engr. (COREN)
Professor Department of Civil Engineering
Faculty of Technology
University of Ibadan, Nigeria

DEDICATION

This thesis is dedicated to the Almighty God, the ultimate source of wisdom, guidance, and inspiration. It is with deep reverence and gratitude that I acknowledge His divine presence in my life throughout this academic journey.

ACKNOWLEDGEMENTS

I begin by expressing my profound gratitude to the Almighty, the Ever-powerful living God. His unwavering guidance, wisdom, and ever-present support have been instrumental in the successful completion of this PhD thesis. Every milestone achieved and every insight gained bear testament to His guiding light.

I owe immense gratitude to the Head of Department, Prof. B. I. O Dahunsi. His exceptional leadership, consistent mentorship, and unwavering support have shaped my research and academic trajectory. Equally invaluable has been the guidance of my supervisor, Dr. W. O. Ajagbe, whose expertise and continuous feedback have been pillars throughout my study. Dr. O. O. Ajide, our Sub-Dean, has also been a guiding hand, and I am thankful for his invaluable contributions.

The dedication and time of Dr. J. O. Labiran deserve special mention. His consistent guidance and invaluable feedback on this thesis have been greatly appreciated. Arch. Joel Taiwo's encouragement and unwavering support, even amidst his own PhD commitments, have bolstered my academic journey.

Dr. Akintayo, our Postgraduate coordinator, has been a beacon with her unfailing support and responsiveness. I am grateful to the postgraduate lecturers of the Department – Prof. O. A. Agbede, Prof. A. O. Coker, and Prof. G. M. Ayininunola – for their invaluable inputs and genuine interest in my research.

My appreciation extends to the entire staff of the Department of Civil Engineering and the Faculty of Technology. Their commitment to academic excellence has been a driving force. I hold a special place in my heart for Engr. Fisayo Animashaun, whose unwavering devotion has made this journey smoother and more meaningful.

To my pillar of strength, my beloved wife, Wuraola – your belief in me, your sacrifices, and unwavering support have been a source of inspiration throughout. My heartfelt appreciation goes to my children, Mofetoluwa and Oluwatamilore. Their understanding, patience, and resilience during this intense period have been a comfort and joy.

I remember with fondness and gratitude my late father, Samuel Olatunde Bucknor. His legacy, combined with the support and love of my mother, Adebola Bucknor, laid the

foundation of my academic pursuits. Their unwavering belief in me has been the wind beneath my wings.

In closing, I wish to recognize the countless individuals who have been a part of this journey, both directly and indirectly. The faith you placed in my abilities and your relentless support have been treasures that I will always cherish.

ABSTRACT

Concrete, a conventional building material is prone to fracture crack propagation, due to temperature and shrinkage stresses development, resulting in strength loss. Efforts in recent times have been directed at improving the resistance of concrete to crack propagation using pozzolanic materials such as Rice Husk Ash (RHA). However, information on fracture characteristics of High Strength RHA blended High Strength Concrete (HSC) are limited. This study was designed to investigate fracture characteristics of modified RHA-HSC using Crack Tip Opening Displacement (CTODc) and Stress intensity factor (K^S_{IC}).

Rice husk obtained from Ire-Ekiti was calcined for six hours at 700°C in a closed furnace and cooled over a 48-hour period. The RHA produced was milled to 5 µm, and the chemical and microstructural properties were determined using ASTM C 618 and Xray Diffraction (XRD), respectively. The BRE/DoE mix design method was used to determine the concrete mix for targeted compressive strength of 60 MPa. Portland limestone cement was replaced with RHA at 0, 10, 20, 30, 40 and 50% by weight of cement. Seventy-six (milled and unmilled each) 150 mm RHA-HSC cubes were cast and tested for compressive strength at 7, 14, 21 and 28 days. Based on the preliminary results 78 beams of milled (0, 10 and 20%) RHA-HSC blends were prepared to obtain CTODc and K^S_{IC} using Reunion Internationale des Laboratoires et Experts des Materiaux method. The CTODc and K^S_{IC} for 60 MPa were modelled using numerical analysis, while Scikit-learn statistical method was used to model varying RHA-HSC blends. Adequacy of the model was determined using coefficient of Regression (R^2).

The RHA comprised of SiO_2 (87.3%), Al_2O_3 (3.1%), and Fe_2O_3 (1.1%). This satisfied the ASTM C 618 70% minimum requirement for oxides. The observed pattern of peak broadening, smaller grain size and distinct peaks in RHA-HSC blends, implied the presence of a periodic crystal lattice structure. The compressive strengths of milled and unmilled RHA concrete blends ranged from 54.5 to 60.2 MPa and 11.3 to 44 MPa, respectively. This implied that RHA concrete did not meet the targeted compressive strength of 60 MPa. The corresponding CTODc at 10% and 20% RHA concrete cement blends were 0.02 and 0.32 mm, respectively while that of K^S_{IC} were 1.32 and 1.42 MPa$\sqrt{m}$, respectively. The corresponding CTODc of 10% milled RHA-HSC increased by 20% crack width, while the 20% milled RHA-HSC increased by 58.5%, when compared with the control mix. The K^S_{IC} of 10% RHA-HSC samples yielded 7.9% increase, while the 20% RHA-HSC concrete yielded a 16.2% increase, when compared with the control mix. The CTODc and K^S_{IC} from varying RHA-HSC blend fracture models yielded 0.02 and 1.24, respectively, and compared favourably with experimental data (R^2=0.873).

The incorporation of rice husk ash enhanced the fracture resistance characteristics of blended high strength concrete. The adopted model is suitable for predicting the potential failure of high strength concrete derived from rice husk ash cement blends.

Keywords: Stress intensity factor, Crack tip opening displacement, Rice husk ash, High strength concrete

Word count: 482

TABLE OF CONTENTS

LIST OF TABLES

LIST OF PLATES

LIST OF FIGURES

LIST OF ABBREVIATIONS AND SYMBOLS

CSI	Cement Sustainability Initiative
RHA	Rice Husk Ash
TPM	Two Parameter Model
FIP	The International Federation for Structural Concrete (Fédération internationale du béton)
CEB	European Committee for Concrete (Comité euro-international du béton)
HSC	High-Strength Concrete
ACI	America Institute of Concrete
DSP	Densified Systems of Homogeneously Arranged Ultra-Fine Particles
ASTM	American Society for Testing and Materials
SCM	Supplementary Cementitious Material
NFRA	National Food Reserve Agency
IRRI	International Rice Research Institute
UNEP	The United Nations Environment Programme
FAO	Food and Agriculture Organization
LOI	Loss on Ignition
Max	Maximum
Min	Minimum
LEFM	Linear Elastics Fracture Mechanics
FPZ	Fracture Process Zone
NLFM	Nonlinear Fracture Mechanics
CCM	Cohesive Crack Model
FCM	Fictitious Crack Model
CBM	Crack Band Model
TPFM	Two-Parameter Fracture Model
SEM	Size-Effect Model
ECM	Effective Crack Model
DKFM	Double-K Fracture Model
DGFM	Double-G Fracture Model
CMOD	Crack Mouth Opening Displacement

RILEM	International Union of Laboratories and Experts in Construction Materials, Systems and Structures
SIF	Stress Intensity Factor
HRWR	High Range Water Reducer
BS	British Standard
OPC	Ordinary Portable Cement
CTM	Compression Testing Machine
TPBT	Three-Point Bending Test
SG	Specific gravity
FIIRO	Federal Institute of Industrial Research, Oshodi
VB	Volume Batching
CST	Concrete Slump Test
F. A	Fine Aggregate
C.A	Coarse Aggregate
CAB	Cement-Aggregate Bond
WIC	Water Immerse Curing
AAC	Ambient Air Curing
XRD	X-Ray diffraction
N	Naira
$CTOD_C$	Critical Crack Tip Opening Displacement
K_{IC}^{s}	Critical Stress Intensity Factor
f_c'	Compressive Strength
$	US Dollar
℃	Degree Celsius
K	Potassium
S	Sulphur
Ca	Calcium
Mg	Magnesium
μm	Micrometer
m^2/g	Meter square per gram
%	Percentage
K_{IC}	Stress Intensity Factor
K_R	Curve Based Cohesive Force

K_I	Stress Intensity Factor
a_c	Critical Effective Crack Length
a_o	Initial Crack Length
Δa	Equivalent Extension in Stress-Free Crack Length at Peak Load
Δl	Change in Length
$CTOD_c$	Critical Crack Tip Opening Displacement
C_u	Unloading Compliance
E	Young Modulus
S	Specimen Loading Span
H_o	Thickness of Clip Gauge Holder
D	Beam Depth
	Beam Width
C_i	The Initial Compliance From P-CMOD Curve
G_f	Fracture Energy
c_f	Critical Effective
B'	Dimensionless constant
D_o	Constant with a dimension of length
f_t	Tensile strength of Material
P_u	Peak Load
w_g	Unit weight
σ_{Ni}	Nominal stress
K_{IC}^{e}	Critical Intensity Factor
K_{IC}^{ini}	Initial Cracking Toughness
K_{IC}^{un}	Unstable Fracture Toughness
K_C^t	Tangency
G_{IC}^{ini}	The Initiation Fracture Energy Release
G_{IC}^{un}	The Unstable Fracture Energy Release
G_{IC}^{C}	Cohesive Breaking Energy
MPa	Mega Pascal
Mm	Millimeter
Kg/m^3	Kilogram Per Meter Cube
w/c	Water/Cement Ratio

a_o	Initial notch
sp_w	Specific gravity of water
sp_{CA}	Specific gravity of coarse aggregate
sp_c	Specific gravity of cement
sp_{RHA}	Specific gravity RHA

CHAPTER ONE
INTRODUCTION

1.1 Background to the study

Fracture mechanics is a branch of mechanics that studies the behaviour of materials and structures under the action of a load or a sudden impact or strain. It involves analysing the response of materials and structures subjected to external forces or stresses and then noting the change in risk of failure or breakage of a material or structure (). The purpose of fracture mechanics is to assess the risk of failure of a material or structure while understanding its physical and mechanical properties. The study of fracture mechanics can help design structural components that can withstand sudden loading or impacts without breaking or becoming damaged beyond their operational life (Meng, Wong, and Zhou, 2021). The principles of fracture mechanics are used in various engineering disciplines, including civil and structural engineering, mechanical engineering, materials science, aerospace engineering, and other disciplines (Fu, Engqvist, and Xia, 2020). Fracture mechanics is a very complex field that combines mechanical, chemical, and material sciences. Because fractures are random, they are often difficult to predict or calculate. To build reliability in the components analysis, fracture mechanics must be understood from both the micro- and macro-levels. At the micro-level, fracture mechanics involves the study of the microscopic effects of displacement or strain within a material.

This study is often done through microscopic observations, X-ray diffraction or other imaging techniques (Wciślik and Lipiec, 2022). This analysis aims to understand a material's behaviour at a small scale and identify the local properties that can influence its response. At the macro-level, fracture mechanics studies the behaviour of materials and structures as a whole, and it seeks to understand how the whole behaves compared to its parts. These studies often involve larger-scale tests, such as anisotropic fracture tests, which aim to simulate the behaviour of a material or structure. This analysis provides insights into how a material or structure responds to different loading forms, such as tension, compression or shear.

Fracture mechanics is increasingly used to analyse how materials and structures behave under harsh conditions, such as during extreme temperatures, pressure or other environments. This is of great value to industries that rely on reliable materials, components and structures that can withstand extreme loading and temperature conditions. Engineers can design materials and components that maintain integrity in these extreme conditions using fracture mechanics. It is an important part of the science of engineering materials. It has applications in many fields such as aerospace, automotive, civil, and materials science (Beaumont, 2020).

Fracture mechanics is used to determine the conditions under which cracks will propagate and to analyse the effects of crack propagation on the performance of a structure. It is also used to design components and structures to prevent cracking or ensure that any cracking does not lead to failure. We study fracture mechanics in modern times because it is a critical tool for understanding how materials behave under various stresses. It is used to design and assess the safety and reliability of structures, machines and components subject to fatigue, fracture, and other types of mechanical stress. By understanding how materials fail and fracture, engineers can design structures and components more resistant to fatigue and fracture, improving safety and reliability. In addition, fracture mechanics has applications in the materials sciences, allowing scientists to understand better the properties of new materials and how they respond to stresses. Finally, fracture mechanics evaluates the integrity of materials used in high-performance applications, such as aerospace and nuclear power.

Fracture mechanics is an important factor to consider when designing concrete structures due to its ability to account for energy required for crack formation, its objectivity in finite element solutions, the lack of yield plateau, the need to predict ductility and energy absorption capability, and the effect of structure size on the nominal strength, ductility, and energy absorption capability (Cervera *et al*. 2022). Recently, people have been researching ways to understand masonry structures better. They tested masonry by bending it and measuring how much energy was released and how much stress it was under. They used different types of bricks that were either hollow or solid and had different levels of grooves. They were trying to figure out how masonry fractures and what affects it. Tests were done on the bricks and the brick/mortar connection and compressive fracture of masonry. Griffith's theory is essential to fracture mechanics and agrees with experimental data for brittle materials such as glass (Petersen, 2013). Using

the energy release rate concept, which suggests that fracture occurs when the energy release rate reaches a critical value, the value is determined by the material's fracture toughness, which measures how much energy is required to break a unit area of the material. Griffith's theory also considers the effect of stress concentration. It provides a mathematical expression to calculate the critical energy release rate. This expression has been tested experimentally and shown to predict glass fracture accurately. Thus, Griffith's theory provides an excellent agreement with experimental data for brittle materials such as glass (Petersen, 2013).

Fracture mechanics was developed during World War I by English aeronautical engineer A. A. Griffith, who first observed the phenomenon of crack propagation in brittle materials. Griffith's work was fundamental in understanding the behaviour of materials under tension and developing methods for predicting and preventing catastrophic failure. His groundbreaking work showed that the amount of energy needed to cause a crack to grow in a material is related to the size and shape of the crack. This knowledge has been used to design materials and structures that withstand extreme mechanical loads. Today, fracture mechanics is used in various industries, from aerospace to civil engineering, and is an invaluable tool for ensuring the safety and reliability of structures and components (Kanvinde, 2016). Griffith crack is a phenomenon that occurs when brittle materials fail under compressive or tensile stress. It is named after the British physicist and mathematician A.A. Griffith, who first described this type of fracture in 1920. Griffith crack is a type of brittle failure in which a crack propagates rapidly through a material (Zhang, 2022). This failure is usually caused by a combination of high stress and a lack of plasticity, which are necessary for the material to absorb the energy of the applied load.

When the material cannot absorb this energy, the stress is concentrated at the crack tip and causes a sudden fracture. This type of failure is common in brittle materials, such as ceramics, glass, and concrete, where the material has low ductility and high strength. Griffith's work was motivated by two contradictory facts. On the one hand, the stress needed to fracture bulk glass was around 100 MPa (15,000 psi). On the other hand, the theoretical stress needed for breaking atomic bonds of glass was approximately 10,000 MPa (1,500,000 psi) (https://mechanicalc.com/reference/fracture-mechanics, 2014). Griffith's work was dedicated to bridging this gap and explaining why glass fractures at such a low-stress level. His work eventually led to Griffith's criterion, which states that

fracture occurs when the energy needed to create a new surface exceeds the surface energy already present. This criterion has been used to explain the fracture of bulk materials since then.

Griffith's work on the fracture of brittle materials was ground-breaking in its ability to reconcile conflicting observations about the behaviour of these materials. His theory was the first to explain the seemingly paradoxical behaviour of brittle materials, where a small increase in applied stress could cause them to fail suddenly and catastrophically. This theory, now known as Griffith's fracture theory, is still widely accepted. In addition to his theoretical work, Griffith also conducted experiments on glass fibres, showing that the fracture stress increases as the fibre diameter decreases (Rani *et al*. 2021). This observation was a key foundation for his theory and is still used today. His experiments also showed that the fracture energy decreases as the fibre diameter decreases, providing further evidence for his fracture theory. Overall, Griffith's work was revolutionary in its ability to explain the behaviour of brittle materials. His fracture theory is still used today and testament to his skill and ingenuity as a scientist. The engineering community largely ignored Griffith's work on fracture mechanics until the early 1950s, when technological advances in materials science and the application of mathematics to engineering problems made his findings relevant (Bažant, Le, and Salviato 2021). Griffith's work was the first to provide a mathematical explanation of how materials fracture, and it revolutionized the field of fracture mechanics.

His work provided insight into the theoretical basis of fracture. It helped engineers design more reliable and durable components, leading to an increased understanding of the behaviour and performance of materials. Griffith's work is now considered a cornerstone of modern engineering design. Griffith's theory postulates that the energy needed to fracture a material equals the work to create a new surface area. This energy is usually called ‘surface energy (Heffer, 2015). The theory is based on the assumption that the surface energy is higher than the internal energy of the material. Although this assumption is often correct for brittle materials, it may be overly optimistic for ductile materials. Ductile materials are often characterized by much lower surface energy than their internal energy, which means that the energy needed to fracture them is much lower than what is predicted by Griffith's theory. Thus, while Griffith's theory can provide a helpful starting point for understanding the fracture of brittle materials, it is often unrealistically high when applied to ductile materials. The group, led by Irwin at the

U.S. Naval Research Laboratory (NRL) during World War II, was composed of engineers and scientists from different disciplines and backgrounds. This multidisciplinary team worked together to investigate the fracture of ductile materials. During their research, they discovered that plasticity must play a significant role in the fracture process, leading to new theories and approaches for understanding and predicting the fracture of ductile materials. Their pioneering work helped to advance the field of materials science and engineering, and their discoveries have had a lasting impact on the design and manufacture of durable products.

The evolution of concrete has had a profound effect on the way structures are built and modern infrastructure is created (Vatan, 2017). Concrete was first used by the Romans over 2,000 years ago. It was revolutionary for its time, allowing them to create structures that were exceptionally strong and durable (Bajaber and Hakeem 2021). During the Middle Ages, concrete was used in many regions, slowly evolving and improving with each century. The Industrial Revolution saw massive advancements in concrete production technology, allowing for increased durability and improved safety of structures. In the late 19th and early 20th centuries, concrete production and technology continued to improve, so today, concrete is used everywhere in constructing roads, bridges, and buildings (Adesina, 2020). This is especially thanks to the invention of Portland cement, which greatly improved the strength and durability of concrete. Over the last 50 years, concrete technology has continued to develop, with construction materials becoming more aesthetic, lighter, and stronger than ever. Companies now specialize in additives to concrete mixtures that allow for greater strength and improved protective qualities from weather and other factors that can damage and wear down concrete (Gandage, 2020). In summary, the evolution of concrete has had a major impact on building modern infrastructure, allowing us to create aesthetically pleasing and exceptionally durable structures.

Concrete is a heterogenous anisotropic, non-linear, inelastic composite material composed of a combination of two or more phases: aggregate and paste. Concrete is an inelastic material due to its aggregate content. It will strain beyond its elastic limit and not return to its original shape or dimensions. Concrete is also non-linear because its strength and performance characteristics increase with age and experience. This effect is known as "ageing" and is caused by the cement paste forming strong bonds with the aggregates over time. Concrete's anisotropic characteristic means that its stiffness,

strength, and shrinkage vary in different directions depending on the type and mixture of the aggregates that make up the concrete. Because of each direction's varying strengths and behaviour, concrete must be designed with specific loading conditions. Finally, concrete is a composite material composed of fine aggregates, coarse aggregates, and binding agents such as cement and water. This composition of materials gives concrete its versatility of form and function, allowing it to be used in various applications, including foundations, pavements, dams, and bridges.

The cement industry is one of the world's largest producers of carbon dioxide ($C0_2$), accounting for approximately 7% of global $C0_2$ emissions. The cement sector is responsible for almost half of all anthropogenic $C0_2$ emissions by the industrial sector, estimated to be around 5 gigatons of $C0_2$ per year. Burning fossil fuels to produce energy is the main source of $C0_2$ production in the cement sector (Ali, Saidur, and Hossain, 2011). Other sources of $C0_2$ include grinding of raw materials, calcination of limestone, and fuel combustion during cement production. Numerous technologies have been developed to reduce the amount of C02 emitted by the industry, such as using alternative fuels instead of fossil fuels, using waste heat recovery systems, reducing fuel use for clinker production and finding alternative processes for clinker production. Industry initiatives such as the Cement Sustainability Initiative have also been established to promote adopting environmentally friendly practices in the cement industry. Despite industry efforts to reduce emissions, the cement sector is still far from becoming carbon neutral. More efforts are needed to reduce emissions, both at the production and consumption ends of the cement value chain, if the industry is to play a significant role in the global climate effort (Ighalo and Adeniyi 2020).

The major environmental impact of cement production is related to air pollution caused by the release of carbon dioxide (CO_2) gas during the clinker calcination process. This CO_2 is released mainly due to burning fuels containing carbon, such as coal, coke or oil. The release of large amounts of CO_2 into the atmosphere contributes to global warming, ozone layer depletion, and acid rain (Ofosu-Adarkwa *et al*., 2020). Additionally, cement production requires large amounts of energy, mostly from burning fossil fuels. This can lead to further environmental impacts, such as air pollutants like nitrogen oxides (NO_X) and sulphur dioxide (SO_2) (Brown, Sadiq, and Hewage, 2014). The use of cement in construction can also contribute to air pollution, and cement production may release dust and particulate matter that can harm public health. Furthermore, cement production can

generate large amounts of liquid and solid waste materials, contaminating soil and water supplies (Mohamad *et al*., 2021).

In recent years, Nigeria has witnessed a significant surge in the development and expansion of diverse industrial sectors, particularly in manufacturing and production. This growth trajectory is emblematic of the nation's concerted efforts to bolster its economic standing and enhance its global competitiveness.

One salient sector that has played a pivotal role in this multifaceted industrial landscape is the cement industry. As a fundamental building material, cement underpins the foundations of infrastructure and development, making it a critical component in Nigeria's journey toward economic progress.

The country's cement industry has experienced notable expansion and transformation, characterized by advancements in production capacity and technology. These developments have been instrumental in addressing the nation's infrastructure needs, facilitating urbanization, and supporting a burgeoning construction sector.

Moreover, Nigeria's cement industry's growth has implications beyond mere economic considerations. It has substantially generated employment opportunities, particularly in the manufacturing and construction sectors, pivotal drivers of socioeconomic advancement. Additionally, the expansion of cement production aligns with broader sustainability objectives by reducing the reliance on cement imports and promoting self-sufficiency in meeting domestic demand.

In light of these developments, Nigeria's cement industry has emerged as a cornerstone of economic growth, contributing to the nation's aspirations for industrialization, infrastructure development, and job creation. It underscores the importance of strategic investments and policy initiatives to enhance this vital sector's production capacity and efficiency."

This growth has been primarily driven by the country’s construction sector and projects to provide infrastructure and housing to rural areas. The Nigerian government has prioritised infrastructure and construction, making investing in the cement sector easier. Nigeria’s cement industry is relatively well-developed, with a strong network of regional distributors and a dedicated sales force. The industry has made significant technological strides, increasing efficiencies and production capabilities (Njoku, Bafuwa, Mgbemene,

and Ekechukwu, 2017). In the future, Nigeria’s cement sector stands to benefit from continued government investment and its strategic geographic position.

Olonade (2013) highlighted that Nigeria's annual cement consumption was approximately 19.5 million metric tons, with nearly half of this amount (9.5 million tons) domestically produced. We witnessed a notable surge in the country's cement production in subsequent years. By 2019, Nigeria had bolstered its production capacity to an estimated 15 million metric tons, positioning itself as a pivotal player in Africa's cement industry (Etim, Babaremu, Lazarus, and Omole, 2021). In recent years, the government has been working to reduce Nigeria's dependence on imports, introducing initiatives such as promoting local manufacturing and allowing lower-priced subsidized imports. It has also invested heavily in infrastructure projects, such as constructing roads, rail lines, and housing to drive cement consumption. With the increasing population and economic development, the demand for cement is expected to grow further in the coming years (Nigeria - Country Commercial Guide, 2023). The growth in cement consumption in Nigeria is driven by the surge in demand stemming from population growth and economic progress.

Additionally, industry-specific factors like enhanced investments from global corporations, improved production efficiency, and better quality play a significant role. "Multinational corporations, leading the charge with foreign direct investments in Nigeria's cement sector, have boosted cement production and consumption. The significant contributions from these major players have profoundly impacted the Nigerian cement industry, leading to remarkable improvements in production capacity and market reach.

The inflow of foreign direct investment has infused the sector with capital, technological know-how, and best practices, enabling the deployment of state-of-the-art manufacturing processes and modern infrastructure. Such enhancements have facilitated the augmentation of cement production capabilities, which has met the burgeoning demand driven by a growing population and increasing construction activities in the country. Furthermore, the infusion of foreign capital has engendered improved operational efficiency, quality control, and environmental standards within the Nigerian cement industry. These advancements align with global sustainability objectives, reducing carbon footprints and enhancing environmental stewardship.

The positive repercussions of increased foreign direct investment extend beyond production, encompassing broader economic implications. This influx of capital has generated employment opportunities, directly and indirectly, contributing to socioeconomic development. Additionally, it has bolstered Nigeria's status as an attractive investment destination within the African continent.

The government of Nigeria has also been instrumental in increasing cement use in the country, implementing policies such as the Mining and Mineral Acts of 2007 that liberalized the licensing and taxation regimes for the cement industry (Ninyio, 2019). This increase in cement consumption is accompanied by growing concerns about its sustainability and environmental impacts. The production and use of cement generates significant amounts of carbon dioxide (CO_2), one of the main contributors to climate change (Oguntade, *et al*., 2023). Nigeria is thus actively working towards reducing its carbon footprint by investing in alternative energy sources such as solar, wind, biomass and hydropower. It also invests in more efficient production systems with co-processing and cement recycling technologies. Despite the increase in cement consumption, Nigeria’s per capita consumption is still relatively low compared to other countries in the region. To keep its cement industry competitive in terms of quality and cost-effectiveness, the Nigerian government should seek to increase the availability of infrastructure and skilled labour and implement policies to stimulate further investments in the sector (Etim, Babaremu, Lazarus, and Omole, 2021). Additionally, measures should be taken to reduce the environmental impacts associated with the industry, such as investing in cleaner production technologies and using alternative energy sources.

The increase in cement prices is linked to the cost of production due to the rising price of fuel, electricity, and gas in Nigeria. The Federal Government of Nigeria's import duty and excise taxes levied on cement account for the high cement price. The government increased the duty and tariffs, rising from zero in 1999 to 15 percent in 2019. The high price of cement has impacted the construction industry in Nigeria, considering the significant role played by cement in the entire building process. The high price of cement has, in turn, led to an increase in the cost of housing, making it more difficult for many people to own a home (Odigure, 2014). This has resulted in a shortage of housing in the country. To address the issue of high cement prices, the Nigerian government has focused on encouraging efficiency in production, price cuts and subsidies, and improved infrastructure to reduce costs (Akinluyi and Adeleye, 2013). The government has also

introduced fiscal incentives, including an export incentive scheme, to stimulate production and encourage exports to other countries.

Additionally, the government has established the National Cement Committee to advise the Federal Government on prices, production, and other areas of the cement industry. Despite this, the cost of cement remains high, leading to a decrease in demand. The government's efforts have so far proved insufficient to bring down the cost of cement in Nigeria. To sustain a healthier building industry, the federal government must revise taxes, incentives, and infrastructure and collaborate with the private sector to make cement production more efficient and cost-effective.

1.2 Statement of the research problem

High-strength concrete, a cornerstone in modern civil engineering, offers unparalleled resilience and durability. However, its behaviour remains intensely scrutinised, especially under strain and fracture. Fracture mechanics, which delves into the intricate behaviour of materials under stress, becomes pivotal when applied to high-strength concrete. A comprehensive understanding of this behaviour is essential for optimizing its performance and ensuring the longevity of structures built from it.

Yet, as the demand for high-strength concrete surges, so does the industry's reliance on traditional cement, which poses both economic and environmental challenges. The increasing importation of cement strains foreign exchange reserves, while environmental concerns underscore the urgency for sustainable alternatives.

Against this backdrop, exploring locally sourced materials as potential substitutes or supplements for cement in high-strength concrete production becomes paramount. Rice husk ash, characterized by its significant pozzolanic properties, emerges as a promising candidate. Rich in silica and other beneficial compounds, this by-product not only holds the potential to enhance the fracture mechanics of high-strength concrete but also offers an eco-friendly avenue by repurposing agricultural waste.

1.3 Justification of the study

The civil engineering discipline is perpetually evolving, driven by the need to address complex structural challenges. Central to this evolution is the study of fracture mechanics in concrete structures. As architectural aspirations advance, necessitating the construction of taller and more intricate structures, a profound understanding of the behaviour of high-strength concrete under various stressors becomes indispensable.

Natural calamities, notably earthquakes and floods, underscore the criticality of this research. The fracture characteristics of concrete are paramount in mitigating risks associated with structural failures, especially in regions prone to significant environmental disturbances. Nigeria, characterized by its unique geographical and climatic challenges, is a testament to this urgency. The nation's susceptibility to heavy rainfall and other environmental factors necessitates a nuanced approach, one that a deep dive into fracture mechanics can inform.

Recent infrastructural developments in Nigeria further accentuate the significance of this study. With burgeoning investments in infrastructure, the nation is witnessing a pronounced shift towards concrete construction. Ensuring these structures' strength, durability, and safety is not merely an engineering challenge; it's a mandate to safeguard both public and private investments. Herein, the insights derived from fracture mechanics can offer invaluable guidance, elucidating potential points of vulnerability and avenues for structural reinforcement.

The global emphasis on sustainability necessitates the exploration of alternative construction materials. Rice husk ash (RHA), a byproduct of the rice production sector in which Nigeria is actively positioning itself (Sun News, 2015), emerges as a promising candidate. Preliminary research indicates that RHA, endowed with significant pozzolanic activity, holds potential as a viable substitute for cement in High Strength Concrete (HSC) production. This not only aligns with environmental imperatives but also augments the structural integrity of the concrete.

The integration of agricultural waste into construction, as highlighted by studies such as Tijani, Ajagbe, and Agbede, (2022), presents a paradigm shift. Materials traditionally deemed as waste are recognized for their potential contributions to structural

engineering. These materials offer cost and environmental benefits and introduce unique structural properties that warrant academic exploration.

Innovative methodologies are emerging in the quest to understand the nuanced behaviour of high-strength concrete. From the integration of nanotechnology to the utilization of geopolymers and recycled materials, the field is ripe for academic exploration. Each of these methodologies, when viewed through the lens of fracture mechanics, can offer profound insights into the unique behaviour of high-strength concrete, especially when integrated with alternative materials.

In summation, exploring fracture mechanics in the context of high-strength concrete is not just an academic endeavour; it's a critical pathway to understanding and optimizing structural behaviour in the modern architectural landscape. By integrating alternative materials and harnessing cutting-edge methodologies, this research seeks to redefine the paradigms of sustainable and resilient construction within the civil engineering discipline, focusing on Nigeria's unique challenges and opportunities.

1.4 Research questions

1. Is the efficacy of the fracture parameter of concrete produced from a rice husk ash–cement mixture in relation to accepted standards worthy of consideration?
2. What are the economic and environmental implications of utilizing rice husk ash in concrete fabrication?
3. Is it possible to gain a more comprehensive understanding of the structural characteristics of high-strength concrete formulated from rice husk ash?

1.5 Hypothesis and testing

It is conceivable that the development of a cement-rice husk amalgam could provide a feasible solution to the problem of high costs incurred due to the production of concrete during building projects by enabling the production of high-quality concrete with desirable structural characteristics.

1.6 The aim and objectives of the study

This research aims to investigate the use of rice husk ash as a partial replacement for cement in determining fracture parameters of high-strength concrete. The specific objectives of the research are to;

1. investigate the potential of utilizing rice husk ash (RHA) as a supplementary cementitious material to produce high-strength concrete blends.
2. investigate the effects of various concrete mix ratios on high-strength rice husk ash concrete by conducting laboratory experiments to determine critical fracture parameters such as the critical stress intensity factor$K_{Ic}^{s}$and the crack-tip opening displacement $CTOD_c$.
3. examine the viability of utilizing rice husk ash as a replacement for cement and comprehending the ecological advantages of such a substitution.

1.7 The scope of the study

The scope of this research is centred on the exploration of rice husk ash (RHA) as a potential partial substitute for cement in high-strength concrete production, with a particular emphasis on its implications for fracture parameters within the construction industry. The study's parameters are defined by incorporating RHA in concentrations ranging from 0% to 50% in high-strength concrete production. This results in a control mix alongside five distinct mixes with RHA concentrations of 10%, 20%,30%, 40% and 50%. Compression cube testing is employed to ascertain the optimal RHA concentration that can be integrated into an M60-grade concrete mix without compromising its structural integrity. For the mix with the highest permissible RHA content, three-point notched bend tests are conducted in alignment with the Two Parameter Model (TPM) as advocated by Shah and Jenq (1990), aiming to discern critical fracture parameters such as K_{Ic}^{s} and $CTOD_c$.

1.8 Limitations of the study

Several logistical and infrastructural constraints circumscribe the scope of the current investigation. Foremost, the laboratory's experimental setup was not comprehensive enough to probe certain fracture parameters. Specifically, the available testing apparatus constrained the research to examine beams with a maximum length of under one meter. Additionally, the spatial separation between the laboratory and the sample casting location curtailed the diversity of samples amenable to testing. A significant logistical

challenge was also posed by the vast distance (approximately 348km) between the rice husk source and its processing facility, which inevitably impacted the volume of rice ash that could be processed and transported for experimental purposes. Given these constraints, the research predominantly focuses on the mode I fracture failure of concrete.

CHAPTER TWO
LITERATURE REVIEW

2.1 Preamble

While concrete stands as a widely utilized construction material, celebrated for its myriad benefits, it is not without its challenges in the modern construction landscape. These inherent limitations have spurred many research endeavours to devise innovative solutions. This academic exposition sheds light on the pronounced shortcomings of concrete in today's construction milieu, buttressed by relevant academic citations.

Over their lifespan, concrete structures are prone to various deterioration mechanisms, including but not limited to cracking, reinforcement corrosion, and susceptibility to sulfate attacks. Such adverse effects often lead to significant maintenance and repair costs. The academic literature deals with studies delving into concrete's durability, offering in-depth analyses and potential countermeasures (Wang *et al*. 2021).

The intrinsic heft of concrete categorizes it as a weighty construction material, which sometimes limits its applicability. This significant weight demands sturdy foundational and structural supports, leading to escalated material and transport costs (Zhang *et al*., 2021). Moreover, concrete's inherent rigidity often results in a monolithic visual aesthetic, limiting design versatility, especially when juxtaposed with materials like steel or glass, making intricate architectural aspirations challenging (Das and Choudhury 2019).

A defining characteristic of concrete is its brittleness, making it prone to crack propagation, particularly under tensile stresses. The onset of such cracks can have manifold repercussions, from undermining the structural soundness to facilitating moisture ingress, culminating in corrosion and aesthetic degradation (Wang *et al.*, 2021). The application of Linear Elastic Fracture Mechanics (LEFM) to concrete encountered hurdles, given concrete's predisposition to cracking and its intricate fracture dynamics stemming from its heterogeneous composition and non-linear mechanical attributes (Berto and Lazzarin, 2014). The evolution of XLEFM aimed to encapsulate the effects of material toughness, strain, and crack trajectory on the fracture mechanism by

incorporating an expanded parameter set (Malitckii *et al.*, 2018). This adaptation sought to render a more nuanced portrayal of concrete behaviour. Adapting LEFM to concrete has been instrumental in forecasting its fracture dynamics and demystifying its intricate properties. By amalgamating material traits with fracture parameters, XLEFM has emerged as a pivotal instrument in the design and scrutiny of concrete edifices. The overarching objective is to delve deeper into the failure modes of such materials, thereby enhancing our comprehension of the degradation mechanisms and the potential triggers for its failure within its operational context. Such insights empower engineers and professionals to preemptively address challenges that might surface during the material's production, processing, and application.

Furthermore, engineers can adapt and refine the parameters responsible for such failure to optimize the material and its usage. By quantifying the necessary parameters responsible for the failure, engineers can identify potential points of failure in the material and ways to avoid, anticipate, and mitigate such issues to maximize performance and efficiency. Engineers can help ensure successful operation and increase material lifespan by doing so. Griffith's brittle fracture theory remains one of the most popular theories in material science and engineering (Li *et al*., 2021). In 1921, he proposed his energy-based failure criterion, which states that material failure occurs when the stored strain energy in a material reaches a critical value. This hypothesis explained the advantage of tougher materials (Denli *et al*., 2020). It provided insight into why certain materials fracture abruptly, which had previously been unexplained. Griffith's idea was ground-breaking in that it could be used to predict the mechanical strength of different materials. As a result of this, engineers and scientists began to measure the fracture energy of various materials to improve design parameters, enhance the material's strength, and promote safety. Griffith's energy-based failure criterion has since been used in a variety of applications, including aircraft design, civil engineering, and even medical surgery (Nicolas *et al.*, 2018). The crack in the glass can be attributed to the applied stress exceeding the material’s tensile strength. This is known as brittle fracture. Brittle materials fail without significant deformation by breaking suddenly under stress instead of yielding like ductile materials.

The analysis revealed that applied remote stress with a magnitude greater than the glass material’s tensile strength was at least partially responsible for the crack in the glass.

This situation is further complicated by two competing activities: in-plane tensile stresses, which widen the crack, and crack-tip shear stresses, which tend to hold the crack closed. The balance between these two activities dictates the growth and propagation of the crack and, ultimately, the failure of the brittle material. In 1961, Kaplan attempted to apply the concept of Linear Elastic Fracture Mechanics (LEFM) to concrete by developing models that could predict the onset of cracking and its progress in unrestrained concrete elements (Chauhan*et al.,* 2018). His models defined how stresses propagate in a body before, during and after the onset of cracking.

One of the objectives of his work was to develop an analytical framework that could be used in the design of reinforced concrete structures. He developed a theoretical model to describe the initiation and propagation of cracks in brittle materials such as concrete. Then, he applied it to the analysis of crack formation in concrete beams and plates. His research established the importance of understanding the behaviour of cracks in structural materials, which can be used to improve structures' structural performance and durability. As a result of his work, LEFM can now be applied to many engineering materials and structures (Chauhanet al., 2018). The energy release rate is a measure of the stiffness and strength of a material. It can be determined for notched concrete beams tested in three- and four-point bending configurations (Ohno *et al.*,2014). The energy release rate for a notched concrete beam can be defined as the energy required to cause the material to fail by fracture. As such, the higher the energy release rate, the less susceptible the material is to fracture. In a three-point bending test, the beam is placed between two points and a third point is applied on the top to apply a uniform load to the beam. The two lower points will cause the beam to bend as the load is applied, and as the load increases, the beam will eventually fracture.

The energy release rate can then be determined by the energy needed to cause the material to fail. In a four-point bending test, the beam is placed between two sets of two points and two loads are applied to the beam, one on each end. The two sets of points cause the beam to bend inwards, and as the loads increase, the beam will eventually fracture. The energy release rate can then be determined by the energy needed to cause the material to fail. Overall, the energy release rate for notched concrete beams tested in both three-point and four-point bending configurations can be used to determine the quality of the material, with higher energy release rates indicating greater stiffness and

strength. Shemirani *et al.* (2017) provide a detailed exploration of fracture mechanics and its application to materials science. Drawing on existing research, the authors provide an overview of how fracture mechanics is used to analyze the macroscopic properties of materials. They discuss the role of stress singularities in fracture, the development of fracture surfaces, and the effects of environmental conditions, fatigue and creep. Additionally, the paper looks at fracture toughness and the fracture toughness of various materials in detail. The paper describes empirical methods to measure fracture toughness and discusses the theoretical models used to describe fracture mechanics. This in-depth exploration of fracture mechanics provides an important resource for materials scientists, providing insight into the mechanics of failure in materials systems. The slow cracking phase before fast fracture failure is an important aspect of fracture analysis that should not be overlooked. In this phase, the material experiences increasing strain, microstructural changes, and thermal stresses, which can cause the material to exhibit unexpected behaviour.

Detailed knowledge of these effects is essential for accurately understanding the fracture process. It helps to explain why some materials may fracture faster than others. Furthermore, carefully considering the slow cracking phase can allow engineers to predict the fracture behaviour of materials more accurately, helping to prevent failure before it occurs. The Griffith concept of a critical energy rate has become widely accepted for analysing brittle failure in materials and engineering structures (Li *et al.*, 2021). In concrete, however, modifications to the theoretical framework are necessary to account for concrete's combined ductile and brittle behaviour. In recent years, several modifications to the Griffith concept have been proposed to make it applicable to concrete. Some of these modifications include experimental analyses of the impact of environmental conditions on the failure process and the incorporation of physical characteristics such as porosity, toughness and tensile strength. Additionally, analytical and numerical models, such as finite element models, have been developed to analyse the effects of mechanical and environmental loading on the dynamic failure processes of concrete (Jin and Yu 2022).

The successful application of the modified Griffith concept of a critical energy rate to the analysis of concrete failure would enable engineers to predict the failure of concrete structures more accurately, particularly when subjected to dynamic loading conditions.

It could, therefore, be used to assess the structural reliability and safety of engineering concrete structures. The experimental investigations utilized a variety of experimental setups and test conditions to simulate the actual field conditions. In addition, various numerical models such as the finite element method, discrete element method, and hybrid finite-discrete element method were used to study the fracture behaviour of concrete. These investigations found that concrete has a wide range of fracture behaviours due to the heterogeneity of its microstructure and material properties. It was observed that the fracture behaviour of concrete depends on several parameters, such as the strain rate, loading mode, loading rate, temperature, and specimen size (Rezaei and Issa, 2021).

Furthermore, it was observed that concrete fractures more easily under dynamic loading compared to static loading conditions. Additionally, the presence of pores and other flaws in the concrete microstructure can also influence the fracture behaviour of concrete. Finally, it was concluded that the fracture behaviour of concrete can be effectively simulated using numerical models.

The widespread adoption of the linear elastic fracture mechanics (LEFM) approach in the 1960s to examine cementitious materials resulted in a significant breakthrough in understanding the behaviour of these materials. Previously, researchers were limited in analysing these materials due to the lack of a single tailored experimental procedure. The recognition that a procedure similar to that used for metals for the determination of critical stress intensity factors K_{IC} could be adapted to include cementitious materials provided a basis for furthering knowledge and facilitating greater understanding. This discovery and subsequent adoption of LEFM allowed for a more comprehensive view of cementitious materials, in particular their fracture behaviour. It enabled researchers to gain further insights into the strength and durability of cementitious materials, which in turn led to the further refinement of design criteria and applications in the field. Ultimately, the LEFM approach incubated a greater understanding of the properties of cementitious materials and enabled the use of more sophisticated and accurate predictive tools.

The stress intensity factor K_{IC} (Xie *et al.*,2021) is a measure for the resistance of a metal to plastic deformation, which can be used to determine the strength and ductility of a metal. It is defined as the square root of the work of fracture energy normalized by the

fracture area and is expressed as $K_{IC} = \sqrt{W/A}$. K_{IC} is based on the strain-energy-release ratio (SERR). With increasing K_{IC}, the ductility of the metal decreases, while its hardness and strength increase. The K_{IC} can be measured directly from the force-displacement curves obtained from tensile tests, or indirectly from microstructural parameters. K_{IC} values typically range from 1 to 700 MPa·m1/2. When the K_{IC} is lower than 1, the metal is more pliable and has a higher ductility; when it is above 700 MPa·m1/2, the metal is more resistant to plastic deformation and has higher strength and hardness. K_{IC} is important for understanding the properties of metals and designing ductile materials. It is instrumental for comparing materials with different microstructural features since the value of K_{IC} is unaffected by scale or variables such as grain size, crystallographic orientation, and type of hysteresis.

In addition, because K_{IC} is based on fracture energies, it is applicable to a wide range of materials, including metals, alloys, and composites. (Iskander and Shrive, 2018), this research focused on the brittle fracture of concrete which is a dominant form of fracture in concrete. Glucklich's research included tests on plain concrete and steel–reinforced concrete specimens. The application of rigorous fracture mechanics principles to concrete structures was studied by examining the relation between tensile strength and stress-intensity factor (K) at the crack-tip. Glucklich identified a linear relationship between stress-intensity factor (K) and the ultimate concrete strength. This was a significant result as it showed that fracture mechanics could be applied to concrete structures. This research also established the concept of fracture toughness as a criterion for controlling the fracture strength of concrete. The fracture toughness was identified as the ratio of critical stress-intensity factor (K) to the strength of the material. Glucklich additionally studied the influence of temperature and humidity on the fracture strength of concrete by repeating fracture tests at different temperatures and humidity levels. This research was able to quantify the effect of temperature and humidity on the fracture strength of concrete. Glucklich's work provides the foundation for future research into the fracture mechanics of concrete. Today, the fracture mechanics of concrete remains an active research field with ongoing efforts to further understand this complex material. Modern research focuses on the development of analytical models for predicting the propagation of cracks in concrete structures, development of parameters for numerical implementations simulating fracture behaviour and the effects of loading rate and concrete structure on the material fracture behaviour. The relatively high value of the

shear modulus for composite materials is largely attributed to their high filler content. Higher filler content leads to increased stiffness, which is due to stiffener-matrix interaction and higher confined matrix.

The shear stiffness of the matrix itself can also influence the material's overall shear modulus, depending on the type and proportion of matrix and its extent of confinement between the stiffeners. Furthermore, the increase in the micro-cracked zone and the heterogeneity of composite materials contribute to the relatively high value. Since the micro-cracked region does not contribute to the load-bearing capacity of the material, the higher shear modulus reflects its increased stiffness in that direction. Additionally, the heterogeneity of composite materials may lead to variation in their shear stiffness, which can affect the overall shear modulus. (Kumar and Barai, 2012) explored the concept of the strain energy release rate in their paper. The strain energy release rate (SERR) is a measure of the energy dissipated in the form of elastic strain energy within a material due to applied forces. It can be thought of as a measure of the energy required to deform the material and thus it is a key parameter in determining the potential failure of materials under static or dynamic loading. Kumar and Barai, (2012) investigated the effects of temperature on Zener-Hollomon coefficients and resulting SERR values.

They explore the temperature dependence of the Zener-Hoollomon coefficients in a range of materials and find that high temperature increases the SERR values in all investigated materials. They also propose the development of an equation to predict the strain energy release rate dependent on temperature. Overall, Kumar and Barai, (2012) provided a comprehensive exploration of the strain energy release rate and its dependence on temperature. Their findings provide valuable insight into the performance of materials under varying temperatures and their proposed SERR equation can be used to aid in the design of components exposed to varying temperatures. Gdoutos (2020) studied the nature of fracture in concrete in order to investigate how it contributes to the mechanical properties of concrete. The two engineers conducted their research by analysing how different variables, such as loading rate, size of the specimen, and type of reinforcement, affect the fracture process in concrete. To analyze this, they designed a testing procedure that included specimen preparation, testing, and data collection. Gdoutos (2020) concluded that the main factors affecting the fracture process in concrete were the size of the specimen and the loading rate. Furthermore, they

highlighted the importance of using the methods of numerical simulation to predict the fracture process in concrete.

This work is considered to be a major contribution to the understanding of the mechanical properties of concrete. In 1972, Walsh showed that the size and type of coarse aggregate can have a significant effect on the fracture toughness of concrete as determined by a three-point bending test (Matouš et al. 2017). He found that for a given concrete composition, the fracture toughness increased with an increase in the size of the coarse aggregate. Walsh also observed that the type of aggregate used can also affect the fracture toughness of concrete. He found that quartzite and limestone aggregates gave higher fracture toughness values than aggregates made from trap rock or marble. In general, Walsh concluded that the size and type of coarse aggregate should be carefully considered when selecting aggregate for concrete in order to achieve adequate fracture toughness. Fracture toughness of geometrically similar notched concrete beams is an important measure of their mechanical properties. The fracture toughness of such beams can be determined using the three-point bending geometry and the (Kesler, Naus, and Lott, 1972)??? method. This method involves loading a beam at two points and measuring the crack opening displacement with a crack-detection device. The ratio of crack opening displacement over the applied load is then determined and used to calculate the fracture toughness of the beam.

Alternatively, the fracture toughness can also be evaluated from the area underneath the fracture toughness curve generated using the three-point bending technique. Shaikeea *et al*. (2022) studied the effects of crack depth and notch shape on the fracture toughness of concrete beams. They found that the fracture toughness increased with the increase of the notch depth and decreased when the notch was filled with a glass bead. It was also observed that, in general, shallow notches had a higher fracture toughness than deep notches. This finding is important because it shows that the depth and shape of the notches should be considered while determining the fracture toughness of geometrically similar notched concrete beams. In summary, Shaikeea *et al*. (2022) proposed a method to determine the fracture toughness of geometrically similar notched concrete beams using three-point bending geometry and a crack-detection device. Their findings shed light on the effects of crack depth and notch shape on the fracture toughness of concrete

beams, indicating that the depth and shape of the notches should be considered while determining the fracture toughness.

Later experiments focused on determining the relationship between specimen size and fracture strength. He suggested that the use of 10 or more specimens from the same specimen size will help to reduce the variability between tests and estimate the true fracture strength more accurately (Matouš *et al*. 2017). He also drew attention to the importance of including specimens with different dimensions when extrapolating laboratory results for use in real-life structures.

This can help to ensure that greater variability between tests does not overestimate a structure's strength, potentially leading to catastrophes. Walshalso studied the effects of boundary conditions on fracture strength, finding that the presence of a boundary layer and the magnitude of the size effect are closely related. Thus, the boundaries could be used to negate the size effect in laboratory tests, as such, proposed a method of combining the results of tested specimens with differing size to correctly extrapolate fracture strength tests of real-life structures with reasonable accuracy (Matouš et al. 2017). He claimed that this estimation method would not differentiate between size effects, making it more accurate and reliable than other traditional methods.

The validity of linear elastic fracture mechanics (LEFM) depends on the extent of micro-cracking, slow crack growth, or other inelastic behaviour around the crack tip. This is because LEFM assumes that all stresses around the crack tip remain within the linear elastic range and do not exceed the material’s ultimate strength. If any of these micro-cracking, slow crack growth, or other inelastic behaviours occur, it causes stresses to exceed the elastic limit of the material, thereby rendering LEFM invalid. Furthermore, these inelastic behaviours can cause an increase in the fracture toughness of the material, which is not accounted for by LEFM and thus further decreases its validity. To ensure that LEFM is valid, it is important to understand and account for any inelastic behaviours occurring around the crack tip. This is because LEFM assumes an ideal stress distribution within the specimen, with the magnitude of the stress reaching a maximum at the crack tip, which decreases linearly as the crack length increases. In such an ideal situation, the crack slip line solution or its variants can be used to calculate the stress intensity factors in the specimen which showed that the macro-crack pattern (meso-level) was more dominant than the micro-crack pattern.

Therefore, it would be necessary to use a failure criterion which considers the interaction between the micro and macro-crack patterns, such as the critical crack load (CCL) or critical distance from the crack/tip approach, which is better suited for modelling the mixed-mode loading conditions. Wang *et al*. 2016) conducted the first full-scale fatigue failure investigation of concrete using the LEFM (linear elastic fracture mechanics) approach. Their experimental data showed that fatigue failure of concrete is progressive, with crack length increasing logarithmically as the number of load cycles increased. The results of the study indicated that a significant increase in the number of fatigue cycles was required when the crack length became larger and that surface cracks were an important factor in increasing the number of fatigue cycles required to cause failure. Furthermore, the results suggested that the fracture process of concrete is similar to that of metals, with a critical fracture toughness being found necessary for fracture.

The results of this study provided a foundation for the further application of LEFM in the study of fatigue failure of concrete. The finding that the presence of a fracture process zone (FPZ) at the tip of a crack makes the concept of linear elastic fracture mechanics (LEFM) in concrete more complex, is important. It means that the classic LEFM approach is not sufficient on its own to capture the behaviour of concrete in the presence of cracks and other flaws. As such, more sophisticated numerical analyses are often required; these involve accounting for the presence of the FPZ and some of its characteristics. Additionally, further empirical investigations may be needed to validate the results of these numerical models. When the structure's characteristics dimension D is less than the size of the FPZ, other cementitious materials may still be applicable depending on the project's requirements. For instance, such materials could offer more flexibility when compared to standard Portland cement, allowing for easier installation and quicker construction times. Other types of cementitious materials include mortars, lime-based cement, fly ash-based cement, expansive cement, hydraulic limes, and blended cement. Each of these materials has its own set of advantages and can be beneficial in certain scenarios. To determine which type is best suited to meet the project requirements, consulting an experienced design-build team can be invaluable. In addition to Portland cement, other cementitious materials commonly used in construction are fly ash, slag, silica fume, geopolymer, and calcium aluminate cement. FPZ size refers to the grain size of the material, usually expressed in mm (millimeters). Fly ash and slag generally have a maximum FPZ size of 0.15mm, silica fume generally

has an FPZ size of 0.03 mm, geopolymer has a FPZ size of 0.45 mm, and calcium aluminate cement has an FPZ size of 0.02mm (Plizzari, 1995). Nonlinear fracture mechanics (NLFM) analysis is a form of fracture mechanics that accounts for variability in the material properties, geometry, and environmental conditions that affect the fracture behaviour of structures. NLFM analysis puts emphasis on the dependence of fracture behaviour on the nonlinear material properties. It is used to assess the effects of localized material damage, small-scale yielding, and large strain effects on the fracture behaviour of structures. NLFM analysis is important for understanding the consequences of static and dynamic loading, as well as the variability in the fracture parameters.

Furthermore, NLFM analysis allows designers to account for the potential risk of failure under the conditions experienced by a structure. The analysis involves examining stress and strain values at critical locations in the structure, as well as identifying the fracture parameters that may affect its behaviour. NLFM analysis is commonly used in engineering applications to assess the safety and reliability of structures and can be used to design parts or components to prevent or reduce the risk of failure. NLFM analysis can provide insights into the effect of various loading conditions on the lifetime of a structure and help prevent premature failure. Over the past few decades, the unavailability of computational tools for the analysis of Nonlinear Fracture Mechanics (NLFM) has limited the extent of understanding related to how damaging loads, stresses and strains result in the fracture of materials. To address this limitation, researchers such as (Carpinteri, 1982), (Hillerborg A. , 1985), (Jenq and S. Shah, 1985), (Bazant and Kazemi, 1990) and (Plizzari, 1995) have proposed various guidelines for determining modified Linear Elastic Fracture Mechanics (LEFM) parameters or conditions that would help validate the use of LEFM. These researchers highlight the importance of studying the complete fracture process from the initial crack formation to complete rupture in the analysis of NLFM, while holding on to the simplifying assumptions of LEFM. The proposed guidelines have highlighted certain LEFM parameters, including stress intensity factors, fracture toughness, crack area, crack length and energy release rate, as the decisive factors of fracture behaviour. By performing careful finite element analysis of NLFM problems, these parameters are determined and appropriately incorporated into LEFM criteria to identify possible fracture locations and mechanisms. Additionally, the various authors have proposed various approaches to estimate the modified parameters in order to ensure the accuracy of the analysis and to ensure that

LEFM methods provide reliable predictions. The various guidelines proposed by these authors have provided a deeper insight into NLFM and provide different approaches for addressing the limitation posed by the lack of computational tools for NLFM analysis. These guidelines have also enabled engineers to identify critical LEFM parameters for NLFM fracture modeling and have allowed them to make well-informed decisions in various fracture mechanics applications.

2.2 Nonlinear fracture mechanics for concrete

Karihaloo, (1995) provided further evidence of this nonlinear behaviour phenomenon by exploring the concept of 'nonlinearity' in greater depth. He suggested that linear models and methods may not accurately reflect the complexity of the system or sufficiently capture the behaviour of the system. He argued that nonlinear models and methods could better capture the dynamic characteristics of the system and could provide a more accurate and comprehensive picture of the system. He also discussed other aspects of nonlinear system behaviour, such as nonlinear feedback and nonlinear bifurcation. His arguments further highlighted the need for more research on nonlinear behaviour in order to better understand and model the systems in question.

The size of the Frature Plastic Zone (FPZ) is directly related to the hardening plasticity seen at the crack tips on various materials. This is due to the fact that the FPZ is a region of the material containing residual stresses and plastic deformation which can reduce the fracture toughness at the crack tip. In this region, when subjected to fracture, the hardness increases significantly, which can protect the material from further fracture and can also reduce the amount of crack growth. Materials with a large FPZ usually demonstrate higher hardening plasticity at the crack tip as a result of their ability to redistribute plastic deformation around the crack tip. This also serves to reduce the amount of crack propagation that can occur. Conversely, materials with a smaller FPZ are more prone to crack growth, as the hardness at the crack tip is not as high and requires a greater force to promote plastic deformation. This can lead to brittle failure of the material. The application of LEFM (Linear Elastic Fracture Mechanics) has been found to be an effective method for predicting the fracture behaviour of various materials. LEFM considers both the material's strength (as measured by its Fracture Process Zone (FPZ) and its plasticity hardening behaviour. Materials with a small FPZ require higher stresses to initiate fracture, as the FPZ tends to be a stronger region of the material. On

the other hand, materials with significant plasticity hardening will have a larger FPZ, meaning that these materials may be able to resist higher levels of stress before failure.

Linear Elastic Fracture Mechanics (LEFM) analysis is a valuable tool for identifying potential flaws and weak points in materials that are susceptible to failure. It also allows for the simulation of crack propagation, providing crucial insights into material failure mechanisms. By considering the material's Fracture Process Zone (FPZ) and plasticity hardening behavior, LEFM can predict the fracture behavior of various materials accurately. This is particularly relevant as it aligns with LEFM's ability to predict fracture behavior given its linear response to fractural loading (as illustrated in Figure 2.1a). However, for materials exhibiting significant FPZ and/or plasticity hardening (Figures 12b and 12c), LEFM becomes inadequate due to their nonlinear behavior, as observed by Kumar and Barai in 2012. Linear Elastic Fracture Mechanics (LEFM) analysis is a valuable tool for identifying potential flaws and weak points in materials that are susceptible to failure. It also allows for the simulation of crack propagation, providing crucial insights into material failure mechanisms. By considering the material's Fracture Process Zone (FPZ) and plasticity hardening behavior, LEFM can predict the fracture behavior of various materials accurately. This is particularly relevant as it aligns with LEFM's ability to predict fracture behavior given its linear response to fractural loading (as illustrated in Figure 12a). However, for materials exhibiting significant FPZ and/or plasticity hardening (Figures 12b and 12c), LEFM becomes inadequate due to their nonlinear behavior, as observed by Kumar and Barai in 2012.

Figure 1a further demonstrates stress deformation relations of various materials under uniaxial tension, emphasizing their nonlinear behavior. In Figure 2.2a, it is evident that brittle materials display almost linear elastic behavior up to the peak load, after which a catastrophic crack propagates through the specimen. In contrast, ductile and quasi-brittle materials exhibit nonlinear behavior before reaching the peak load, as depicted in Figures 12b and 12c. Specifically, quasi-brittle materials showcase nonlinear behavior initiating before the peak load, with crack localization occurring at peak load, resulting in a reduction of the material's stress transfer capability (Kumar and Barai, 2012).

Figure 1a further demonstrates stress deformation relations of various materials under uniaxial tension, emphasizing their nonlinear behavior. In Figure 12a, it is evident that brittle materials display almost linear elastic behavior up to the peak load, after which a

catastrophic crack propagates through the specimen. In contrast, ductile and quasi-brittle materials exhibit nonlinear behavior before reaching the peak load, as depicted in Figures 12b and 12c. Specifically, quasi-brittle materials showcase nonlinear behavior initiating before the peak load, with crack localization occurring at peak load, resulting in a reduction of the material's stress transfer capability (Kumar and Barai, 2012).

2.2.1 Modified linear elastic fracture model concept

As discussed in the preceding section, the conventional LEFM is unable to accurately capture the fracture behaviour of concrete in the presence of a finite process zone (FPZ) and a cohesive force ahead of a traction-free crack (Tang and Chen, 2019). This is because the linear elastic fracture mechanics (LEFM) model assumes that a sharp crack exists and fails to incorporate any form of dissipative behaviour that may occur due to the presence of a FPZ. The primary challenge that the conventional LEFM fails to incorporate is the cohesive force, which acts ahead of the traction-free crack. This is because the LEFM neglects the dissipative effect of the FPZ and instead assumes the crack to open instantaneously, thus failing to capture any form of delay between the applied stress and the response of the material. This is a significant limitation of the model, as it fails to incorporate the crucial effect of the cohesive forces. Furthermore, LEFM predicts the fracture toughness of concrete to increase with increasing fracture width, while experiments and more advanced models show otherwise. This is due to the fact that LEFM ignores the effect of microcracking that occurs in the FPZ and is generally unable to accurately account for the dissipative behaviour of concrete. To conclude, the conventional LEFM is unable to accurately account for the fracture behaviour of concrete due to the presence of a FPZ and the cohesive force ahead of a traction-free crack, as it neglects the dissipative behaviour of the material and fails to incorporate the effect of microcracking. Various fracture models were proposed to predict the crack propagation and to account for the influence of the FPZ on the fracture behaviour of the materials in question (see Figure 13)

As shown in the Figure 13, the modified LEFM models use a critical effective crack length a_c derived via computation based on experiments on the assumption of peak load. This crack length can be related to the initial crack length by Eq. (2.1) below:

$$\boldsymbol{a_c = a_o + \Delta a} \qquad \textbf{(2.1)}$$

Where Δa is the equivalent extension in stress-free crack length at peak load with a corresponding stress intensity factor $K_I = K_{IC}$ determined using the LEFM principles. With the aim to shed more light on modified LEFM concepts, the various models will be discussed in the proceeding paragraphs.

Two-Parameter Fracture Model (TPFM)

This model was proposed by (Jenq and S. Shah, 1985). In TPFM, the real crack is being substituted by an equivalent fictitious crack. The central concept of this model is based on two fracture parameters for cementitious materials; (**a**) Critical stress intensity factor ($\boldsymbol{K_{IC}^{s}}$) fracture toughness defined as the stress intensity factor calculated at the critical effective crack tip, (**b**) Critical crack tip opening displacement ($\boldsymbol{CTOD_c}$) defined as the crack tip opening displacement calculated at the original notch tip of the specimen.

To determine these parameters, an unloading and reloading procedure is carried with the setup shown in Figure.15 in Appendix. Here, based on the unloading compliance $\boldsymbol{C_u}$at 95% of peak loadderivedfrom the P – CMOD curve as shown in the Figure 15 in the Appendix, the effective crack length $\boldsymbol{a_c}$can be evaluated and with the value of the $\boldsymbol{P_{max}}$measured from the experimental procedure, the $\boldsymbol{K_{IC}^{s}}$ and $\boldsymbol{CTOD_c}$ can be evaluated using the Tada et al. (1985) LEFM formula.

$$\boldsymbol{E = \frac{6Sa_oV_1(\alpha_o)}{C_iW^2B}} \qquad \textbf{(2.2)}$$

For S/D = 4, the function $V_1(\alpha)$ is given by

$$\boldsymbol{V_1(\alpha_o) = \frac{0.76 - 2.28\alpha_o + 3.87\alpha_o^2 - 2.04\alpha_o^3 + 0.66}{(1-\alpha_o)^2}} \qquad \textbf{(2.3)}$$

Where;

E = Young Modulus to be determined;

S = Specimen loading span;

$$a_o = \ initial\ crack\ length;$$

$\alpha_o = \frac{a_o + H_o}{D + H_o}$;

H_o = thickness of clip gauge holder;

D = beam depth;

B = beam width;

C_i = the initial compliance from P-CMOD curve;

From the experimental results, the value of $\boldsymbol{K_{IC}^s}$obtained from the TPFM is said to be independent of the specimen geometry (Jenq and Shah, 1988, Kumar and Barai, 2012). The same result is in agreement with the compact test, wedge splitting cube test and large tapered double-cantilever beam results of (Jenq and Shah, 1988), conclusion on the likelihood of $\boldsymbol{K_{IC}^s}$and$\boldsymbol{CTOD_c}$being geometry-independent fracture parameters. However, further research by same author and other researchers on the geometrical effect on $\boldsymbol{K_{IC}^s}$ and $\boldsymbol{CTOD_c}$ indicate a significant influence of geometry on their value (Jenq and Shah , 1988; Planas, 1990). In view of (Kumar and Barai, 2012), the determination of $\boldsymbol{K_{IC}^s}$ and $\boldsymbol{CTOD_c}$ neglects the inelastic part of the total CMOD which might result to underestimation of the value of $\boldsymbol{a_c}$ due to the nonlinear fracture behaviour of concrete associated with stable crack propagation. One of the drawbacks of the model lies in the experimental setup using a closed-loop testing system.

2.2.2 Size-Effect Model (SEM)

The phenomenon of size effect, which pertains to the variance in fracture behaviour of cementitious materials across macro-scale and nano-scale specimens, has been meticulously examined by Bažant and his colleagues. This effect arises from fracture energy and surface area disparities between different specimen scales. Typically, smaller specimens exhibit a reduced fracture energy compared to their macro counterparts, primarily due to their elevated surface area-to-fracture energy ratio. This makes them more susceptible to failure under identical stress conditions. Moreover, the crack formations in smaller specimens tend to adopt a more 'snail-shell' configuration than those in larger specimens, complicating crack control.

Bažant's seminal contributions have elucidated the interplay between specimen size, shape, and fracture energy. His findings, validated for materials like Portland cement, concrete, and mortar composites, have informed the development of models that can predict size-effect behaviour and strategies to enhance specimen resilience. In essence, the pioneering work of Bažant and his team has deepened our comprehension of the size effect on cementitious materials' fracture behaviour, offering models that forecast this behaviour. Their insights have significantly influenced construction industry practices.

One of the pioneering explorations into the impact of specimen size on fracture behaviour was the Size-Effect Model. Bažant and Kazemi, in 1986, postulated a power law linking fracture toughness to specimen size. Concurrently, a similar formulation was proposed by Gettu et al, (1990). Both models employed two parameters to characterize the size effect: a loading-independent specimen size scale and an exponent denoting loading intensity (Shaikeea *et al*. 2022). Efforts were made to refine the Size-Effect Model by incorporating parameters accounting for behaviours like limiting stage and crack-tip bridging, encompassing interface strength, crack velocity, and material properties. This enhanced model was subsequently employed to simulate diverse size effects in materials, spanning from highly ductile metals to specific brittle materials. Despite the model's capabilities, further investigations are imperative to thoroughly decipher the nexus between specimen size and fracture behaviours.

Two pivotal parameters to quantify fracture behaviour include (a) Fracture Energy.$\boldsymbol{G_f}$ (alternatively represented as$\boldsymbol{G_{FB}}$), and (b) the critical effective crack length extension $\boldsymbol{c_f}$(at peak load for infinitely large test specimens). As Kumar and Barai (2012) highlighted, quasi-brittle materials like concrete manifest a transitional size effect, oscillating between two size effect extremes, as depicted in Figure 16 in the Appendix.

The Size-Effect Model (SEM) determines fracture parameters using geometrically analogous notched specimens of varying sizes, prioritizing maximum loads. Bažant and Jaime (1997) proposed an intricate yet streamlined methodology centred on the transitional size effect in articulating these parameters. They conceptualized a notched plate of width D and thickness B, accompanied by an infinitesimal crack extension$\boldsymbol{\Delta a}$, as illustrated in Figure 17 in the Appendix. Consequently, the estimated energy released is equated to the energy requisite for a crack extension, as delineated in Eq. (2.4).

$$\frac{\boldsymbol{2k\left(a_o + c_f\right)B\Delta a\sigma_N^2}}{\boldsymbol{2E}} = \boldsymbol{BG_{FB}\Delta a} \tag{2.4}$$

Which can be further reduced to;

$$\boldsymbol{\sigma_N = \frac{B' f_t}{\sqrt{1+\beta}}} \tag{2.5}$$

Where;

$\beta = \frac{a_o}{c_f} = \frac{D}{D_o} = constant$;

$f_t = tensilestrengthofthematerial$;

$B' = dimensionlessconstant$;

$D_o = constantwithadimensionoflength$;

$c_f = materialconstantintermsofelasticequivalentcrackextension$;

$G_{FB} = Fractureenergy\ (ameterialconstant)$;

From the Eq (2.5) above, the transitional size effect for most practical size range concrete structure is being represented and provide an insight into the two extreme size effects exhibited by plastic limit analysis and LEFM. Kumar and Barai, (2011) reiterated that the size effect seen in concrete structures is due to the existence of large and variable length of FPZ ahead of the crack tip. (Shah and Carpinteri, 1991) gives a detailed explanation on the methodology of using SEM to determine the nonlinear fracture properties is well documented. With reference to this procedure using a three-point bending test (TPBT) specimen (see Figure 14 in the Appendix), the maximum load $\boldsymbol{P_u}$including self-weight per unit of beam$\boldsymbol{w_g}$is given as follows;

$$\boldsymbol{P_u} = \boldsymbol{P_{u,test}} + \frac{\boldsymbol{w_g S}}{\boldsymbol{2}} \tag{2.6}$$

Taking, $\boldsymbol{\sigma_N = \frac{P_u}{BD}}$, $\boldsymbol{\sigma_{Nu} = \frac{c_n P_u}{BD}}$. Thus, Eq. (2.6) can be expressed as;

$$\left(\frac{\boldsymbol{1}}{\boldsymbol{\sigma_N}}\right)^{\boldsymbol{2}} = \left(\frac{\boldsymbol{D}}{\boldsymbol{D_o(B' f_t)^2}}\right) + \left(\frac{\boldsymbol{1}}{\boldsymbol{B' f_t}}\right)^{\boldsymbol{2}} \tag{2.7}$$

$$\boldsymbol{Y_i} = \left(\frac{\boldsymbol{1}}{\boldsymbol{\sigma_{Ni}}}\right), \qquad \boldsymbol{C} = \left(\frac{\boldsymbol{1}}{\boldsymbol{B' f_t}}\right)^{\boldsymbol{2}}, \qquad \boldsymbol{X_i} = \boldsymbol{D_i} \tag{2.8}$$

$$\boldsymbol{Y = AX + C} \tag{2.9}$$

With the above relation established, a scatter plot of Y and X can be plotted on X-Y plot as shown in Figure 19. With the aid of linear regression analysis, the constants of the Eq. (29) can be determined. (Kumar and Barai, 2012) noted that the coefficient of the variation of the slope of the regression line, coefficient of variation of the intercept and the relative width of the scatter band should not exceed about 0.1, 0.2 and 0.2 respectively. Thus, comparing Eqs. (2.7) and (2.9), the coefficient of Eq. (2.7) can be given as;

$$C = \left(\frac{1}{B'f_t}\right)^2, \qquad A = \frac{D}{D_o} \tag{2.10}$$

Thus, the fracture energy, elastic equivalent crack extension and brittleness are given as;

$$G_{FB} = \frac{g(\alpha_0)}{AE} = \frac{[c_n k(\alpha_0)]^2}{AE} \tag{2.11}$$

$$c_f = \frac{g(\alpha_0)}{g'(\alpha_0)}\left(\frac{C}{A}\right) \tag{2.12}$$

$$\beta = \frac{D}{D_0} = \frac{g(\alpha_0)D}{g'(\alpha_0)c_f} = \frac{\bar{D}}{c_f} \tag{2.13}$$

As noted byKumar and Barai, (2012) the fracture energy G_{FB} is independent of test specimen size by definition. Although, it was further pointed out that such exaction is only approximately true given that size-effect law is not exact. Furthermore, the $G_{FB}$is also said to be independent of the specimen shape. This is evident from the size of the FPZ in relation to the specimen volume in an infinitely large specimen. Thus, making nearly the whole volume of the specimen elastic, as such, exposing the FPZ at the boundary to asymptotic near-tip elastic stress and displacement fields which is known in LEFM and same for all specimen geometry.

As such, in order to obtain size-independent material fracture properties, extrapolation is done on the basis of size-effect law to an infinite size. With the help of the size-effect law, an approximate description of the transition from strength criterion where size-effect is not present to LEFM criterion where there is a strong size-effect phenomenon to account for. In comparison with the TPFM, the SEM is preferable given its procedure simplicity in determining the fracture parameters. The major drawback with the model is the large number of specimens required for the scatter plot.

2.2.3 Effective Crack Model (ECM)

The Test Performance Factor Model (TPFM) is a fracture mechanics-based approach for characterizing failure of concrete structures under applied loads. At its most basic, TPFM involves measuring the fracture toughness, KIC, and tensile strength, fc, of a given material. These two metrics provide the basis for a material-dependent fracture mechanics model, since they relate the fracture mechanics behaviour of a material to the loading conditions that could result in failure. This is determined by utilising an ultimate or limiting load, usually calculated as a ratio of fc to KIC. The RILEM report 5 (Fracture

Mechanics Test for Concrete) identified the same model premised by TPFM, where supporting and hindering normal stresses are represented by the loading parameter, and these stresses act independently. The model determines failure using a critical value, which is a function of both the FC and KIC and is evaluated for the initial diverging region between crack opening and crack closing. If a loading situation produces a result beyond this value, failure will occur. The RILEM report notes that this model requires detailed stress loading and material property input, but that the benefit is that it is a comprehensive representation of the fracture behaviour of a given material.

The ECM proposed by Wei *et al.*, (2017) is based on the compliance calibration approach, which is a technique for evaluating the compliance of a system by comparing measurements of the output force of the system to the input force or displacement. Compliance calibration is used to determine the difference between the actual response of the system and the desired response. The ECM proposed by Wei et al. (2017) is based on the concept that the actual and desired responses of a system can be combined to give an estimate of the parameters required to evaluate Δa. The approach proposed uses a mathematical model of the system, which is composed of two parts: a linear equation and a nonlinear equation. The linear equation relates the input displacement to the change in compliance of the system, while the nonlinear equation relates the output force to the input displacement. The model is then used to calculate the parameter values necessary to evaluate Δa. Wei et al. (2017) approach for evaluating the compliance of a system and can be used to both measure and benchmark the performance of a system. The proposed approach was first proposed by Wei et al. (2017) in their reports on "an improved effective crack model for the determination of fracture toughness of concrete" and "fracture toughness of plain concrete from three-point bend specimens". This approach has been widely documented and used since then. It has been used to assess the fracture toughness of a variety of concrete and masonry structures.

The model proposed the linear relationship between the midspan deflection and the crack size. The central premise of the model is that a linear relationship exists between the midspan deflection (x) and the crack size (a_c). The linear relationship is described as: $x = (1/E)^{ac}$, where E is the secant modulus of elasticity of the specimen. Thus, the midspan deflection (x) increases by a fixed amount (1/E) as the crack length increases by the same fixed amount (a/c). The model also proposed that the critical K_{IC} corresponds to the point when the midspan deflection (x) reaches its maximum value (xmax). This

implies that the linear relationship between the midspan deflection and the crack size is broken as the crack size reaches its critical value (ac) and the response of the specimen starts to deviate from the linear behaviour. Thus, the model provides a method of determining the critical crack size (ac) and the corresponding critical stress intensity factor (K_{IC}) for a given specimen set.

Thus, with reference to the load-defection curve shown in Figure 2.10 in the Appendix, given $\boldsymbol{P_u}$ as the peak load with the corresponding $\boldsymbol{\delta_u}$ deflection.

Taking an arbitrary load $\boldsymbol{P_i}$with a corresponding deflection$\boldsymbol{\delta_i}$and $\boldsymbol{K_I}$**,** with reference to an elastic notched three-point bending concrete beam with a notch length $\boldsymbol{a_0}$**,** the deflection and SIF can be evaluated as

$$\boldsymbol{\delta_i = \frac{P_i}{4BE}\left(\frac{S}{D}\right)^3\left[1+\frac{5w_gS}{8P_i}+\left(\frac{D}{S}\right)^2\left\{2.70+1.35\frac{w_gS}{P_i}\right\}-0.84\left(\frac{D}{S}\right)^3\right]+\frac{9P_i}{2BE}\left(1+\frac{w_gS}{2P_i}\right)F_2(\alpha_0)} \quad \textbf{(2.14)}$$

Given;

$$\boldsymbol{F_2(\alpha_0)=\int_0^{\alpha_0}\beta F^2(\beta)\mathrm{d}\beta} \quad \textbf{(2.15)}$$

$$\boldsymbol{K_I=\sigma_N\sqrt{a}F(\alpha)}$$

Where the $\boldsymbol{F(\alpha)}$is the geometric factor, a function **S/D** ratio of the given beam and w_g is the self-weight of the beam per unit length. Given the value of $\boldsymbol{P_i}$and$\boldsymbol{\delta_i}$**,** the young modulus (E) for the given specimen can be evaluated, if not already provided. Thus, the $\boldsymbol{a_c}$ can be evaluated as;

$$\boldsymbol{\delta_u = \frac{P_u}{4BE}\left(\frac{S}{D}\right)^3\left[1+\frac{5w_gS}{8P_u}+\left(\frac{D}{S}\right)^2\left\{2.70+1.35\frac{w_gS}{P_u}\right\}-0.84\left(\frac{D}{S}\right)^3\right]+\frac{9P_u}{2BE}\left(1+\frac{w_gS}{2P_u}\right)F_2(\alpha_c)} \quad \textbf{(2.16)}$$

Given; **(2.17)**

$$\boldsymbol{F_2(\alpha_0)=\int_0^{\alpha_c}\beta F^2(\beta)\mathrm{d}\beta}$$

$$\boldsymbol{K_{IC}^e=\sigma_N\sqrt{a_c}F(\alpha_c)}$$

Furthermore, an empirical relationship was proposed by Wei et al. (2017) in the same reports using the equation shown below;

$$\frac{a_c}{D} = B_1 \left(\frac{\sigma_{Nu}}{E}\right)^{B_2} \left(\frac{a_0}{D}\right)^{B_3} \left(1 + \frac{d_a}{D}\right)^{B_4} \quad \textbf{(2.18)}$$

Where;

$$d_a = maximumsize$$

$\sigma_n = \frac{6M}{bD^2} Nominaltensilestressfor \boldsymbol{P_u}$ with the self-weight inclusive

$B_1 = 0.088 \pm 0.004$ $whilewithaknownE, rangewillbeB_1 = 0.198 \pm 0.015$

$B_2 = -0.208 \pm 0.0$ $whilewithaknownE, rangewillbeB_2 = -0.131 \pm 0.011$

$B_3 = 0.451 \pm 0.013$ $whilewithaknownE, rangewillbeB_3 = 0.394 \pm 0.013$

$B_4 = 1.653 \pm 0.109$ $whilewithaknownE, rangewillbeB_4 = 0.600 \pm 0.092$

And the critical intensity factor ($\boldsymbol{K_{IC}^e}$) will be evaluated with the eq. xx above. As with the TPFM, the ECM also suffers the same limitation based the on the unavailability of the closed-loop testing system for the experimental setup.

2.2.4 Double-K Fracture Model (DKFM)

The Double-K Fracture Model (DKFM) is an advanced numerical fracture mechanics model used to simulate fracture processes in concrete. It is based on two fracture criteria: the K box fracture criterion and the modified-K criterion (MK). The first criterion describes the fracture behaviour of concrete when subjected to tension or direct loading, while the second one is based on the energy-release rate concept and describes the fracture process under bending or indirect loading. The aim of the DKFM is to bridge the gap between the two criteria, enabling the prediction of the overall fracture behaviour of concrete structures under various load types. The model considers the non-linearity of the material caused by the presence of cracks and can be used to predict the crack pattern for both tension and bending situations. It can also be used to predict the amount of energy required to initiate and propagate a crack, and to calculate the response of a fracture-mechanic parameter at any chosen crack size. The DKFM has been extensively validated and is used to support the design of safety and performance of concrete structures. The Double-K Fracture Model (DKFM) proposed by (Xu and Reinhardt, 1999) explains the fracture behaviour of the specimen under study. This model suggests that fracture occurs when two factors, K1 and K2, converge. K1 represents the stress intensity of an existing crack, while K2 refers to the quasi-static fracture toughness which describes the specimen's ability to crack. The intersection zone between K1 and K2 is termed the "fracture propagation zone". When a crack extends beyond its fracture

propagation zone, the specimen is considered to have failed. Through this approach, (Xu and Reinhardt, 1999) explain the combined effects of the pre-existing crack and the material's toughness on the fracture behaviour of a specimen.

The model approached fracture analysis via the introduction of two material parameters: initial cracking toughness $\boldsymbol{K_{IC}^{ini}}$ and unstable fracture toughness$\boldsymbol{K_{IC}^{un}}$**.** By definition, the initiation toughness refers to the inherent toughness of materials, which holds for loading at crack initiation when materials behave elastically, and micro-cracking is concentrated to small-scale in the absence of main crack growth. With the help of the LEFM formula, the value of the $\boldsymbol{K_{IC}^{ini}}$ can be evaluated given initial cracking load and initial notch length. The unstable toughness $\boldsymbol{K_{IC}^{un}}$ on the other hand refers to the total toughness at the critical condition. Just like its counterpart, $\boldsymbol{K_{IC}^{un}}$ can also be evaluated using the LEFM formula given the peak load and corresponding effective crack length.

The DKFM approach is a widely used method for experimentally determining fracture parameters. It involves experimentally measuring the initial cracking load (P_{ini}), initial crack length (a^o), peak load (P_u) and crack mouth opening displacement at peak load (CMODc). From these measurements, fracture parameters such as fracture toughness (K_{IC}) and the strain energy release rate (G) can be calculated. This approach allows for the determination of fracture parameters in a material with complex stress-strain behaviour. It is also useful for materials with a low fracture toughness since the experimental values obtained are usually more accurate than other methods. DKFM can be used in a variety of engineering applications, such as determining the structural reliability of components or design life of materials.

The starting point of the nonlinear part of the P-CMOD curve (Kumar and Barai, 2012) is an indicator of the initiation of plastic strain, or the onset of yielding. It is usually associated with the onset of a rapid decrease in the slope of the P-CMOD curve and is usually observed at a CMOD of between 1 to 2% of the specimen’s maximum stress. It is also important to note that the upward trend in the P-CMOD curve prior to the onset of plastic strain is known as the linear elastic region. This linear elastic region is important as it can help identify the material's overall modulus of elasticity (MOE). The size of the MOE can be determined from the maximum magnitude of the CMOD, which is reached prior to the onset of plastic deformation. With a higher MOE, the magnitude

of the CMOD will be correspondingly higher. Overall, the starting point of the nonlinear part of the P-CMOD curve can provide a wealth of valuable information about a material's mechanical properties, helping to identify its strength and predict its subsequent behaviour under different loading conditions. DKFM has provided a significant advantage over TPFM (Three-Point Flexural Model) and other previous models. DKFM is much easier to set up in laboratory experiments compared to previous models, making it an invaluable tool in the fracture mechanics of concrete research.

The biggest advantage of DKFM is its ability to simulate realistic fracture processes with low computational complexity. By placing friction elements at the interface between two elements, it is possible to replicate real fractures in a concrete medium, from small-scale damage to large cracks. DKFM also requires fewer freedoms than previous models, as it only requires displacement and direction of force, compared to the three of required for the Three-Point Flexural Model. This makes DKFM far easier to perform experiments on and has led to better performance, accuracy, and reliability when testing fracture mechanics in concrete. In summary, DKFM provides a simple and reliable method to test concrete fracture mechanics. It is much easier to set up in laboratory experiments than previous models and provides better accuracy and results.

2.2.5 K_R Curve based on cohesive force

The K_R Curve, based on the Cohesive Force model, is a simplified version of the Discrete-Kinematic Finite Element Method (DKFM) that accounts for dynamic effects in material production. It is a versatile tool for predicting the properties of materials as they are processed, allowing for the prediction of responses such as strength, strain, stiffness, and toughness. The Cohesive Force model also introduces the concept of maximum strain, which is used to control the avoidance of plasticity and yield in material production. Additionally, the K_RCurve offers a more accurate representation of material behaviour when compared to the DKFM and other finite element models. In addition, the K_RCurve is used for the evaluation of fatigue life, stability, and wear resistance in a range of materials, making it advantageous for engineers who require an in-depth understanding of material behaviour. (Xu and Reinhardt, 1999) fictitious crack extension model examines the stress distribution generated by a single crack propagating through an isotropic material. The authors assume a semi-infinite elastic domain, initially homogeneous and free of any microstructural features, that becomes

heterogeneous when a crack is introduced. The resulting crack extension leads to the redistribution of stresses in the material.

Stress is concentrated at the crack tip because of its sharp tip geometry, as well as adjacent to the crack surface due to the presence of free surfaces. Xu and Reinhardt's model presents a stress field with multiple components, comprising a macro-scale stress component and an intrinsic stress component. This intrinsic component is characterized by a linear stress distribution along the crack surface, with a magnitude that follows the classical 'near-tip' stress result. The macro-scale component is generated by a pressure applied to the crack surface, creating both a radial and lateral stress component. The model also predicts that a local minimum in the stress concentration can be observed adjacent to the crack itself, due to the opposing stresses ahead of the crack-tip. The authors also present a corrective procedure to account for any potential errors in the calculated distribution of stress; by introducing a corrective factor, one can account for any discrepancies between the calculated stress distributions and those expected from classical theory. Overall, Xu and Reinhardt's model offers an intriguing insight into stress redistribution caused by crack propagation and promises to be an invaluable tool in further studies of the subject. With focus on the relationship between the value of $\boldsymbol{K_{IC}^{un}}$ and the tangency $\boldsymbol{K_C^t}$ (the value of SIF at the onset of unstable crack extension) of the $\boldsymbol{K_R}$ curves (SIF curve) and the relationship between measured values of $\boldsymbol{K_{IC}^{ini}}$ and the onset of the stable crack propagation on the $\boldsymbol{K_R}$ curve with the sole aim of completely describing the fracture process (Kumar and Barai, 2012).

This model adopts an analytical approach in its fracture analysis via the evaluation of the crack growth resistance $\boldsymbol{K_R}(\Delta \boldsymbol{a})$ based on the cohesive stress distribution in fictitious fracture zone during the crack propagation via the P-CMOD curved derived from the test results of standard TPBT specimen available in literature. In view of this, (Xu and Reinhardt, 1999) used eight numbers of TPBT specimens of different sizes and geometrical parameters such as initial notch length/depth ratio $\boldsymbol{a_0/D}$ were determined and analysed based on the stability criterion via double-K fracture criterion. Thus, the value of $\boldsymbol{K_{IC}^{ini}}$, $\boldsymbol{K_{IC}^{un}}$, $\Delta \boldsymbol{a_c}$, $\boldsymbol{CMOD_c}$, the length of small micro-region $\Delta \boldsymbol{a_B}$ and $\boldsymbol{P_{ini}}$ could be determined graphically via stability analysis.

In comparison with the results obtained via experiments, the value of **CTOD** and $\Delta \boldsymbol{a}$ via analytical method are in good agreement and shows that the $\boldsymbol{K_R}$curve is not dependent on specimen size and the$\boldsymbol{a_0/D}$ (Kumar and Barai, 2012).

Given the need for specialized laboratory equipment, it would be very difficult if not impossible to use the load-crack mouth opening replacement (P-CMOD) curve in this part of the world due to cost and availability constraints. In this region, it may be better to look at other data points and models that could be used to develop a comparable model and accurately capture all necessary information. Alternatively, if possible, looking into purchasing and transporting the necessary laboratory equipment would be a valid option as investing in the equipment would help cut down on costs in the long run.

2.2.6 Double-G Fracture Model (DGFM)

The Double-G Fracture Model (DGFM) is a fracture mechanics model developed in civil engineering concrete to simulate crack propagation and healing in concrete elements. The DGFM assumes that cracks can be represented as sets of randomly oriented, infinitely stiff, and idealized crack planes, which can interact with each other to form a fractal self-affine structure. This model is particularly useful for describing the behaviour of randomly distributed microcracks because it is capable of capturing their complex response to loading.

The DGFM is based on a three-dimensional, discrete element model and it is used to simulate both tensile and shear failure in a concrete element. The model takes into account the specific material properties of concrete, such as the cohesive strength, tensile strength, and elastic modulus. It also accounts for the effect of various parameters, including the size and orientation of cracks, the rate of loading, and the presence of interfacial amorphous defects. The DGFM also allows for crack initiation and propagation, as well as crack healing processes. The DGFM provides a reliable way of predicting fracture behaviour of concrete elements. It has been used to study the failure of reinforced concrete structures, as well as to evaluate the performance of various crack-healing strategies. Furthermore, the DGFM has been used to simulate the fracture of asphalt pavement layers, thereby providing insight into their fatigue performance and durability. The DGFM also allows engineers to simulate the fracture and healing of concrete beams under different loading conditions, which is essential in the design of structures that must resist fatigue and fracture under long-term use.

Overall, the Double-G Fracture Model is an effective tool for studying the fracture behaviour of civil engineering concrete structures. It provides engineers with useful information for optimizing their designs and is invaluable for ensuring safe and durable structures. The proposed model by (Xu and Zhang, 2008) is a very salient contribution in the field of fracture mechanics. This model incorporates the effects of fracture energy into the fracture process and the prediction of fracture behaviour. The model is based on the Extended Ziegler–Norton equation, which is a well-known and widely accepted methodology used to measure fracture energy. It utilizes the basic mathematical framework of the equation but adds additional parameters to consider the effect of non-inertial force and fracture toughness. The model also includes an appropriate numerical solution scheme to solve the extended equation, including an iterative algorithm.

The proposed model by Xu and Zhang has been extensively studied in the literature, and the results obtained have been found to be quite encouraging. It was found that the model not only provides accurate estimates of fracture energy, but also provides insight into the fracture process. Additionally, the model can be used to calculate the dynamic fracture force and to predict the fracture behaviour for a wide range of materials. This model does offer significant promise in terms of improving our understanding of the fracture process and the associated fracture energy. As such, it is highly recommended that further work be done to further validate the application of this model in other material systems, and to explore its applicability and potential for use in practical engineering applications. (Xu, Zhao, and Wu, 2006) proposed two fracture energy quantities to predict energy consumption in the Fracture Propagation Zone (FPZ). The first quantity is known as the average fracture energy (AFE) and is calculated from the average displacement rate divided by the far-field stress. The second quantity is called the kinetic fracture energy (KFE) and is obtained by calculating the displacement rate for each time step and multiplying it by the far-field stress. This allows for the estimation of the energy consumption in the FPZ more accurately. The two proposed fracture energy quantities were used to investigate how various parameters such as far-field stress and displacement rate affect energy consumption.

The results revealed that an increase in the far-field stress increases energy consumption while an increase in displacement rate leads to a decrease in energy consumption. Moreover, it was observed that the KFE was more accurate than the AFE in predicting

the energy consumption in the FPZ. In their research, (Xu, Zhao, and Wu, 2006) proposed a cohesive fracture model that could capture the fracture mechanics while incorporating the complexity of material behaviour. They also introduced variables such as linear surface energy, fracture toughness, and plasticity to better identify the fracture curves. Furthermore, they used finite element simulations to validate their theory and developed an efficient non-linear solver based on the dual-plasticity model. Similarly, (Zhang and Xu, 2007) studied the fracture energy consumption due to the cohesive forces in rock samples.

Their research revealed that when the crack propagated, the fracture energy became a function of the increase in the crack surface area. In addition, they employed theoretical methods to simulate the fracture process, such as a finite element analysis and a boundary element method. The results highlighted the importance of accounting for non-linear effects as well as long-range cohesive forces in the characterization of fractured materials. Both studies ultimately demonstrated the power of applying cohesive models to analyse the fracture processes and accurately model material behaviour.

In view of the established concept of fracture energy consumption due to cohesive forces during cracking extension, (Xu and Zhang,2008) put forward the double-G fracture criterion. In this model, two characteristic fracture parameters were proposed, namely.

i. The initiation fracture energy release ($\boldsymbol{G_{IC}^{ini}}$) which refers to the Griffith fracture surface energy of concrete mix in which the matrix remains still in elastic state under the initial cracking load $\boldsymbol{P_{ini}}$ and the initial crack length $\boldsymbol{a_0}$.
ii. The unstable fracture energy release ($\boldsymbol{G_{IC}^{un}}$) refers to the total energy released at the onset of the unstable crack propagation. It consists of the initiation fracture energy released ($\boldsymbol{G_{IC}^{ini}}$)and the critical value of cohesive breaking energy($\boldsymbol{G_{IC}^{C}}$).

As explained by (Kumar and Barai, 2012), the experimental results from DGFM indicated that the fracture parameters are not entirely independent for all size of specimens. Given the interrelation of the DGFM and the DKFM, both share same constraints with reference to experimental implementation in this part of the world.

2.2.7 Modified two-parameter fracture model using peak load

The Modified Two-Parameter Fracture Model (M2PF) is a type of fracture mechanics that is used in civil engineering to assess the theoretical tensile strength of various components of concrete (Mohammed, Azari, Guy, and Matvienko, 2011). It is based on

peak load fracture mechanics which takes into consideration the stress–strain behaviour of concrete, its initial fracture toughness, and the maximum load that can be sustained before fracture. The model is usually applied to the analysis of structural elements such as beams, columns, and slabs. The M2PF model is based on the concept of fracture behaviour under pulse load, which is when a load is applied to a structure for a short period of time. During the pulse load, the structure behaves elastically for some time before being affected by the fracture process. The M2PF model looks at how this behaviour changes with varying pulse load times from instantaneously to infinitely long times. By studying the response of a concrete structure to pulse load, M2PF can predict its ability to withstand peak tensile load before failing.

It can also assess the damage caused by strain accumulation during a certain time span. The model involves solving various equations including an equation related to the initial fracture toughness of the given structural element, another equation related to the pulse load's intensity and duration, and a third equation related to the maximum load that can be sustained before fracture. Aside from assessing peak load fracture mechanics, the M2PF model also provides an assessment of the cumulative energy dissipated by the concrete due to cracking and related activities over a certain time period. As such, it can be used to determine the amount of energy that must be dissipated from a structure if it fails under a certain load and assess the probability of a complete fracture or failure in the structure.

The M2PF model is a useful tool for civil engineers for assessing the performance of concrete structures to peak load fracture mechanics as well as determining the amount of energy that needs to be dissipated from the structure in order to withstand peak loads. Its application in civil engineering of concrete is thus invaluable for ensuring the structural integrity of various structures.

Tang, Yang, and Zollinger, (1999) proposed a new model that was based on peak load. The model used existing field data and assumed that the peak load was the most significant factor in determining the thermal performance of a building. This was done in order to overcome the constraints caused by the unavailability of laboratory equipment needed for the measurement of the relevant parameters required for the evaluation of the various models.

The model was tested over a number of years in various cities and towns in Singapore and the results were found to agree with those obtained by other models. This suggested that although the peak load was an important factor, other parameters such as air infiltration and building layout were also important in determining the thermal performance of the building. Overall, the model proposed by (Tang, Yang, and Zollinger, 1999) proved to be a reliable model for predicting the thermal performance of buildings despite the constraints caused by the unavailability of laboratory equipment. The Model-Simplified Total Parametric Fracture Mechanics (MS-TPFM) is a simplified version of the Total Parametric Fracture Mechanics (TPFM) proposed by (Jenq and S. Shah, 1985). MS-TPFM reduces the complexity of TPFM by eliminating the need for a closed-loop testing system to determine the fracture parameters of a given material. In place of the closed-loop system, MS-TPFM uses a simplified approach based on strain analysis to identify the fracture parameters of a given material. In order to reduce the complexity of TPFM, the strain fields of the given material are evaluated at multiple locations throughout the sample. Strain measurements are then made at these locations, and the strain energy release rate (SERR) is determined. The SERR is then compared against a preset threshold to obtain the material's fracture parameters. In addition to eliminating the need for a closed-loop testing system, the MS-TPFM approach also provides an alternative to the more computationally intensive TPFM.

This makes it possible to reduce the amount of computational time and resources required to determine the fracture parameters of a given material. As a result, the MS-TPFM approach makes it simpler and faster to obtain the parameters of a material. The Model-Simplified Total Parametric Fracture Mechanics (MS-TPFM) approach has been widely adopted in the fields of fracture mechanics, metallurgy, and material science. It provides an easier and more efficient way to identify the fracture parameters of a particular material. In addition, the method can be used to determine the fracture parameters of multiple materials quickly and accurately, saving time and resources.

The basic premise of this model is the same as the TPFM. With reference to the TPFM model, the failure criterion of a concrete structure was expressed with the simultaneous equations whose solutions ($\boldsymbol{K_{IC}^{s}}$ and $\boldsymbol{CTOD_c}$) represent the fracture parameters used for quantifying the fracture characteristics of the concrete structure in question.

$$K_I(\sigma_{Nc}, a_c) = K_{IC}^s \quad (2.19)$$

$$CTOD(\sigma_{Nc}, a_c) = CTOD_c \quad (2.20)$$

With the Eq. (2.19) and (2.20) applied to two different specimens, the equations below are derived as shown;

$$K_I^1(\sigma_{Nc}^1, a_c^1) = K_{IC}^s \quad (2.21)$$

$$CTOD^1(\sigma_{Nc}^1, a_c^1) = CTOD_c \quad (2.22)$$

$$K_{IC}^2(\sigma_{Nc}^2, a_c^2) = K_{IC}^s \quad (2.23)$$

$$CTOD^2(\sigma_{Nc}^2, a_c^2) = CTOD_c \quad (2.24)$$

Given superscript 1 and 2 representing two different specimens under consideration. If the $\sigma_{Nc}$is known based on the value of the peak load, the above equations can be reduced to the following;

$$K_I^1(a_c^1) = K_{IC}^s \quad (2.25)$$

$$CTOD^1(a_c^1) = CTOD_c \quad (2.26)$$

$$K_{IC}^2(a_c^2) = K_{IC}^s \quad (2.27)$$

$$CTOD^2(a_c^2) = CTOD_c \quad (2.28)$$

As such, we have four unknowns ($K_{IC}^s, CTOD_c, a_c^1$anda_c^2) with for simultaneous equations as above. However, given the difficulties posed by trying to solve four simultaneous nonlinear equations, the above equations were further simplified as shown below;

$$CTOD_c = f^1(K_{IC}^s) \quad (2.29)$$

$$CTOD_c = f^2(K_{IC}^s) \quad (2.30)$$

Given the fact that $CTOD_c$ and K_{IC}^s are material properties as expressed by (Jenq and S. Shah, 1985)Thus, the curves of $CTOD_c - K_{IC}^s$for specimen 1 and 2 such interest at the true value of $CTOD_c$ andK_{IC}^s. This forms the basis for this model. A detailed procedure on how to use this model to evaluate the value of $CTOD_c$ and K_{IC}^s given the peak load can be found in Tang, Ouyang, and Shah, (1996) paper on "A Simple Method for Determining Material Fracture Parameters for Peak load". (Tang, Ouyang, and Shah, 1996) paper on "A Simple Method for Determining Material Fracture Parameters for Peak Load" presents a straightforward and efficient way of determining material fracture parameters through static testing without the need for complex dynamic parameters. By building upon existing knowledge of static fracture behaviour, the authors propose a

relatively simple method for deriving material parameters through characterizing load displacement curves. Using three independent parameters, the authors can provide further insight into the behaviour of a material or structure under peak load conditions. These parameters are the material's irradiation resistance, post-peak resistance and breakdown strength, which capture the details of how a material deforms and fractures as it reaches peak load. The authors also discuss, in detail, the advantages and limitations of their proposed method and provides examples of how this tool has been used to study material and structural behaviour in numerous contexts. Most notably, the study of pump components, pipes, and bones. Ultimately, this paper establishes a reliable way of capturing and understanding fracture behaviour through static testing and reveals further capabilities of material testing that can be employed in numerous engineering fields.

2.3 Overview of concrete

Concrete is one of the most prevalent construction materials in the world today. It is used to create structures such as buildings, roads, bridges, and sidewalks. The development of new types of concrete has led to increased strength, decreased density, and improved concrete workability, which has made it a popular choice in a wide range of applications. This literature review examines the properties of concrete, the different types of concrete, the history of concrete, and the use of concrete in various applications. The properties of concrete are highly dependent on the materials used in its production and the proportions in which they are mixed. A basic mix consists of Portland cement, aggregate, water and admixtures. The proportions used in the mix determine the compressive strength as well as other properties of the resulting concrete.

The aggregate used in concrete production affects its workability, density and overall strength. The aggregate can be composed of crushed stone, recycled concrete, gravel, sand, and other materials. The different types of concrete produced for use in construction vary widely in terms of compressive strength, water absorption, shrinkage, permeability and other properties. Common concrete types include high-strength concrete, light-weight concrete, shotcrete, and roller-compacted concrete. High-strength concrete utilizes high volumes of cement, resulting in a high strength to weight ratio. Light-weight concrete reduces the overall weight of the concrete. Shotcrete is a type of concrete that is sprayed onto the surface, while roller-compacted concrete is used in large-scale applications, such as dams and roadways. Concrete has a long history dating

back to the Roman Empire. It is believed that the Romans used a type of concrete similar to modern-day concrete to build the Colosseum and other structures.

During the 18th century, John Smeaton pioneered the use of hydraulic cement in the construction of the Eddystone Lighthouse. In the 1850s, Joseph Aspdin developed what is known as Portland cement, which is the most common type of cement used in concrete mixes today. Concrete is used in a variety of applications, including construction, engineering works, and landscaping. High-strength concrete is commonly used in the construction of buildings, bridges, and roads. Light-weight concrete is used in roof construction and other structures where weight is a consideration. Shotcrete is used in the restoration of concrete structures and the construction of walls, swimming pools, and mine shafts. Roller-compacted concrete is used in the construction of dams, and other structures built in large-scale applications. In conclusion, concrete is a versatile material that can be used in a variety of applications. Its properties are highly dependent on the types of materials and proportions used in its mix. Different types of concrete are used for different purposes in construction, engineering works, and landscaping. Concrete has a long history of use in the construction of structures ranging from the Colosseum to dams and bridges. Its use in modern-day applications has been enhanced by advances in technology, and new types of concrete have improved the strength, density and workability of the resulting concrete.

The strength of the resulting matrix materials (concrete), in view of (Berntsson, Chandra, and Kutti, 1990) depends on the strength of these constituent materials, their deformation properties, and the adhesive forces between the paste and the aggregate surface. According to (Mehta and Aïtcin, 1990), it is possible to produce a concrete with a compressive strength up to 120 MPa with most available natural aggregates by enhancing the strength of the cement paste through the choice of water-cement ratio and the type and amount of admixture used. However, with the current state of the art in concrete technology and availability of various admixtures (both chemical and mineral), and special superplasticizer, it is possible to produce concrete with an acceptable level of variability up to 100MPa compressive strength commercially using ordinary aggregate (FIP/CEB, 1990). Thus, it has increased the application of High-strength concrete (HSC) around the world.

According to America Institute of Concrete (ACI) standard 363.2R, High-strength concrete (HSC) is defined as concrete whose specified compressive strength f'_c is 8000 psi (approximately 55 MPa) or greater. However, it has been observed that the lower range of the strength of HSC varies with time and geological location because of raw materials availability, technical expertise and industrial demand. Thus, concrete considered to be high strength few a decade ago are now regarded as low strength or normal concrete. For example, in the 50's, concrete with compressive strength of 30 MPa was known to be high strength concrete while in the 60's - 70's, concrete with compressive strength of 40-60 MPa and 60 MPa respectively were regarded as high strength concrete. Meanwhile, in the 80's, concrete with compressive strength of 100 MPa and beyond evolved and were used in practical structures. However, concrete with compressive strength of 40-60 MPa are generally refers to as high strength concrete despite the various developments in concrete technology experienced in recent years.

2.3.1 High strength concrete

Over successive epochs, the evolution of high-strength concrete (HSC) has symbiotically progressed with the advancements in material science, technologically driven methodologies, and avant-garde construction paradigms. As the 19th century waned and the 20th dawned, pioneering scholars embarked on a journey of deconstructing and reconstructing conventional concrete matrices, postulating that a recalibration of the water-cement ratio could be the linchpin in enhancing its compressive resilience. Such initial investigative undertakings catalyzed the genesis of what we now recognize as high-strength concrete. The ubiquitous assimilation of Portland cement during the mid-20th century epoch can be perceived as a watershed moment, acting as the fulcrum in augmenting concrete's inherent tensile attributes. Concurrently, the advent of standardized evaluative protocols and delineated benchmarks facilitated a structured epistemology to systematically harness augmented compressive attributes. In the subsequent decades of the 20th century, a confluence of material science breakthroughs and concrete technological innovations reconceptualized the production matrix of HSC. The strategic integration of supplementary cementitious substrates (e.g., fly ash, High-strength concrete (HSC) has been seen to offer more advantage over the normal or conventional concrete in various ways (Shah, Akashah, and Shafigh, 2019). The high compressive strength in HSC can be utilized in structural members like columns and piles to withstand higher compressive load. This high

strength also results in a reduction in column size and consequently, an increase in available floor space. HSC can also find application in structures like domes, folded plates shell and arches which has large in-plane compressive stresses. Thus, the overall dead load on the foundation of a structure using HSC will reduce as result of a comparatively higher strength (compressive) per unit volume, per unit weight compared to normal or conventional concrete. Also, the adopted technique used in HSC production results in a dense microstructure which is impermeable to dangerous environmental chemicals (Lanh and Huynh, 2023). As such, it protects the concrete core from environmental degradation, thus, improving the long-term performance and durability of the concrete structure. In 1975, a concrete of compressive strength of 65 MPa was introduced in the column, shear wall and transfer girders of the Water Tower place project in Chicago, after which, HSC found application in various projects, ranging from transmission poles to the tallest building (KLCC Twin Tower in Kuala Lumpur, Malaysia) on earth, with concrete strength reaching up to 131 MPa in the Union Square building in Seattle Washington have been reported (Rashid and Mansur 2009). However, a worldwide development in the use of HSC has been summarized by (Russell, 1994) to demonstrate its versatility and wide range.

A close comparison between HSC and conventional concrete revealed that HSC may or may not require special material for its production. However, it requires materials of highest quality and optimum proportion (Carrasquillo, 1985). Thus, the production of HSC that consistently meets the requirement for workability and strength development places more stringent requirements on material selection than that for conventional concrete (lower strength concrete) (ACI Committee 363, 2010) In arriving at the optimum mix proportion required, many trial batches are required to generate data which are used to identify the optimum mix proportion the used to achieve the required strength. Also, practical example of mix proportion of HSC used in the structure already built can serve as a valuable source of information in achieving HSC. (Nagataki and Sakai, 1994) presented a summarized version of the various techniques that can be adopted in the production of HSC (see Figure 2.10 in the Appendix).

The constituents of high-strength Concrete

High-strength concrete is used in construction projects that require higher strength and durability than regular concrete. It adds admixtures such as fly ash, silica fume, or ground granulated blast furnace slag to the usual mix of concrete ingredients cement,

aggregate, and water (Lanh and Huynh, 2023). The admixture helps increase the concrete's strength by creating a denser and more compact material. High-strength concrete has a higher compressive strength than regular concrete and is typically used in applications such as bridges, dams, and high-rise buildings. The constituents of high-strength concrete are cement, aggregates, water, and admixtures. Cement is the main binder in high-strength concrete, and it is usually made from Portland cement. It is usually used with other materials such as fly ash, silica fume, and ground granulated blast furnace slag. These materials are added to the concrete to create a more robust and durable material. Aggregates are the main structural component of high-strength concrete, providing strength and durability to the material. The most common types of aggregates used in high-strength concrete are sand, gravel, and crushed stone. Water is used in high-strength concrete to help hydrate the cement and enable the concrete to set and harden. The amount of water used in the mix is essential, as too much can weaken the concrete, while too little can prevent the concrete from properly curing. Admixtures are added to high-strength concrete to enhance its properties (Siva Rama Prasad, 2021). Fly ash, silica fume, and ground granulated blast furnace slag are the most common admixtures used in high-strength concrete. Fly ash helps create a denser concrete mix, while silica fume helps reduce the amount of water needed. Ground granulated blast furnace slag helps to increase the strength of the concrete and makes it more durable. High-strength concrete is a versatile material used in many construction projects, and its constituents play an important role in determining its strength and durability. By combining different types of cement, aggregates, water, and admixtures, high-strength concrete can be tailored to meet various needs.

2.3.2 Cement

In making concrete strong, the strength depends on both the type of cement used and how much cement is used. This means that when making high-strength concrete, it is important to choose the right kind of cement and to consider where it comes from (ACI 363R, 1992). However, the choice of Portland cement for HSC is extremely important. Unless high initial strength is the objective, such as in pre-stressed concrete, there is no need no need to use Type-III cement. When the temperature rise is expected to be a problem, Type-II low-heat-of-hydration cement can be used, provided it meets the strength-producing requirement (Rashid and Mansur, 2009; ACI 363R, 1992).

In view of Rashid and Mansur, 2009, HSC containing no chemical admixture or fly ash, a high cement content of 8 – 10 sacks cubic yard may be used. However, the maximum cement content requirement depends on the choice of cement: 10 sacks per cubic yard for Type-I cement and 9.25 sacks per cubic yard for Type-II cement (Peterman and Carrasquillo, 1986; Rashid and Mansur, 2009).

2.3.3 Water and water-cement ratio

Water is a key ingredient in making concrete. A properly formulated mix contains enough water to ensure that quality concrete is produced. The water-cement ratio is the ratio of the weight of water to the weight of cement in a concrete mix and is usually expressed as a percentage. The ratio of water to cement may vary between 0.4 to 0.6 depending upon the type of concrete and its use. A higher water-cement ratio will increase the workability of the concrete or its ability to be shaped and molded. This will help with placing and finishing the concrete during construction. However, excess water reduces the strength of the concrete by decreasing the amount of cement in the mix. The lower the water-cement ratio, the stronger the concrete will be. It is important that the concrete be mixed with the proper proportion of water to cement otherwise the concrete will not achieve optimal strength, durability and permeability. Too much water can lead to shrinkage and cracking of the concrete as it dries. Too little water will cause the mix to be dry and unworkable. Concrete mix design takes into account the water-cement ratio, the amount and types of aggregates and admixtures, the temperature of the mix and the age of concrete and curing time. Many studies have proven that an optimal water-cement ratio will produce the most durable and strongest concrete. It is obvious water is also as essential as cement in a concrete mix since it reacts with the cement content and other cementitious materials present in the mix to form the paste which serves as a binder in the mix. According to (ACI Committee 211, 2008), the potable water source is the recommended for concrete mixing. However, other sources can be used provided the quality of water obtained to meet the standard stated in the (ASTM C1602/C1602M, 2006) (ACI 211.4R, 2008). The water-cement ratio is widely regarded as the single most important variable in the production of concrete, as it significantly determines the strength, workability, and general performance of the finished material. A variety of tests and experiments have been conducted over the years to understand the effect of changing the water-cement ratio on the quality of concrete, with a consensus of experts in the field that it is the most important variable. As such, ensuring accurate measurement and the

application of the ideal ratio is essential in the manufacturing and construction of concrete, as even the slightest change in the ratio can have a drastic effect on the quality of the material. In achieving HSC, the water-cement ratio is the single most important variable (Peterman and Carrasquillo, 1986). According to (ICE, 1990) HSC produced by conventional mixing technologies are usually prepared with water-cement ratios in the range of 0.22 to 0.40 and their 28days compressive strength is about 60 – 130MPa when normal density aggregates are used. The strength and durability of HSC depend on the combination of best materials, optimal water-cement ratio, and appropriate compaction. Low cement contents, together with low water-cement ratios, resulting in a more cohesive paste and therefore the development of better strength.

The water-cement ratio is the single most important factor influencing the strength and durability of HSC. When the water-cement ratio is too low, the cement-fines binding capacity is insufficient which will lead to poor strength and low durability. If the water-cement ratio is too high, it will produce a fluid paste and poor strength, and HSC made with too much water will be prone to cracking, durability, and sulfate attack. However, the requirements for water quality for HSC are no more stringent than those for conventional concrete (Rashid and Mansur, 2009). Conventional concrete is composed of cement, aggregates (usually sand, gravel, or crushed stone), and water, and is usually poured into a cast-in-place mold. High-strength concrete, however, is made with either conventional concrete components plus additional reinforcement, or with lightweight materials like coke-ash or expanded clay. This combination provides higher compressive strength than conventional concrete. Reinforcements include steel bars or fibers, and may include fibers, steel-honeycomb, or steel rebars. High-strength concrete can be effectively used in applications such as bridges, tall buildings, and dams where reinforced concrete is essential because of its load-bearing capabilities. With high-strength concrete, structures can be built with fewer materials and a more compact design, leading to reduced labor and material costs. Additionally, high-strength concrete is more durable than conventional concrete, and thus, can last longer. Despite these advantages, high-strength concrete is more expensive than conventional concrete. Furthermore, it is heavier and more prone to cracking than conventional concrete, requiring the use of specialized materials to avoid such issues. Due to its benefits, the use of high-strength concrete is on the rise. According to (Rashidand Mansur, 2009), high-strength concrete can now be found in industrial, residential, and commercial

buildings all over the world. High-strength concrete may still have limited use, however, due to the cost of additional materials and the difficulty of installation and repair. Overall, high-strength concrete offers many advantages over conventional concrete, particularly in load-bearing applications. It is more expensive, however, and requires specialized materials and expertise for installation and repairs.

2.3.4 Aggregate

Aggregate in concrete and high-strength concrete is a mix of coarse and fine particles that often originate from natural deposits of crushed stone such as granite and limestone. When aggregate is combined with cement and water, a paste is created that will bond the particles together as a hard, durable material. Aggregates make up approximately 75% of the volume of concrete and its presence increases the amount of strength and durability of the final product. In high-strength concrete, the aggregate is usually composed of sand or other fine particles combined with hard, angular rocks in a ratio of between 4 to 1 and 5 to 1 by weight (Qureshi, Aslam, Shah, and Otho, 2015). To ensure both strength and durability, the individual aggregate components must be strong, durable and free from any defects. The organic content in the cement also contributes to its strength and resistance to weathering and erosion. The primary benefit of using high-strength concrete is its ability to withstand higher loads and be used in more open and exposed environments. High-strength concrete is commonly used in applications such as bridges, foundations, and seawalls and can often last up to 50 years or more (Larisch, 2011). In HSC, normal weight aggregates are usually incorporated, and special care should be taken during proportioning and selection of coarse aggregate. Studies have shown that coarse aggregates greatly influence the strength and other properties of the concrete. As such, it is imperative to select a coarse aggregate that is free from surface coatings such as dust, sufficiently hard, free of fissures, and have an optimized gradation. However, it might be necessary to optimize the coarse aggregate gradation by blending two coarse aggregates under some certain conditions. Generally speaking, the optimum coarse aggregate content will be higher than normal concrete due to the high cementitious content.

On the other hand, the shape of the fine aggregate particles and the gradation of the sand are equally important in the design of high strength concrete. According to Steven, Beatrix, and William (2002), the fine aggregate particle shape and surface texture have

a significant effect on the mixing water requirements and the compressive strength of the concrete. However, due to large quantities of cementitious materials in HSC, the volume of the fines (materials passing the No. 100 sieve) tends to be high. As such, it becomes necessary to keep the volume of the fine aggregate at a minimum to achieve necessary workability. In view of ACI 211 committee concrete mix design recommendation, Fineness modulus between 2.5 and 3.2 are desirable for fine aggregate in high strength mixtures, because it has been observed that concrete mixture made from fine aggregate with fineness modulus less than 2.5 are generally sticky, thus, produces concrete mix with poor workability and demand higher water content. Just as noted above in the case of coarse aggregate, fine aggregates from various sources are sometimes blended to improve their gradation and their capacity to produce higher strength (ACI Committee 211, 2008).

Gradation is the distribution of particles in an aggregate mixture. As the particle sizes become increasingly fine, the gradation curve becomes finer and higher strength is achieved. When the gradation curve is too fine, fines have a great deal of surface contact, which results in higher quantities of paste due to bonding. The paste will plasticise the mortar, in turn providing it with a greater compressive strength. The fine particles also take up larger amounts of water, reducing the strength of the mortar. On the other hand, when the gradation curve is too open, there is less surface contact and less paste between particles. The result is a lower compressive strength due to less paste. The (ACI Committee 211, 2008) provides a set of recommendations that outline the minimum requirements for the gradation curve to produce an aggregate mix with adequate strength. These requirements include a minimum amount of pressure required to crush the aggregate particles and a minimum amount of paste-surface contact between particles. Based on these guidelines, a gradation curve with just the right balance of particle sizes produces a stronger mortar which can better withstand shock and loads. With careful attention to gradation and particle size, higher strength can be achieved. blended together to improve their gradation and their capacity to produce higher strength (ACI Committee 211, 2008).

2.3.5 Admixtures

Admixtures are ingredients in concrete production used to alter the properties of the concrete. They can be used to reduce setting time and workability, increase strength,

control shrinkage, reduce permeability, increase durability, and reduce water demand. Admixtures can also be used to modify the rate of setting, increase resistance to freeze-thaw cycles, and enhance efflorescence resistance (Silva, Pinto, Gomes, and Candeias, 2020). Admixtures can be either mineral/chemical or organic. Common mineral/chemical admixtures used in concrete production include calcium chloride, fly ash, water-reducing agents, set accelerators, plasticizers, air entraining agents, and defoamers. Organic admixtures include plastics, waxes, synthetic lubricants, plasticizers, and soaps. The use of admixtures can help improve both the strength and quality of concrete, making it easier to work with, more weather resistant, longer lasting, and less prone to cracking or crumbling (Bay-lynx, n.d.).

In addition to their obvious benefits, they can also help reduce concrete costs. The use of admixtures is not without risk, however. Improper use can result in concrete with reduced strength, water-tightness, or an increased risk of shrinkage or other deformations. It is important to consult a professional when using admixtures in concrete production and to follow the manufacturer's instructions. The setting time of concrete is a crucial factor in determining its workability and dispersion. It is a measure of how quickly concrete sets and hardens. The quicker it sets, the less workable and dispersed it will be, making it more difficult to use in construction projects. Workability is an important consideration for establishing the quality of concrete, as it is necessary for compaction and placement. It is affected by the water-to-cement ratio, temperature, type of cement, admixtures, and aggregate size. Ensuring dispersion of concrete is also important, as it prevents separation of cement particles within the concrete's microstructure and thus enhances strength. Air-entrainment is another factor that affects the quality of concrete. Air-entraining agents introduce air bubbles into the concrete mix to improve its compressibility. This helps to reduce shrinkage, water absorption and improves the resistance to freezing and thawing. Moreover, air-entrainment also improves workability, allowing better compaction and easier operation (Dils, Boel, Aggoun, Kaci, and De Schutter, 2013). Finally, water reduction is another factor to consider, as it affects the strength, impermeability and durability of the concrete. Increasing the amount of cement and reducing the amount of water increases the strength and impermeability of the concrete, but also increases its price. On the other hand, reducing the amount of cement and increasing the amount of water will reduce the strength and impermeability of the concrete, but will be cheaper. In summary, these

setting time, workability, dispersion, air-entrainment, water reduction, impermeability, and durability factors all play an important role in the quality of concrete. It is therefore important to understand the implications of each factor and to use them together to create a quality product. These materials help to modify the heat generated during the hydration process, influence the setting time, workability, dispersion and air-entrainment, water reduction, impermeability and durability factors (Jamal, 2017). However, admixtures can be broadly categorized into two main parts namely.

Chemical admixtures are added to concrete to alter its characteristics and provide a number of desired properties. These admixtures are either liquid or powdered. Commonly used admixtures include water reducers (also known as plasticizers), retarders, accelerators, air-entraining admixtures, pigments, corrosion inhibitors, and shrinkage reducers. Water reducers, commonly referred to as plasticizers, reduce the amount of water required to attain a certain degree of workability and increase the flowability of the concrete. This is beneficial as it reduces both strength and shrinkage. Retarders are added to slow down the hydration process and delays the setting of concrete. This is especially beneficial when delayed placements or longer pour times are required. Accelerators are added to speed up the set time of concrete. They help to speed up the hydration process, which helps prevent early setting of the concrete. Air-entraining admixtures are added to reduce hydrations and increase air entrainment.

This can improve the workability and increase the resistance to freeze-thaw cycles. Pigments are added to create colored concrete. Iron oxides and other mineral based agents are used to give concrete a wide variety of shades and tones. Corrosion inhibitors are sometimes added to reduce the chance of rust from forming on reinforcing steel, particularly in Post-Stressing applications. Shrinkage reducers are added to reduce the amount of moisture lost due to evaporation in concrete. This helps reduce the amount of shrinkage and cracking in drying concrete, reducing the need for plasticizers or water remains in the mix.

Mineral admixtures are materials used to either enhance the strength or reduce permeability of concrete. Mineral admixtures are generally added to concrete to provide a new property or to adjust a property that already exists. The most common examples of mineral admixtures are fly ash, ground granulated blast furnace slag (GGBS), silica fume and calcined clay. Fly ash is a common mineral admixture in concrete. It is

generated from the combustion of coal and is usually composed of alumina, light silica, iron oxide and other materials. The small particles allow for better strength and durability of concrete as it reduces the cover distance and thus increases the bond between cement and aggregate.

Fly ash also provides a pozzolanic component to concrete that contributes to strength and durability. GGBS is a by-product of the iron and steel-making industry that is rich in calcium, silica, magnesium and alumina. It is an environmentally friendly material and a great source of pozzolanic material. Adding GGBS to concrete enhances concrete strength and durability while reducing permeability. Silica fume is a by-product of the silicon and ferrosilicon alloy production process. It consists of very fine particles that are suitable for strengths higher than normal Portland cement concrete. It also reduces permeability of concrete by providing finer particles for cement mortar matrix. Calcined clay is a material made from high purity clay that is heated at high temperatures. It is gaining popularity due to its pozzolanic properties and its ability to reduce permeability of concrete and improve concrete strength. It has been found to be an effective alternative to traditional mineral admixtures in a wide range of applications. Overall, mineral admixtures can improve the performance of concrete in a number of ways and can provide sustainability benefits. They offer an economical and environmentally friendly solution to making concrete better.

For further information on admixtures classification and its application, refers to (ACI Committee 212, 2010) Report on chemical admixtures for concrete, (ACI Committee 232, 1996): Use of Fly Ash in Concrete, (ACI Committee 232, 2012): Use of Raw or processed Natural Pozzolans in concrete, (ACI Committee 234, 1996): Guide for the use of Silica Fume in concrete and (Sandor, 1992) - “concrete materials, properties, specification and testing”.

Table 2.1: Density Classification of Concrete Aggregates, Mindess

Category	Unit Weight of Dry-rodded Aggregate (kg/m^3)	Unit Weight of Concrete (kg/m^3)	Typical Concrete Strength (MPa)	Typical Application
Ultra-Lightweight	<500	300-1100	<7	Non-structural
Lightweight	500-800	1100-1600	7-14	Insulating material
Structural Lightweight	650-1100	1450-1900	17-35	Masonry units structural
Normal weight	1100-1750	2100-2550	20-40	Structural
Heavyweight	>2100	2900-6100	20-40	Radiation shielding

Source: Department of Civil Engineering Lecture note, University of Pennsylvania, n.d.

2.4 Rice husk ash

Rice husk ash, also known as rice husk ash, is a natural and organic product, made up of finely powdered glass-like material that is a by-product of burning rice husks. Rice husk ash is composed of silica and amorphous alumina, and it is used as a pozzolanic material to increase the strength and water resistance of cement and concrete. It is also used in agricultural applications, as a soil fertilizer, to improve soil stability and nutrient retention. Rice husk ash also has agricultural benefits, such as increasing crop yields and preventing soil erosion. In addition, because it contains no organic material, rice husk ash is considered non-toxic and eco-friendly, making it an attractive additive for sustainable building materials. It can also be recycled, making it an increasingly popular material to use in the production of a variety of products. (Sathy, Satyanarayana, and Pramada, August 2003) conducted a detailed study on the chemical composition of Rice Husk from six different locations in India.

The study found that there are significant variations in the chemical composition of Rice Husks from different locations, such as ash, silica, nitrogen and carbon content. The amount of silica present in Rice Husks were found to vary from 4.24 - 8.35%, while the ash content varied from 1.37 - 7.99%. The relative amount of nitrogen and carbon present in the husks also varied significantly across the locations. The study concluded that the chemical composition of Rice Husk varies significantly between locations, which has a profound effect on the overall quality and value of the Husk. The findings of the study are important for farmers, producers and consumers of Rice Husk, as a better understanding of the chemical composition of this commodity can help maximize its value and ensure better regulation of its trade. The husk forms a protective coat around the seed to protect it during the growing season; the hulk contained hard materials, including opaline silica and lignin. When the rice husk is properly brunt, its ash contains high SiO_2 content and can be used as supplementary cementitious material (SCM) in combination with cement to make concrete products. It was estimated that 200kg of husk can be obtained from 1000kg of rice grains which 20% of the resulting husk can be converted to RHA after processing (Mehta, 1986). It has a variety of uses, from agriculture to building materials, and is an increasingly popular material in the construction industry. Studies have found that, when processed, up to 20% of the resulting husk can be converted to RHA (Barua, Rahman, Chowdhury, Abul Hasan, and Mohiuddin, 2018). This material can be used as a partial substitute for cement, creating

a strong and durable material at a fraction of the cost. It is also non-toxic, resistant to fires, and offers excellent thermal insulation properties. As a result, RHA is gaining popularity in industrial applications, and it is becoming increasingly clear that it is an effective, sustainable resource that could potentially revolutionize many industries. As an active pozzolana, it has several applications in the cement and concrete industry and by extension, the construction industry. Due to its similar micro-silica properties with silica fume, it can be used as an economical substitute for silica fume as SCM. Thus, reducing the overall production cost of concrete is less expensive compared to silica fume and also, reducing the cement requirement leading to less environmental pollution by cement factories, therefore, providing economic and environmental benefits along with providing a way of disposing the agricultural waste products which otherwise has little alternative use (Das, Saha, Jena, and Panda, 2021).

In (Ramezanianpour, Mahdi, and Ahmadibeni, 2009) studied the effect of RHA on the mechanical properties and durability of sustainable concrete. In their report, they noted that concrete incorporating RHA has higher compressive strength, splitting tensile strength and modulus of elasticity at various ages in comparison with the controlled cement concrete. Furthermore, their results also showed that RHA as an artificial pozzolanic material has enhanced the durability of RHA concrete and reduced the chloride diffusion (Chalee, Sasakul, Suwanmaneechot, and Jaturapitakkul, 2012)

2.4.1 Rice production in Nigeria and prospects

Rice, a leading staple food crop in Nigeria, is derived from a monocot plant of Oryza sativa or Oryza glaberrima. It is cultivated in virtually all the agro-ecological zones of Nigeria, from the mangrove and swamps environment of the coastal areas to the dry zones of the Sahel in the North (Ayanwale, Akinyosoye, Yusuf, and Oni, 2011), (Akande, 2002)]. According to (Ramezanianpour A. , 2014), it is the grain with the second-highest worldwide production, after corn. In respect to National Food Reserve Agency (Agency-NFRA, October 2008), it was estimated that 1.7 million hectares of land in Nigeria were under rice cultivation in 2007 with an estimated national production of 3.4 million metric tons. Also, in the same report, 2 metric tons per hectares of rice yield was reported in the same year with a negligible decrease of 0.03 percent with respect to the previous year production output coupled with a percent annual growth rate from 1999(Ayanwale, Akinyosoye, Yusuf, and Oni, 2011). However, in the report

published in (Institute, Annual Report 2010), the national production output in 2008 was estimated to be 5.3 million metric tons as result of 2.3 million hectares cultivated and a yield rate of 2.3 metric tons per hectares. However, due to the population explosion experienced in recent years coupled with rapid urbanization, increased income levels, and associated changes in family occupational structures, the consumption rate has increased to 10.3 percent per annum (Akpokodje, Lançon, and Erenstein, 2001; Akande, 2002); Ayanwale, Akinyosoye, Yusuf, and Oni, 2011). This has created a wide margin between the domestic supply of rice and the associated demand. To accommodate this shortage in supply, the country engages in the massive importation of rice. According to the report published by (Newspaper, This Day, 2014), it noted that Nigeria expends US$1.3 billion every year to import 2.2 billion kg of rice in order to fulfil its domestic requirements. As such, a substantial part of our foreign exchange is being spent on rice importation. With the current significant drop in the foreign exchange earnings due to global drop in oil price, there have been serious moves by the government to boost the local production of rice in the recent years to cut down foreign exchange spending on importation of food items Import Substitution in Nigeria: Feasibility and Path towards Reduced Import Content.

Table 2.2: Rice production trends in Nigeria (1961-2005)

Period	Average area cultivated (hectares)	Average Output (tons)	Average Yield (tons/hectares)
1961 – 1965	179,200	207,200	1.147
1966 – 1970	234,000	321,000	1.360
1971 – 1975	288,800	470,000	1.670
1976 – 1980	332,000	596,200	1.710
1981 – 1985	630,000	1,300,200	2.063
1986 – 1990	1,060,200	2,216,064	2.090
1991 – 1995	1,678,000	2,979,600	1.784
1996 – 2000	1,742,582	3,011,028	1.733
2001 – 2005	2,270,800	3,139,440	1.096

Source: (Project Coordinating Unit (PCU), 2002)

2.4.2 Rice husk and its application

As pointed out in previous paragraphs, the rice husk serves as a hard-protective covering for the rice grain. However, the rice husks have proven to be more than a mere covering for the grains during growing seasons. Below are some of the current and potential applications of rice husk.

a) **Chemical application:** According to (Siriluk, Thanita, and Nurak, 2007) report, rice husk can be used in the production of mesoporous molecular sieves which can be used as a catalyst in various chemical reactions, as a support for drug delivery system and adsorbent in wastewater treatment.

b) **Industrial application:** In (Krishnarao and Mahajan, 1996) reported that rice husks are a cheap source of materials for the manufacture of silicon carbide "whiskers" which are used as reinforcement in ceramic cutting tools to enhance their strength tenfold.

In additional, rice husk has been used as a source of fiber pet food, building material, fuel in some industrial application and fertilizer.

Various researchers have shown that the demand for low-cost materials for building activities has been the major drive for the use of rice husk. It has been demonstrated that a concrete mix of 10 percent of cement, 50 percent of aggregate and 40 percent RHA in addition to water produced test blocks with the average compressive strength of $12\ N/mm^2$ as oppose to the result reported using a normal concrete without RHA which gives an average compressive strength of $4.5 - 7\ N/mm^2$ or high strength concrete blocks which have a compressive strength of 10 N/mm2. In (Ramezanianpour A. , 2014) report, higher strength concrete with RHA allows lighter weight products to be produced such as hollow blocks with enhanced thermal insulation properties, which provides lighter walls for steel framed buildings. It also leads to reduced quantities of cement and aggregates. In Nigeria, the use of rice husk has not been tapped into fully. With reference to (Okpala, 1987)works, he noted that in Nigeria, the majority of the rice growing areas are located in rural areas where housing is mainly of mud walls and other non-durable materials. Rice husks, which abound in such places, are seen as waste materials are normally burnt off. However, it would have been beneficial in the rural areas if the technology for utilizing rice husk is properly developed in Nigeria.

2.4.3 Rice husk ash production

Rice husk has been reported to contain unusually high ash content compared to other biomass fuels - close to 20 percent. The ash is 92- 95 percent silica (SiO_2), highly porous and lightweight, with a very high external surface area. Its absorbent and insulating properties are useful to many industrial applications and the ash has been the subject of many research studies (Ramezanianpour, 2014). However, it has been reported that RHA can find application in various industrial processes due to its excellent insulation properties such as steel foundries and in the manufacture of refractory bricks insulation. As an active pozzolan, it can be used for various purposes in the cement and concrete industry. In addition, its high absorbent properties can be applied to hard surfaces to absorb oil and potentially to filter arsenic from water.

The production of Rice Husk Ash in Nigeria is accomplished through various processes. The dry process involves burning and crushing the husks into a fine powder before storing it in a large container. The wet process involves boiling the husks first and then breaking it down with a hammer mill before storing in containers. The advantage to the wet process is that it produces a smoother ash with lower levels of impurities. The production of Rice Husk Ash provides employment opportunities in the rural communities. The ash can also be used as an alternative to bricks and stones, thereby reducing the cost of building operations. Additionally, it has the potential to help reduce the amount of waste output in the country, thus contributing to a more sustainable environment. Rice Husk Ash production in Nigeria is a growing industry that has the potential to make a positive impact on the environment and to provide economical benefits to the rural communities. With the right strategies in place, Nigeria can tap into this potential and reduce its environmental impact while generating revenue and creating jobs.

Meanwhile, significant research findings on RHA revealed that its chemical composition depends on temperature and the burning time, but the variations in compositions are not significant (Ramezanianpour, 2014). In addition, studies revealed that the ash derived from open field burning (or from non-controlled combustion in industrial furnaces) contains a higher proportion of non-reactive silica minerals such as cristobalite and tridymite. Thus, it is required to ground into very fine particles in other to develop pozzolanic activities in such ash. However, research has shown that highly pozzolanic

ash can be produced by means of controlled combustion when silica is kept in a non-crystalline form. As such, the silica can react with the calcium hydroxide when added to cement in the presence of water to give cementitious compounds. Nonetheless, it has been established by various researchers that burning temperature is a critical point amorphous reactive ash production (Ramezanianpour, 2014). In general term, RHA is used to denote all form of ash produced from the burning of rice husk. But in practice, the type of ash produced varies considerably with respect to the burning technique. In addition, the silica in the ash goes through a structural transformation process depending on the temperature regime employed during combustion. It has been established that a temperature range of $550 - 800\,℃$ produced amorphous silica while a higher temperature regime produced a crystalline form of silica. As a result of differences in structural makeup, it has been established that these two forms of silica exhibit different properties, thus, it is essential to produce ash with the right specification for the required use.

However, further studies have revealed that the form of silica obtained after combustion of rice husk is not only dependent on the temperature regime as pointed out above but also on the duration of combustion. In view of this, (Mehta, 1979) pointed out that amorphous silica can be readily produced by maintaining the combustion temperature below $500\,℃$ under oxidizing conditions for prolonged periods or up to $680\,℃$ with a hold time less than 1 min. But in (Yeoh, Bidin, Chong, and Tay, 1979)reported, that amorphous form of RHA can be produced at a combustion temperature of up to $900\,℃$ and the combustion time is less than an hour, while crystalline can be produced at $1000\,℃$ with combustion time greater than 5 min. In 1981, Chopra et.al observed, with the help of X-ray diffraction, that amorphous silica can be produced at burning temperature up to$700\,℃$. In addition, the inherent differences in burning temperatures and the chemical composition of rice husk were further studied in 1989 by Hwang and Wu. In their reports, it was observed that at $400\,℃$, polysaccharides begin to depolymerize. Above this temperature, the sugar units undergo dehydration. At $700\,℃$ the sugar units underwent decomposition. And at temperature above$700\,℃$, the unsaturated products react together and form a highly reactive carbonic residue. Based on the data obtained by (Hwang and Wu, 1989), it was observed that the higher the burning temperature, the greater the percentage if silica obtained in the ash. Although, K, S, Ca, Mg and several other components were found to be volatile. A report based on

(Della, Kuhn, and Dachamir, 2002)work shows that heat-treating the ash for 6 hours at 700 ℃ can produce 95 percent of silica powder. In addition to this, he further explained that a wet milling procedure can enhance the surface area of the particles from $54\ to\ 81\ m^2/g$.

2.4.4 Physical and chemical properties of RHA

A significant amount of silica (SiO_2) can be obtained from rice husk when it is well processed. It has been established that a well burnt and well-ground rice husk ash has a very high pozzolanic properties and can considerably enhance the strength and durability of cement and concrete. However, such pozzolanic characteristics can be obtained only by burning rice husk under well-defined conditions to improve its physical and chemical properties.

2.4.5 Physical properties

RHA is made up of very fine particles. As reported by various authors, its average particle size ranges from $5-10\mu m$. Table 2.3 below shows some of the physical properties as reported by various authors.

Table 2.3: Physical properties of RHA

Properties	Value			
	Mehta (1992)	Zhang et.al (1996)	Feng et.al (2004)	Bui et.al (2005)
Mean particle size (μm)	-	-	7.4	5
Specific gravity	2.06	2.06	2.10	2.10
Fineness: passing 45 μm (%)	99	99	-	-

Source: Ramezanianpour, 2014

2.4.6 Chemical properties

Based on its high silica content, generally, more than 80 – 85%, RHA is very reactive to calcium hydroxide in cement in the presence of water. Table 2.4 below shows the chemical composition of RHA as reported by various authors. However, for RHA to serve as pozzolans in cement and concrete, it should satisfy the requirements for the chemical composition of pozzolans as per ASTM C618 (Ramezanianpour, 2014). In addition, the combined proportion of silicon dioxide SiO_2, Aluminium oxide Al_2O_3, and iron oxide Fe_2O_3 in the ash should not be less than 70 % and loss on ignition (LOI) should not exceed 12 % as stipulated in ASTM requirement (Ramezanianpour, 2014). See Table 2.5 below.

Table 2.4: Chemical Composition of RHA

Constituents	**Percentage**		
	Mehta (1992)	**Zhang et.al (1996)**	**Bui et.al (2005)**
Silica (SiO_2)	87.2	87.3	86.98
Alumina (Al_2O_3)	0.15	0.15	0.84
Iron Oxide (Fe_2O_3)	0.16	0.16	0.73
Calcium Oxide (CaO)	0.55	0.55	1.4
Magnesium Oxide (MgO)	0.35	0.35	0.57
Sodium Oxide (Na_2O)	1.12	1.12	0.11
Potassium Oxide (K_2O)	3.68	3.68	2.46
Sulphur Oxide (SO_3)	0.24	0.24	-
LOI	8.55	8.55	5.2

Source: (Ramezanianpour, 2014)

Table 2.5: Comparison of chemical and physical specifications of produced RHA with ASTMstandard C618-03

	ASTM	RHA Results
Chemical requirements		
$SiO_2 + Al_2O_3 + Fe_2O_3$, min., %	70	89.9
SO_3, max., %	4	0.15
Moisture content, max., %	3	0.23
Loss on ignition (LOI), max., %	6	5.9
Physical requirement		
Fineness: amount retained when wet-sieved on 45 μm sieve, max., %	34	8
Strength activities index (20 % RHA) at 3-days, min % control	-	102
Strength activities index (20 % RHA) at 7-days, min % control	75	106
Strength activities index (20 % RHA) at 28-days, min % control	75	110

Source: (Ramezanianpour, 2014)

2.4.7 High-strength concrete mix proportioning

In concrete production, the procedure adopted in the selection of constituent materials and determination of the amount of each material as required in producing a concrete in accordance to the specified strength, workability, and durability with strong consideration to the cost is referred to as "**concrete mix proportioning**". In (Murali and Kandasamy, 2009) view, mix proportioning is not unique given the impracticability in measuring all parameters involved and the inability to amend such parameters using mathematical manipulation. The proportioning of HSC varies with strength requirement, test age, material properties and application of the concrete, Economic and structural requirements, manufacturing practicality, curing conditions and time of the year. In view of available literature, there are several methods available for the proportioning of HSC such as New British Method, ACI Method, British Method, Fineness Modulus Method, Maximum Density Method, Road Note No. 4 Method and Minimum Voids Method.

However, all these methods give a channelize procedure for proportioning the basic ingredients of the conventional concrete. But in the case of HSC, there is no single channelized and branded procedure available for it given the numerous varying parameters and materials quality variation with geographical location. In response to this, Canadian Portland Cement Association explicitly suggested the use of trial mixes as the best way to approach the concrete proportioning of HSC. However, with the aim to save materials and time in the process of trying to find the optimum materials proportioning for the required concrete mix via trial mixed, the mix design should be based on some known empirical procedures to create a base mix whose constituents can be varied further to arrive at the intended mix. In view of this, The America Concrete Institute (ACI) provided a broad guide in HSC proportioning in their ACI 211.4R Standard Practice (See the appropriate standard for details of the procedures).

CHAPTER THREE
METHODOLOGY

3.1 Preamble

The study will involve two stages of the investigation. The first stage will focus on analysing the fracture parameter of the rice husk ash concrete as it is composed and how it varies over time. This will involve determining the fracture measurement of the concrete for each time period (7,14, 21 and 28 days) and examining the effect of water saturation on the fracture parameters. The second stage of the research will explore the effect of the fracture parameter on the compressive strength of the concrete. This will involve assessing the impact of varying fracture parameters on the compressive strength of the concrete over different time intervals and determining the optimum values of fracture parameters which will result in the highest compressive strength. The results of this study may be used to optimize the compositions of the concrete about fracture parameters and water saturation and increase the durability and life of the concrete product. Important amongst these were the physical properties of the aggregates and binders to be used, workability and setting time tests of the mixes at varying percentages of replacements. The compressive tests of the cubes, specific gravity and density test were also carried out.

3.2 Material constituents

The materials used for the experiment include the following listed below:

i. Rice Husk Ash
ii. Fine aggregate
iii. Coarse aggregate
iv. Ordinary Portland cement
v. Potable water
vi. High range water reducer (HRWR)

3.2.1 Fine aggregate

The fine aggregate used in the experiment came from the Oworoshoki area of Lagos, specifically from the bed of the Lagos lagoon. To make sure that no clay, loam, dirt, or organic/chemical substances were mixed in, the sand particles were carefully separated. This separation process involved passing the particles through a sieve with holes measuring 4.75mm, while making sure that particles smaller than 0.06mm were caught on a finer sieve. This method effectively eliminated any dust particles present in the sand.

3.2.2 Coarse aggregate

The coarse aggregate used in this research study were crushed granite of igneous origin. There are different sizes used but the preferred size is 2.36 to 12.70mm, this size produces concrete of better quality.

3.2.3 Cement

Cement is a binder and defined as a finely ground inorganic material which when mixed with water, forms a paste which sets and hardens by hydration reaction and through this process hardening retains its strength and stability even under water. The cement used for these experiments was (Ordinary Portable Cement OPC). This cement used meets the laid down standards for Ordinary Portland Cement (OPC), and this guarantees quality.

3.2.4 Rice Husk Ash

The rice hush waste used for the production of Rice Husk Ash (RHA) was sourced from Ire Ekiti in southwestern part of Nigeria. The production process of Rice Husk Ash (RHA) in a closed furnace involves a few steps. Dry Pyrolysis: The husk is then heated in an oxygen-free environment to over 700 °C. This pyrolysis process breaks down the complex chemical compounds and removes any moisture from the husk. Combustion: The dried husk is then combusted under specific conditions. This combustion process creates a char which is mostly composed of inorganic materials, such as silica, calcium and magnesium. Collection: The ash is collected in the furnace and transferred to a storage tank. Milling: The ash is then milled to reduce its particle size and create a uniform ash-powder. Quality Control: The quality of the ash is inspected for composition, fineness, and other properties, based on varying standards set by the user.

Packaging: The RHA powder is then packaged for sale and use. The product is checked for packaging security, labeling and documentation. This is the general process to produce RHA in a closed furnace. The process may vary from one furnace to another, depending on the customer's requirements, type of furnace and the quality of the product desired. By following this process, RHA can be produced of a consistent quality, helping to ensure its use as a valuable raw material in various industries.

Plate 3.1: Rice Husk in production using the closed furnace.

3.2.5 Water

Water is a key ingredient in concrete production and is used to hydrate the cement, control the rate of hardening of the concrete and control the temperature of the product. The chemical composition of the concrete also depends on the water used in the production process. In most concrete production processes, freshwater is used and the water should meet specific limits for alkalinity, impurities, chloride, and other compounds. The amount of water added to the concrete mix is determined by the desired consistency; this is usually determined by the aggregate size and the workability requirement of the concrete. The use of too much water can cause significant strength loss and should be avoided. It can also increase shrinkage, segregation and settlement of the concrete during hardening, as well as creating weak mortar pockets. Too little water can also weaken the resulting concrete due to the lack of a complete chemical reaction between the cement and water. The portable water used in this experiment was obtained from the taps in the laboratory. The quality of water used meets safe to drink standards and does not contain impurities which can influence the quality of concrete in both its tough and fresh states, as stated in standards.

3.3 Apparatus tools and equipment

The apparatus tools and equipment to be used for the tests and observations in the laboratory are briefly outlined below:

3.3.1 Avery weighing machine

The Avery weighing machine is a digital scale specifically designed for use with concrete production. It is a user-friendly and highly accurate system that provides accurate readings of up to 250 pounds with a 1/10th of one pound resolution. The machine includes a digital indicator giving the weight of material placed on the platform and an adjustable-length weighbridge to accommodate various types of mixing and mixing equipment. This machine also features an easy-to-read LCD display, an adjustable-height scale platform, and a manual zero-detect feature. In addition, the Avery weighing machine is designed to be resistant to dust and water and features adjustable feet for stability and easy leveling. Its open system design allows for easy access and maintenance and its heavy-duty steel construction ensures durability.

Plate 3.2: Avery weighing machine

These have a capacity range 0-50kg, which was used to measure the concrete constituent and other materials used for the experiment consisting of a gauge.

3.3.2 Cube moulds

These are iron cast with inner dimensions of $\mathbf{150 \times 150 \times 150}\ \boldsymbol{mm}$used to cast the cubes for the compressive strength. Iron cast with inner dimensions of 150x150x150 mm are generally used in the production of concrete to form a mould for concrete bricks, blocks and other building elements. These iron casts are typically made using a casting-iron process and are strong and durable enough to withstand large amounts of pressure from the concrete mixture. Moreover, the small dimensions of these castings allow them to fit into tight spaces and narrow gaps, making them ideal for use in small-scale construction projects. Iron castings are also often used in the construction of outdoor structures, as the material is resistant to rust, corrosion and environmental damage. In addition to their strength and durability, these castings are also cost-effective and can be reused in multiple construction projects.

3.3.3 Slump mould

A slump mould is a tool used in the production of concrete. It is used to measure the consistency of the concrete by analysing the "slump" or deformability of the freshly mixed concrete when it is dropped from a given height. The slump test is a measure of the consistency, workability, and cohesiveness of concrete. The mould consists of a metal cone-shaped vessel with a base plate and handle, usually having a volume of 1000 cm3 (0.035 ft3). The sample of freshly mixed concrete is placed in the cone and then dropped onto a hard surface from a given height (usually 15 cm (6 in)). The amount by which the cone deforms is a measure of the slumping characteristics of the concrete and can be used to judge the consistency of the mixture. The slump mould is an indispensable tool used in the production of concrete and provides important insights into the quality and consistency of the concrete. The slump mould is a metal hollow frustum of a cone having the following dimensions.

i. Diameter of top – 100mm
ii. Diameter of base – 200mm
iii. Height of mould – 300mm

It is used to determine the workability of a mix by measuring the slump height.

3.3.4 Concrete mixer

This is a diesel engine powered tilting drum device which homogeneously combined cement, aggregate such as sand or gravel, and water to form concrete required. A concrete mixer is an important piece of equipment in the production of concrete. It is used to combine cement, sand, gravel, and water together to make concrete that is of a uniform consistency. The mixer works by rotating its drum within a bed of dry ingredients, slowly introducing water until the desired consistency is achieved. The mixture is then agitated and poured into the forms, where it is allowed to harden and form a solid mass. The exact type of concrete mixer used in production will depend on the application and the amount of concrete needed. For larger projects, such as streets or sidewalks, a large ready-mix truck with a revolving drum is used. For smaller applications, such as patios or driveways, an electric or gas-powered concrete mixer is usually adequate. The cost of owning and operating a concrete mixer can vary significantly, depending on the size and scope of the project. Concrete mixers are a versatile tool, offering a wide range of options for a variety of applications. Many mixers feature a variety of accessories, such as different blades, agitators, and hoppers, which allow them to reduce and refine the ingredients in the mix and create specific mixes according to a user's specifications. Most mixers are easy to operate and maintain, although the size and weight of some of the larger machines can make them difficult to maneuver. They require regular inspection and cleaning in order to avoid problems with the mixture, and safety should always be taken into account when working with concrete mixers. Overall, concrete mixers are essential for the production and use of concrete in various projects, from small repairs to large buildings. They provide an efficient way to combine and control the ingredients to create a uniform mixture that can be poured and shaped into various forms.

3.3.5 Vicats apparatus

The equipment was used to determine the initial and final setting time of the plastic mix. Vicats Apparatus is a device used in the production of concrete. It is used to measure the workability of concrete, which is a measure of how easily concrete can be handled, molded, and placed. It measures the amount of force required to press a plunger into a sample of concrete. The measured force is then used to calculate a concrete's workability, consistency, and other characteristics. It is an important tool for quality control of concrete production and is used in quality assurance tests required by many

building codes. The apparatus can also be used to measure the cube strength of concrete, which is used to measure the strength of a concrete sample when tested under standard conditions. Vicats Apparatus is a standard tool in most concrete production facilities and is used to ensure that concrete is manufactured consistently and to the necessary quality standards.

3.3.6 Compression testing machine

This was used to obtain the compressive strength of the cubes cast. A Compression Testing Machine is an important piece of testing equipment used to evaluate the structural strength of concrete. The machine works by using a hydraulic cylinder or screw mechanism to apply a compressive force on a concrete specimen. The compression force is measured against the failure load, or the maximum amount of force the concrete specimen can take without breaking apart.

The test can also measure the elasticity and ductility of concrete. This is essential in order to gauge the material's ability to withstand extreme conditions, such as earthquakes, heavy winds, and other natural disasters. This testing machine is an invaluable tool in the construction industry because it helps evaluate the safety and structural integrity of a building or a bridge. By measuring the strength and stability of concrete, architects and engineers can design resilient structures that will withstand extreme conditions and last for years to come. Compression testing machines are also used to determine the compressive strength of soil, which is essential information when designing foundations. In addition, concrete production facilities use compression testing machines to test the quality of the concrete before sale. Companies will ensure that their products meet their customer's requirements and have the necessary levels of compression strength and durability needed for their building projects. A compression testing machine can help certify that the customer is receiving a high-quality product that is reliable and resistant. Compression testing machines are a must-have in the concrete production industry, as they provide vital information regarding the performance and safety of concrete products. This testing machine can help evaluate the structural integrity of a building and guarantee customer satisfaction.

3.3.7 Tapping rod

Tapping rods are used in concrete testing to assess the density of concrete. It is a simple and effective test that helps determine how well a concrete mix has been blended and placed. The test involves tapping the side of a concrete block with a rod. The degree of sound produced provides an indication of the compaction of the concrete. A dull sound usually indicates excess entrapped air in the concrete, while a hard, ringing sound indicates high density. Tapping rods are usually lightweight steel rods, and the size and shape may vary depending on the specific application. The procedure is inexpensive, fast, and non-destructive, meaning the concrete block can be reused for other testing and construction purposes. The tapping rod test is widely used in the quality inspection of concrete products. **Sieve** It is of different apertures of sizes used to obtain the grain sizes classification of aggregate.

3.3.8 Sieve

A sieve is used in concrete testing to assess the particle size of the concrete, which helps to determine its overall quality. The sieve consists of a cylinder with a series of comparatively spaced metal plates, which act as screens. A sample of dry, powdered concrete is placed into the sieve and vibrated for a set period of time. The concrete material that passes through each metal plate is weighed, and the cumulative percentages of the material passing through each plate are calculated, providing an overall profile of the particle size distribution. This information can be used to assess the particle size of the concrete sample and, hence, the quality of the material.

3.4 Experimental Test Procedure

The experiment started by examining the quality of cement, Rice Husk, granite and cement. The next step was to conduct laboratory trials to determine the appropriate concrete mix proportions that would result in a strength of 60 MPa, following the guidelines provided by the ACI committee 211 (2008) and to obtain CTODc and K^{S}_{IC} using Reunion Internationale des Laboratoires et Experts des Materiaux method (based on preliminary results) was conducted for the fracture parameters determination. The rice husk ash was varied at a proportion of 10%, 20%, 30%, 40% and 50% used as cement replacement.

3.4.1 Preliminary investigation

The preliminary investigation carried out is to determine the properties of each which include the following testes list below;

i. Sieve analysis
ii. Bulk density
iii. Specific gravity
iv. Moisture content
v. Chemical analysis of rice husk ash
vi. Physical properties of Rice of husk ash

A. Sieve Analysis/Graduation of Aggregates

Sieve analysis (or gradation test) is a practice or procedure used to evaluate the particle size distribution of aggregates by allowing the material to pass through a series of sieves of progressively smaller mesh size and weighing the amount of material that is stopped by each sieve as a fraction of the whole mass. Before the commencement of the experiment the aggregates (sand, granite, rice husk ash and cement) were thoroughly dried and before passing through sieves.

Apparatus:

i. Mechanical sieve shaker
ii. Sieve brush
iii. Weighing balance
iv. Various sizes of sees ranging from 2.36 mm to 6.5 mm
v. Evaporating pans

Plate 3.3: Mechanical Sieve Shaker

Procedure:

a) I cleaned the sieves of the sieve shaker, ensuring no particles remained stuck in the openings.
b) I recorded the weight of each sieve and the receiving pan.
c) If the specimen wasn't already dried, I dried it in the oven for 3-4 minutes.
d) After drying, I weighed the specimen and noted down its weight.
e) I arranged the sieves in order, placing the one with the smallest openings at the bottom and the one with the largest openings on top, as per the guidelines in Table 3.1.

Table 3.1: Sieve Number

Sieve Number	Diameter (mm)
#4	4.75
#10	2.00
#20	0.85
#40	0.43
#60	0.25
#200	0.075
Pan	-

B. Specific Gravity

Specific gravity is the ratio of the density of a substance to the density mass of the same unit volume of the reference substance. Apparent specific gravity is the ratio of the weight of a volume of a substance to the weight of an equal volume of the reference substance.

The specific gravity of a soil is often used to describe the relationship between the weight of the soil and its volume as soil contains different particles with different specific gravity is the term $\boldsymbol{GSS}$ represent the average value for all particles.

Specific gravity is commonly used in industry as a simple means of obtaining information about the concentration of solutions of various materials, or of quality control for polymer materials: to evaluate physical changes or determine the degree of uniformity between samples or lots.

Apparatus:

- **i.** Density bottle
- **ii.** Glass world wash bottle containing distilled water (W1)

Procedure:

a) I weigh the dry density bottle ($\boldsymbol{W_1}$).
b) I obtain about 25g of the oven dry material and transfer into the density bottle. Replace the stopper and weigh the bottle and contents ($\boldsymbol{W_2}$).
c) I added distilled or tap water so that the soil in the bottle is covered. Thoroughly stirred the mixture with a glass rod or shaker to remove air trapped in the soil.
d) I fill the bottle with distilled or tap water and replace the stopper shake the density and its contents carefully to remove any remaining air ($\boldsymbol{W_3}$).
e) I empty the contents of the bottle and fill the bottle will be distilled water only ($\boldsymbol{W_4}$).

The specific gravity is used in the laboratory to help with the calculation of the void ratios of soil specimens in the determination of moisture content of a soil and in the particle size analysis also known as sedimentation test.

C. Moisture Content

Water content or moisture content is the quantity of water contained in a material it is the ratio of water present in a soil mass to the weight of the soil solids.

The natural moisture content will give an idea of the state of soil in the field. The natural water content also called the natural moisture content is the ratio of the weight of water to the weight of the solids in a given mass of soil. This ratio is usually expressed as a percentage.

D. Chemical Analysis of Rice Husk Ash (RHA)

The chemical analysis of rice husk ash was carried out in Federal Institute of Industrial Research, Oshodi (FIIRO) and compared with that of Ordinary Portland Cement. This is done to determine the composition of rice husk ash material.

3.4.2 Secondary investigation

The secondary investigations carried out in the course of this research study include the following:

i. Test on cement paste
ii. Slump test (workability)
iii. Casting of cubes
iv. Compressive strength test

A. Test on cement paste

The aim is to get the consistency of the standard cement paste to calculate the initial and final setting time of the cement paste and the compressive strength. It is essential that cement set neither too rapidly nor too slowly. In the first case, there might be insufficient time to transport and place the concrete before it becomes hardened while longer setting time slows down the work unduly and might postpone the actual use of the structure because of inadequate strength at the desired age.

Initial setting time test is important for transportation, placing and compaction of cement concrete while the final setting time is the time when the paste completely loses its plasticity. In other words, it is the time taken for the cement paste or cement concrete to harden sufficiently and attain the shape of the mould in which it is cast.

Apparatus:

i. V-ICAT Apparatus
ii. Digital weighing scale used to measure the weight of dry cement
iii. Glass graduates used to measure the volume of water
iv. Mixing bowl
v. Ordinary Portland cement
vi. Water

Procedure:

A. Test Block Preparation:

a. Before commencing the setting time test, the consistency test was done to obtain the water required to give the paste a normal consistency (P).

b. A mixture of 400g of cement and 0.85P of water by weight of cement was used to prepare a neat cement paste.

c. A gauge time was kept between 3 – 5 minutes. The stopwatch was started at the instant when the water was added to the cement. The recorded time was taken as ($\boldsymbol{t_1}$).

d. With the cement paste gauged as described above, the Vicat mould was filled while resting on a glass plate with the surface smoothen off the paste to make it level with the top of the mould. This is taken as the test block.

B. Initial Setting Time:

a. The test block was confined within the mould and resting on the non-porous plate, under the rod bearing the needle.

b. The needle was lowered gently until it was in contact with the surface of the test block, it was quickly released to allow penetration into the test block.

c. As discussed above, the needle completely pierces the test block. Step (b) was repeated after every 2 minutes till the needle failed to pierce the block beyond 5 mm measured from the bottom of the mould and the time recorded as ($\boldsymbol{t_2}$).

C. Final Setting Time:

a. The Vicat's apparatus needle was replaced with an annular attachment.

b. The cement is considered finally set when upon applying the final setting needle gently to the surface of the test block; the needle makes an impression thereon, while the attachment fails to do so. The was recorded as ($\boldsymbol{t_3}$)

Calculation:

$$Initial\ setting\ time = \boldsymbol{t_2 - t_1} \quad \textbf{(3.2)}$$

$$Final\ setting\ time = \boldsymbol{t_3 - t_1} \quad \textbf{(3.3)}$$

Where,

$$t_1 = Timeatwhichwaterisfirstaddedtocement$$

$$t_2 = Timewhenneedlefailstopenetrate\ 5\ mmto\ 7\ mmfrombottom\ of\ the\ mould$$

$$t_3 = Timewhentheneedlemakesanimpressionbuttheattachmentfailsto\ do\ so.$$

B. Concreting and curing

Batching of concrete means measuring different ingredients of concrete (i.e. cement, sand, coarse aggregate and water) before mixing it. When this measurement is done on the basis of volume, we call it Volume Batching. For the purpose of this experiment the materials used were batched by weight.

C. Slump test

The concrete slump test is the empirical test that measures the workability of fresh concrete. It measures the consistency of the concrete with reference to a specific batch. This test is performed to check the consistency of the freshly made concrete. Consistency, in close relation to workability, is a term which describes the state of fresh concrete in relation to the ease with which the concrete flows and an indication of the degree of wetness.

Apparatus:

i. Slump cone (Height = 30 cm, Base diameter = 20 cm, Top diameter = 10 cm)
ii. Tamping rod (Length = 60 cm, Diameter = 16 mm)
iii. Stopwatch
iv. Hand Trowel
v. Head pan

Procedure:

a. The internal surface of the mould was thoroughly cleaned and freed from superfluous moisture before commencing the test. And if the cone is in completely dry condition, then dampen it using a damp cloth.
b. The mould was then placed on a smooth, horizontally levelled rigid and non-absorbent surface such as a rigid plate. It was held firmly in place during filling by the operator by standing on the two-foot pieces provided in the slump cone.
c. The mould is filled with concrete in four layers, each approximately one-quarter of the height of the mould, and each layer is tamped down with 25 strokes of tamping rod with the pointed end in a uniform manner.
d. After tamping the top layer, the concrete is struck off level with a trowel and any mortar leaked out between the mould and base plate is cleaned away.
e. The mould is then removed from the concrete immediately by raising it slowly and carefully in a vertical direction.

Calculation:

The slump is measured immediately by determining the difference between the height of the mould and that of the highest point of the specimen.

D. Curing

Curing is a procedure of promoting the hydration of cement for development of concrete strength and controlling the temperature. As a result of curing, we can achieve higher strength and reduced permeability which is very vital for long-term strength or durability. At this stage of the experiment, the samples were allowed to cure using both immersion and ambient air for periods of (7, 14, 21, 28 days).

Apparatus:

i. Concrete mixer
ii. $150 \times 150 \times 150\ mm$ three cube moulds
iii. Tamping rod (16 mm)
iv. Slump Cone
v. Shovel
vi. Scoop
vii. Curing tank
viii. Compression test machine
ix. Head pans
x. Weigh machine

Table 3.2: Concrete Mix Design Material Specification (Grade M60)

Percentage RHA Replacement	Cement Content (kg/m^3)	Water Content (kg/m^3)	Coarse Aggregate Proportion (%)	Fine Aggregate Proportion (%)
0	449.28	178.64	37.93	62.07
10	475.71	177.13	37.93	62.07
20	422.86	178.12	37.93	62.07
30	370	179.45	37.93	62.07
40	317.14	179.74	37.93	62.07
50	264.28	180.03	37.93	62.07

3.4.3 Concrete mix design for Grade M60

Calculations for 0%, 10%, 20%, 30%, 40% and 50% of replacement of Rice Husk Ash (RHA) in the concrete mix design for Grade M60 using the BRE/DoE mix design method.

Procedure:

To obtain a concrete mix design material specification for Grade M60 concrete using the BRE/DoE mix design method, you would typically follow these steps:

1. Determine the target strength: Identify the required compressive strength for Grade M60 concrete. In this case, the target strength is M60, which means a compressive strength of 60 megapascals (MPa).
2. Determine the water-cement ratio (w/c): The water-cement ratio is a crucial parameter that influences the strength and durability of concrete. It can be determined based on past experience and local conditions.
3. Select the water content: Determine the appropriate water content considering factors such as workability requirements, aggregate characteristics, and the desired w/c ratio.
4. Select the cement content: Calculate the cement content based on the water-cement ratio and water content determined in the previous steps.
5. Determine the aggregate content: Determine the proportions of coarse and fine aggregates based on standard guidelines and requirements for achieving the desired concrete properties.
6. Adjust the mix proportions: Fine-tune the mix proportions of cement, water, and aggregates to ensure the desired workability, strength, and durability. This adjustment may involve iterative calculations and adjustments.
7. Verify the mix design: Conduct laboratory tests to validate the mix design and ensure it meets the desired strength and durability requirements. These tests typically include compressive strength tests and other relevant tests as per the design standards.

0% replacement calculation:

Target Compressive Strength: 60 MPa

Water-Cement Ratio (w/c): 0.35

Water Content (W): 185 kg/m³

Maximum Aggregate Size: 20 mm

Superplasticizer Dosage: 1.5% of cement weight

Percentage Replacement of RHA: 0%

Step 1: Calculate Cement Content (C):

C = (W / w/c)

C = (185 kg/m³ / 0.35)

C ≈ 528.57 kg/m³

Step 2: Adjust Cement Content with RHA:

Adjusted Cement Content = C

Adjusted Cement Content = 528.57 kg/m³

Step 3: Calculate Water Content:

Adjusted Water Content = W - (Superplasticizer Dosage * Adjusted Cement Content)

Adjusted Water Content = 185 - (0.015 * 528.57)

Adjusted Water Content ≈ 176.63 kg/m³

10% replacement calculation:

Coarse Aggregate: 60%

Fine Aggregate: 40%

Percentage Replacement of RHA: 10%

Step 1: Calculate Cement Content (C):

C = (W / w/c)

C = (185 kg/m³ / 0.35)

C ≈ 528.57 kg/m³

Step 2: Calculate Rice Husk Ash (RHA) Content:

RHA Content = (10/100) * C

RHA Content = (10/100) * 528.57

RHA Content ≈ 52.86 kg/m³

Step 3: Adjust Cement Content with RHA:

Adjusted Cement Content = C - RHA Content

Adjusted Cement Content ≈ 528.57 - 52.86

Adjusted Cement Content ≈ 475.71 kg/m³

Step 4: Calculate Water Content:

Adjusted Water Content = W - (Superplasticizer Dosage * Adjusted Cement Content)

Adjusted Water Content = 185 - (0.015 * 475.71)

Adjusted Water Content ≈ 177.13 kg/m³

20% replacement calculation:

Coarse Aggregate: 60%

Fine Aggregate: 40%

Assumed values:

Target Compressive Strength: 60 MPa

Water-Cement Ratio (w/c): 0.35

Water Content (W): 185 kg/m³

Maximum Aggregate Size: 20 mm

Superplasticizer Dosage: 1.5% of cement weight

Percentage Replacement of RHA: 20%

Step 1: Calculate Cement Content (C):

C = (W / w/c)

C = (185 kg/m³ / 0.35)

C ≈ 528.57 kg/m³

Step 2: Calculate Rice Husk Ash (RHA) Content:

RHA Content = (20/100) * C

RHA Content = (20/100) * 528.57

RHA Content ≈ 105.71 kg/m³

Step 3: Adjust Cement Content with RHA:

Adjusted Cement Content = C - RHA Content

Adjusted Cement Content ≈ 528.57 - 105.71

Adjusted Cement Content ≈ 422.86 kg/m³

Step 4: Calculate Water Content:

Adjusted Water Content = W - (Superplasticizer Dosage * Adjusted Cement Content)

Adjusted Water Content = 185 - (0.015 * 422.86)

Adjusted Water Content ≈ 178.12 kg/m³

30% replacement calculation:

Coarse Aggregate: 60%

Fine Aggregate: 40%

Percentage Replacement of RHA: 30%

Step 1: Calculate Cement Content (C):

C = (W / w/c)

C = (185 kg/m³ / 0.35)

C ≈ 528.57 kg/m³

Step 2: Calculate Rice Husk Ash (RHA) Content:

RHA Content = (30/100) * C

RHA Content = (30/100) * 528.57

RHA Content ≈ 158.57 kg/m³

Step 3: Adjust Cement Content with RHA:

Adjusted Cement Content = C - RHA Content

Adjusted Cement Content ≈ 528.57 - 158.57

Adjusted Cement Content ≈ 370 kg/m³

Step 4: Calculate Water Content:

Adjusted Water Content = W - (Superplasticizer Dosage * Adjusted Cement Content)

Adjusted Water Content = 185 - (0.015 * 370)

Adjusted Water Content ≈ 179.45 kg/m³

40% replacement calculation:

Coarse Aggregate: 60%

Fine Aggregate: 40%

Target Compressive Strength: 60 MPa

Water-Cement Ratio (w/c): 0.35

Water Content (W): 185 kg/m³

Maximum Aggregate Size: 20 mm

Superplasticizer Dosage: 1.5% of cement weight

Percentage Replacement of RHA: 40%

Step 1: Calculate Cement Content (C):

C = (W / w/c)

C = (185 kg/m³ / 0.35)

C ≈ 528.57 kg/m³

Step 2: Calculate Rice Husk Ash (RHA) Content:

RHA Content = (40/100) * C

RHA Content = (40/100) * 528.57

RHA Content ≈ 211.43 kg/m³

Step 3: Adjust Cement Content with RHA:

Adjusted Cement Content = C - RHA Content

Adjusted Cement Content ≈ 528.57 - 211.43

Adjusted Cement Content ≈ 317.14 kg/m³

Step 4: Calculate Water Content:

Adjusted Water Content = W - (Superplasticizer Dosage * Adjusted Cement Content)

Adjusted Water Content = 185 - (0.015 * 317.14)

Adjusted Water Content ≈ 179.74 kg/m³

50% replacement calculation:

Coarse Aggregate: 60%

Fine Aggregate: 40%

Percentage Replacement of RHA: 50%

Step 1: Calculate Cement Content (C):

C = (W / w/c)

C = (185 kg/m³ / 0.35)

C ≈ 528.57 kg/m³

Step 2: Calculate Rice Husk Ash (RHA) Content:

RHA Content = (50/100) * C

RHA Content = (50/100) * 528.57

RHA Content ≈ 264.29 kg/m³

Step 3: Adjust Cement Content with RHA:

Adjusted Cement Content = C - RHA Content

Adjusted Cement Content ≈ 528.57 - 264.29

Adjusted Cement Content ≈ 264.28 kg/m³

Step 4: Calculate Water Content:

Adjusted Water Content = W - (Superplasticizer Dosage * Adjusted Cement Content)

Adjusted Water Content = 185 - (0.015 * 264.28)

Adjusted Water Content ≈ 180.03 kg/m³

3.4.4 Determination of compressive strength

The compressive strength of the hardened concrete depends on the cement type, aggregate, cement-aggregate bond, water/cement ratio, mix ratio and the degree of compaction of plastic concrete.

The compressive strength of each sample was determined by dividing the average load each sample group by their corresponding nominal cross-sectional area.

The compressive strength is the most important property of concrete. The compressive strength of concrete is determined in the laboratory in controlled conditions. Based on the experiment result the quality of concrete was determined.
Using the Avery crushing machine the cubes were placed on the machine and the load was applied until the failure occurred and recorded accordingly.

A. Material quantities

A total of 144 cubes (72 cubes for water immerse curing and 72 cubes for ambient air curing). The whole cubes were divided into 6 groups (A – F) corresponding to the various cement percentage replacement of 0 – 50% at 10% increment (see table 3.3 below). In addition, 78 beams (18 controls and 60 experimental specimens), all air cured.

Table 3.3: Cube specimen classification

% Replacement	Cube Group	Days 7	14	21	28	Total
0	A	3	3	3	3	12
10	B	3	3	3	3	12
20	C	3	3	3	3	12
30	D	3	3	3	3	12
40	E	3	3	3	3	12
50	F	3	3	3	3	12

Table 3.4: Beam specimen classification

Group	Wi(mm)	S(mm)	L(mm)	b(mm)	a0(mm)/W	a0(mm)
1	102.00	381.00	481.00	76.00	0.290	29.580
2	102.00	381.00	481.00	76.00	0.320	32.640
3	102.00	381.00	481.00	76.00	0.460	46.920
4	102.00	381.00	481.00	76.00	0.520	53.040
5	102.00	381.00	481.00	76.00	0.620	63.240
6	102.00	381.00	481.00	76.00	0.670	68.340

Source: (Bucknor, *et al.*, 2020)

3.5 Three-Point Bending Test (TPBT)

Based on the optimum percentage replacement observed from the compressive strength test conducted, the results of 10 percent and 20 percent replacement concrete mixes were used to prepare 78 concrete beams (18 control beams inclusive) for fracture parameter test. Due to the laboratory set-up limitation, a modified TPFM was adopted. As discussed in chapter two, this model focus on the peak load, as such, an experimental set-up is arranged to capture the maximum load a beam will stand before failure. Thus, the TPBT experimental set-up was adopted in this regard (see Figure 2.10 in the Appendix).

The RILEM TC 50-FMC standard is an international standard method developed by the RILEM Technical Committee 50 (TC 50) for obtaining fracture mechanics parameters, such as fracture toughness and crack initiation strength. The standard consists of a number of tests that must be performed in a strictly controlled environment. The experiment typically begins with a preparation of the sample materials. This includes preparing the test specimen to the dimensions specified by the TC 50-FMC standard. This will involve grinding or polishing the sample surface with an abrasive cloth and subsequent cleaning with a solvent.

The specimen is then loaded into the testing apparatus. This usually comprises an Instron universal testing machine or other suitable device. The loading rate is then set to the pre-determined value of 10 mm/min as specified by the TC 50-FMC standard. The specimen is then loaded to the fracture toughness or crack initiation strength value required. Once the test is completed, the resulting strain and displacement values can be used to calculate the fracture toughness or crack initiation strength. These values can then be compared with the minimum standards specified by the TC 50-FMC standard. Finally, the test data is checked for accuracy and repeatability. This is done by comparing results with similar specimens and those obtained previously. If the results meet the minimum requirements specified by the standard, the specimen is accepted. In the event of any discrepancies, the experiment must be repeated to verify the results.

Recommended test and analysis procedure

A test and analysis procedure for the proposed peak load method is summarized as follows:

i. Prepare fracture specimens (notched beams and or notched cylinders) and cylindrical specimens for the compressive strength. Fracture test specimens are grouped according to specimen shape, specimen size and notch length. When all the fracture test specimens are of the same shape and same size, the notch length distinguishes specimen groups. There should be at least three groups of fracture test specimens.

ii. Conduct fracture tests of all the specimens and record the peak load in each test. Conduct compression tests for the elastic modulus E. if the lab is not able to measure E, obtain the compressive strength f'c from the compressive test.

iii. Calculate the average of the peak-load values from the specimens of the same group. If E is not obtained in step ii, calculate it from the compressive strength f'c (in unit of MPa) using the formula in the ACI Building Code: $E = 0.043w^{\frac{3}{2}}f'^{\frac{1}{2}}$ in MPa, where w is the unit weight of concrete in kg/m^3 or $E = 0.043w^{\frac{3}{2}}f'^{\frac{1}{2}}$ in MPa for normal weight concrete.

iv. Calculate $k_{ic}^{s}$and $CTOD_C$ for a series of assumed values of the critical effective crack length a_c for the specimen under the average peak-load for one specimen-group. A spread program on the personal computer is suggested for this and following steps. The first column of the spreadsheet be filled by assumed critical crack length a_c and the following columns be filled by the formulas for k_{ic}^{s} and $CTOD_C$as a function of a_c

v. Correlate $CTOD_C$ and k_{ic}^{s} corresponding to the same value of crack length a_c to establish a function for $CTOD_C$ in terms of k_{ic}^{s}

vi. Repeat steps iv and v for other specimen groups.

vii. Calculate the average $CTOD_C$- k_{ic}^{s} curve for all specimen groups

viii. Calculate values of s^2 values using Eq $E = 0.043w^{\frac{3}{2}}f'^{\frac{1}{2}}$. Find out the minimum of s^2.

ix. The k_{ic}^{s}value corresponding to the minimum s^2 is the solution k_{ic}^{s}. Substituting the obtained k_{ic}^{s} into the average $CTOD_C$- k_{ic}^{s} curve to determine the value $CTOD_C$.

Plate 3.4: Three-point bending test

CHAPTER FOUR
RESULTS AND DISCUSSION

4.1 Preamble

This chapter aims at discussing the results of the various tests done. Essentially, the whole experimental programme was divided into two phases aside the preliminary tests done on the materials and related concrete tests. In the initial phase of the work, varying RHA percentages ($0\% \; to \; 50\%$) were used to supplement cement in the production of HSC with the aim of finding the optimal cement percentage replacement without compromising the strength of the concrete. In the next phase of this study, with help of fracture mechanics, the fracture parameters of the HSC based on optimal cement percentage replacement were studied. Given the laboratory limitation with respect to fracture mechanics experiment on concrete. For the experimentation involving fracture parameters, the method employed was based on the paper titled "Simple Method for Determining Material Fracture Parameters from Peak Loads" by (Tang, Ouyang, and Shah, 1996).

To make the RHA more effective in the concrete mix, it was finely ground to create a larger surface area. This helps the RHA react better with the other materials in the mix. Additionally, a substance called high range water reducer (HRWR) was added to the mix. This makes the concrete easier to work with and helps the pozzolan in the mix to hydrate more effectively. In other to determine the optimum percentage replacement of RHA in the concrete mix, a total of 72 cubes were cast for 0 – 50% replacement for 7, 14, 21 and 28 days respectively. The BRE/DoE design guide was adopted for the laboratory trial mixes to produce grade M60 concrete and necessary adjustments were made to arrive at the needed mixed design.

Based on the compressive strength result, 10 and 20 percentage replacement were chosen for the second phase of the experiment given their compressive strength close agreement with the control mix value of 60MPa. As such, the fracture performances of

the two mixes were evaluated and compared with that of the control mix with the aim of understanding the fracture characteristics of RHA-based HSC.

4.2. Preliminary tests and results

This section aims to discuss the test results of the various preliminary tests conducted to understand the characteristics of the materials used for the experimental studies.

4.2.1. Sieve analysis

The aim of the sieve analysis is to understand the aggregate particle size distribution to check its compliance to ACI 363R-10 report recommendations on the selection of materials for HSC. Given the critical contribution of aggregate in HSC, it is essential to carefully selectaggregate for HSC production.

A. Sieve analysis of fine aggregate

Figure 11 Appendixsummarires the sieve analysis of the Fine aggregate. The initial weight of the soil sample was 1200g and the final sample weight is 1189.10g with a 0.90% deviation from the initial sample weight. Given the percentage deviation being less than 1%, this result is within the acceptable standards.

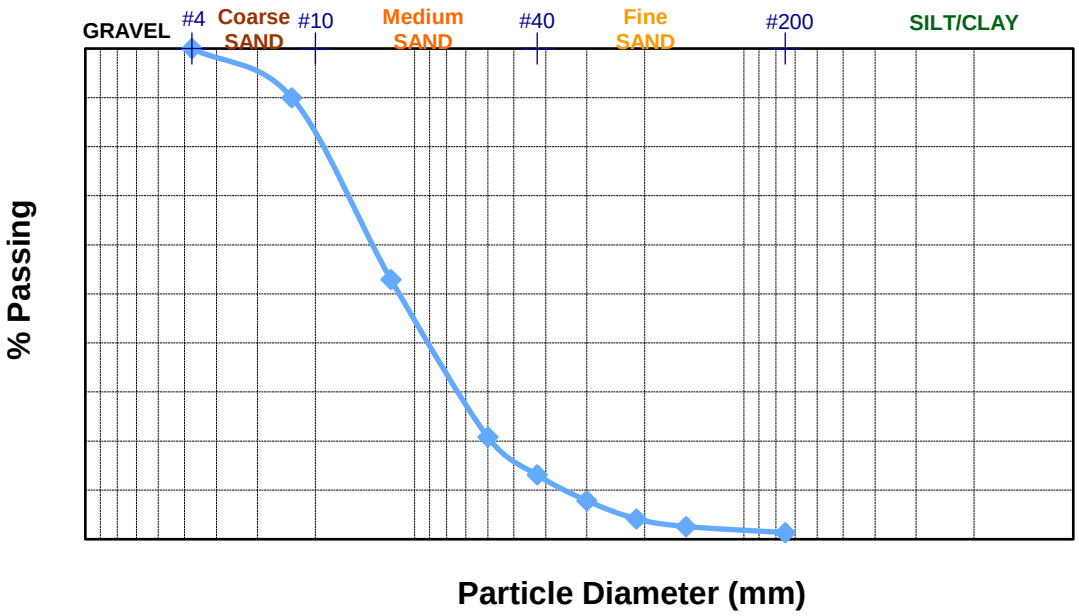

Figure 4.1: Fine aggregate sieve analysis

The test results indicate that the largest amount of aggregate stayed at a size of 1.18mm, representing 37.08% of the total weight. Going by the results data summarized, it can be inferred that the soil sample is well graded given the particle sizes distribution in the sample. As stated in the preceding chapters, particle size distribution of the fine aggregate has a significant influence on void content and invariably impact the overall strength of the concrete.

B. Sieve analysis of coarse aggregate

Figure 4.2 in the Appendix, it summarises the result of the coarse aggregate with respect to particle size distribution. With the result, the weight of the aggregate after the experiment was recorded to be 4998.40g with 0.032% deviation of the initial sample weight. Given the percentage deviation being less than 1%, this result is within the acceptable standards. The particles in the size range of 10-20mm make up 83.04% of the sample weight, and there is only a small amount of fine aggregate present. Because of this, the impact of the fine aggregate on the properties of the concrete is very small. However, if there is a lot of fine aggregate mixed in with the larger particles, it will affect the amount of water needed for the mix, which can then impact the strength of the concrete.

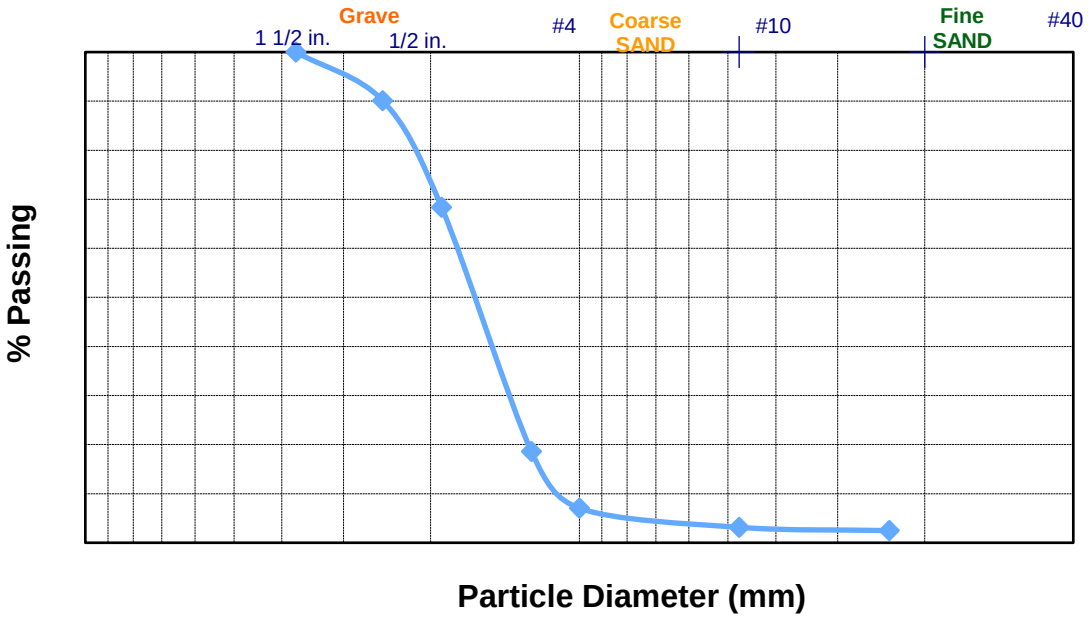

Figure 4.2: Coarse aggregate Sieve analysis

4.3. Rice Husk Ash (RHA)

As discussed in chapter 2, the RHA adopted was closed furance at a controlled temprature. As earlier discussed, the nature of the ash formed is a function of the combustion temperature. Given numerous researches conducted on the use of RHA in concrete production, the amorphous silicate dominant RHA has been proven to be more pozzolanic reactive compared to the crystalline type. The chemical structure (XRD) of the RHA conducted shows it contains a more non-crystalline form of silicate (see Figure 13). In view of this, (Della, Kuhn, and Dachamir, 2002) pointed out that the surface area of the RHA can be improved with wet milling. So, to follow this suggestion, the RHA was ground into smaller particles to make its surface area larger.

In this research, different amounts of RHA were used to replace cement, ranging from 0% to 50%, with increments of 10%. The goal was to find the best amount of replacement that would work well in the concrete mix. And fracture mechanic analysis was explored to further understand the fractural characteristics of optimum replacement concrete.

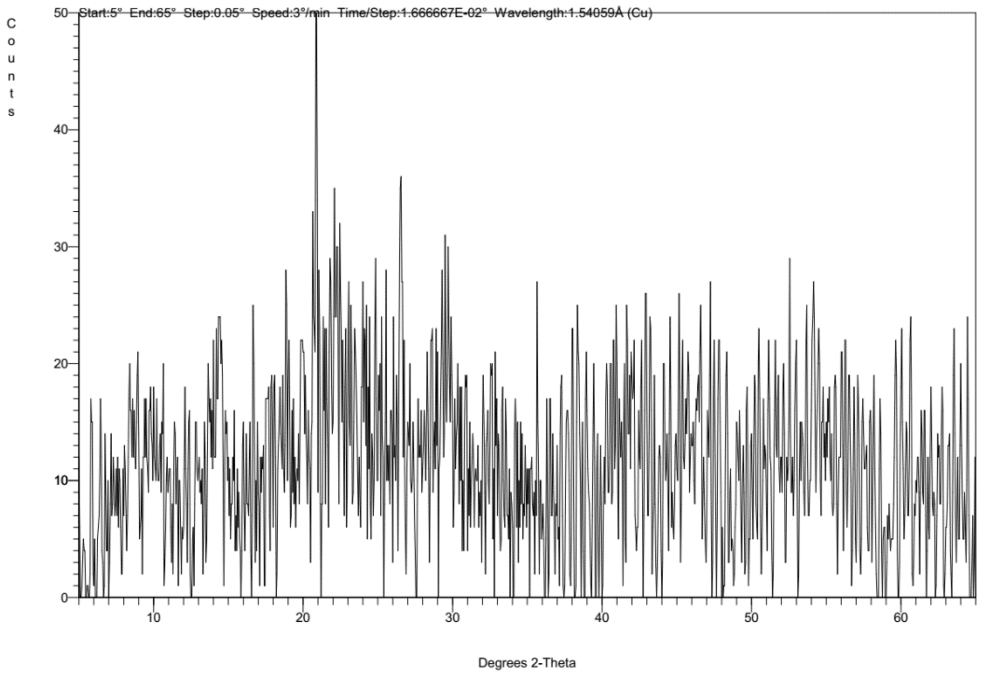

Figure 4.3: X-Ray Diffraction (XRD) analysis for RHA after milling.

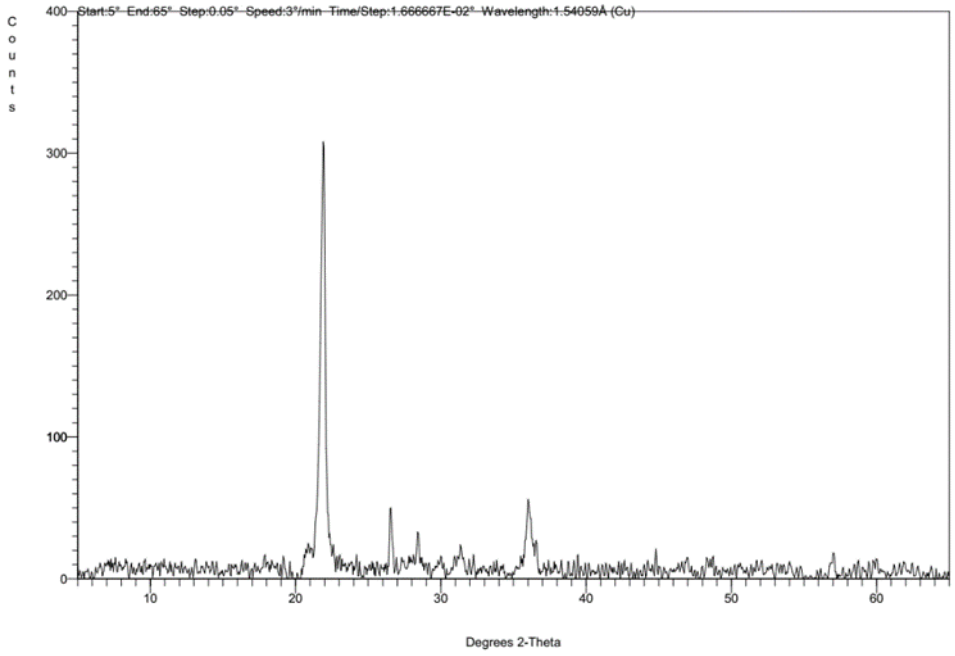

Figure 4.4: X-Ray Diffraction (XRD) analysis for RHA before milling.

4.4. Concrete compressive strength test

For the compressive test, six batches of concrete were prepared. The first batch was a regular mix without any rice husk ash, serving as a reference. The other five batches had different amounts of unmilled rice husk ash added, at 10%, 20%, 30%, 40%, and 50%.

Figure 15 in the results shows a comparison of the compressive strength test between the regular mix (the reference) and the concrete mixes with varying amounts of unmilled rice husk ash. The tests were conducted at room temperature and the results were recorded after 28 days.

It's important to note that the percentage of RHA replacement is measured based on the weight of the total cement material.

Additionally, Figure 4.7 in Appendix shows the first compressive test conducted between the regular mix and the concrete mixes with different amounts of RHA at room temperature for 28 days.

The results clearly indicate that as the percentage of RHA replacement increases, the compressive strength of the concrete with unmilled RHA decreases. However, it was observed that the strength of the concrete cubes increases as the number of days goes by.

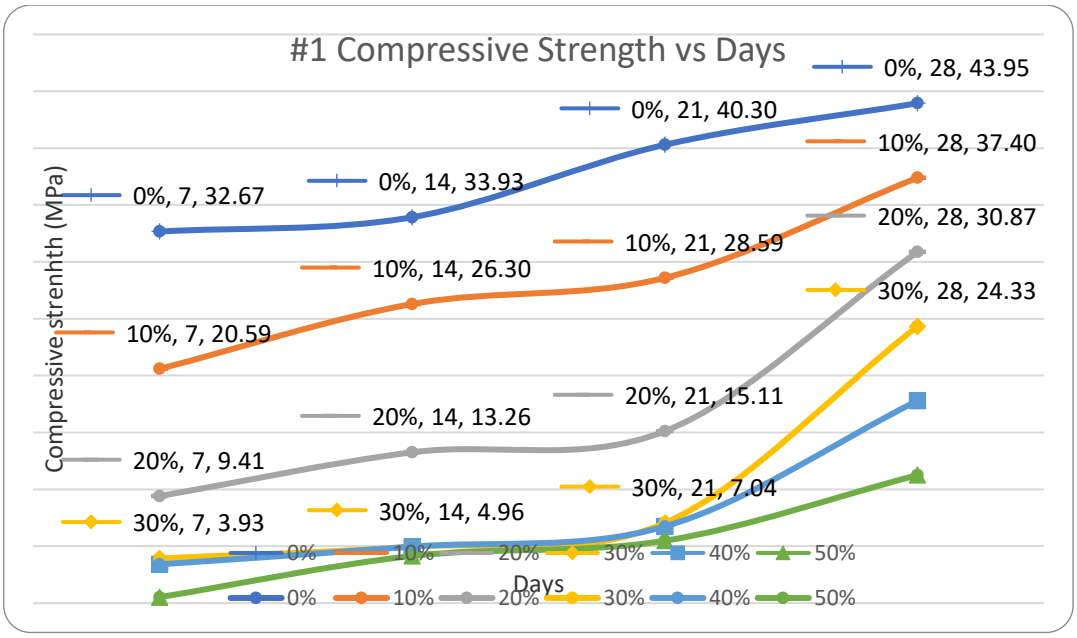

Figure 4.5: Unmilled RHA compressive strength

The unmilled did not meet the target strength due to the crystalline content of the structure responsible for the week pozzolanic properties. The high crystalline structure for our unmilled RHA resulted in low pozzolanic reactivity affecting the lowering the compressive strength (Hwang and Wu, 1989; Muthadhi, 2010; (Khalaf and Yousif, 1984) presented that pozzolanic activity improves as the specific surface area increases. (Della, Kuhn, and Dachamir, 2002) stated that the surface area of the RHA can be improved with wet milling, based in this wet milling was done to improve our RHA structure.

In the second compressive test, we conducted six batches of concrete. The first batch served as a reference and did not contain any rice husk ash (RHA). The other five batches included different amounts of milled rice husk ash, namely 10%, 20%, 30%, 40%, and 50%.

Figure 16 in the Appendix displays a comparison between the compressive strength test results of the reference mix and the concrete mixes with varying percentages of milled RHA. These tests were conducted at room temperature and the results were recorded after 28 days.

We observed that the compressive strength steadily increased and reached its highest point at the 10% RHA mix. However, from the 10% to the 20% mix, the strength started to decrease. Nonetheless, the results for the 20% mix were very close to our target strength.

The data also showed that the strength of the concrete increased as the number of days passed for each batch.
Furthermore, in Figure 18 in the Appendix, you can find the results for the unit weight of the different concrete mixes with varying percentages of RHA replacement.

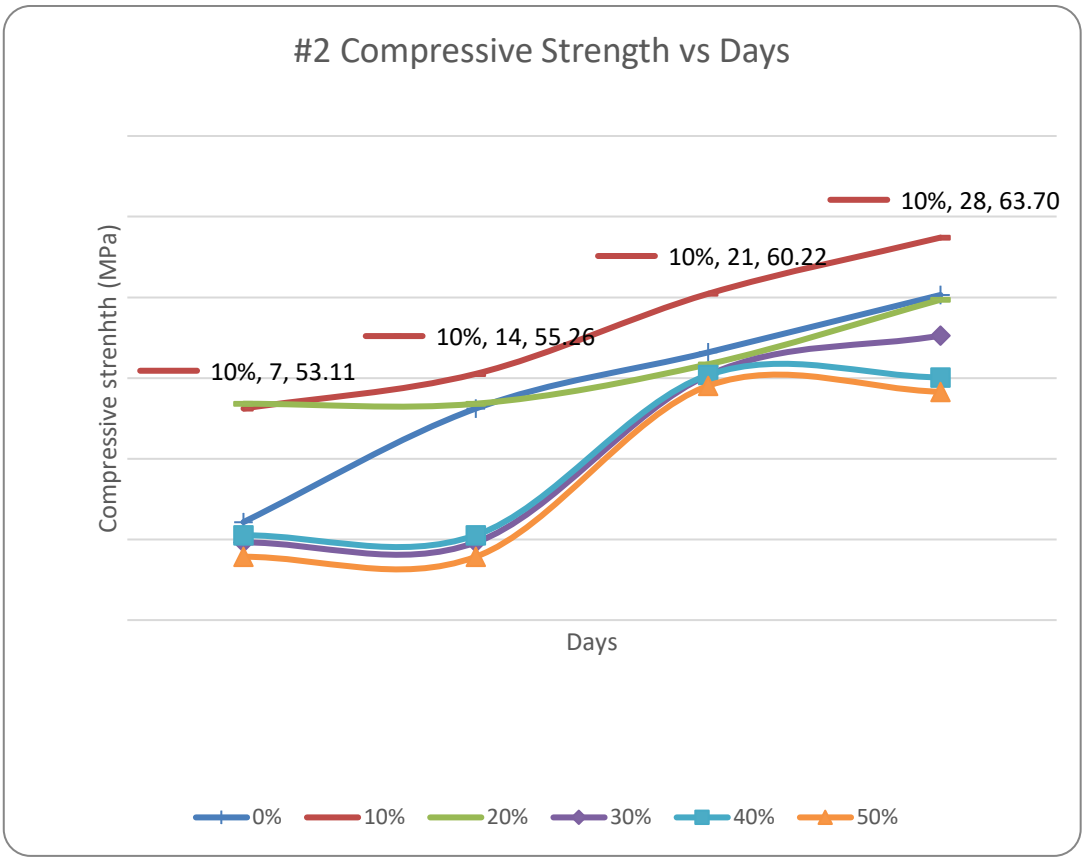

Figure 4.6: Milled RHA compressive strength

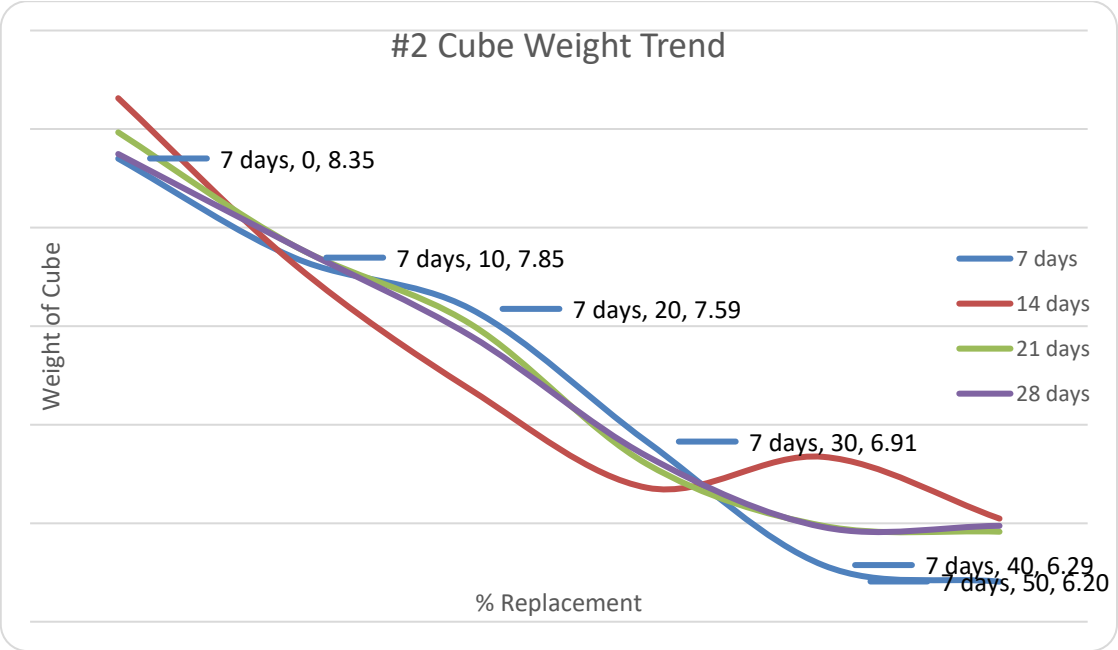

Figure 4.7: Unit weight for milled RHA concrete

4.5. Fracture parameter analysis

As mentioned in the earlier sections, the fracture parameters of the concrete structure were determined using the method outlined in the publication titled "Simple Method for Determining Material Fracture Parameters from Peak Loads" by (Tang, Ouyang and Shah, 1996). This approach was selected based on its applicability. Referring to the compressive test outcomes, as depicted in Figure 19 Appendix, further analysis was conducted. It was observed that the compressive strength increases progressively and peaked at 63.70MPa at 10%. However, the 20% replacement shows promises with a compressive strength of 59.85MPa. As such, Fracture parameter analysis was conducted on the two replacement percentages along with the control to further understand their fractural characteristics of the concrete mixes.

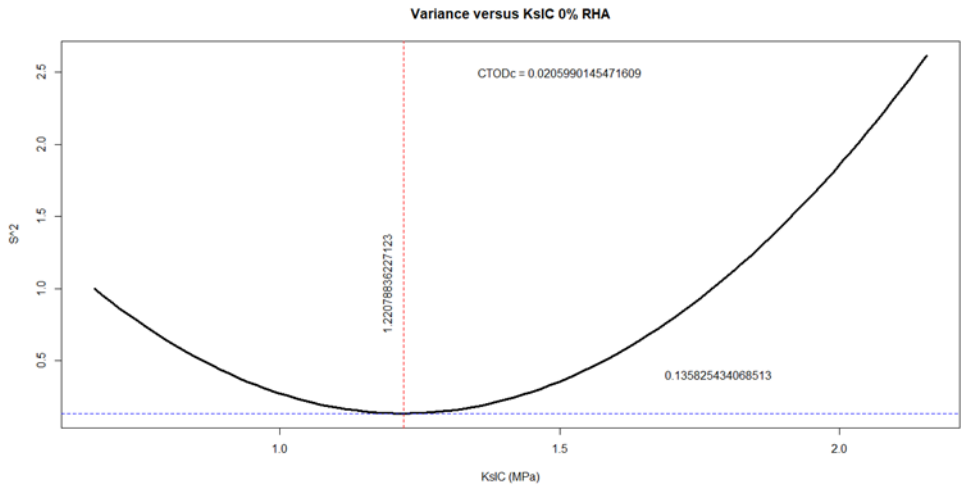

Figure 4.8: $CTOD_c$ and K^S_{IC} for 0% RHA

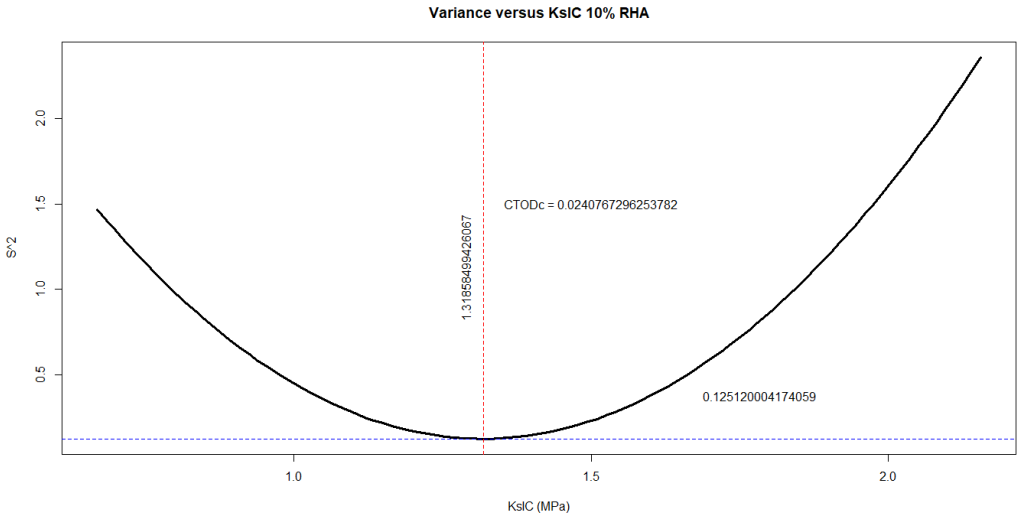

Figure 4.9: CTODc and KSIC for 10% RHA

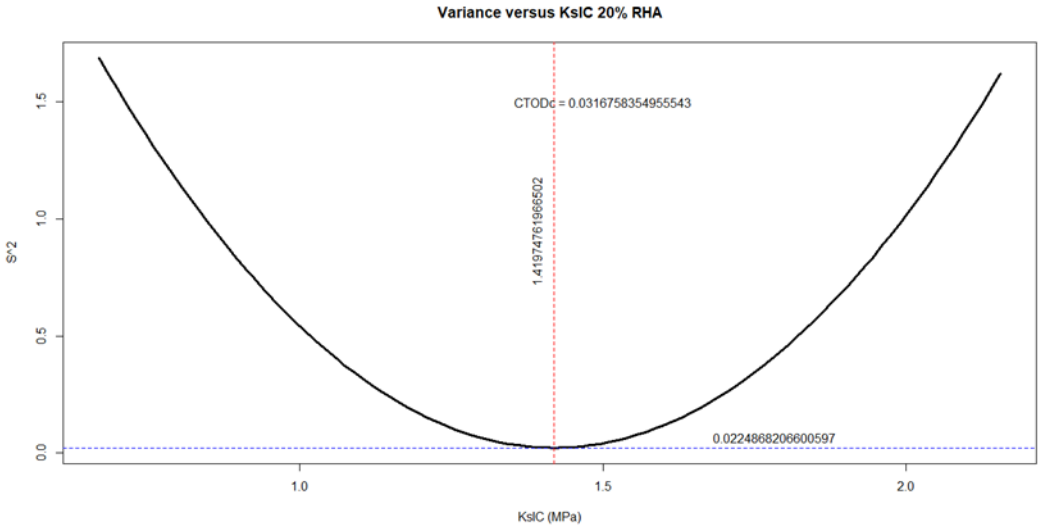

Figure 4.10: CTODc and KSIC for 20% RHA

In total, 78 beams were used in the study, with 18 beams serving as the control group, 30 beams for the 10% replacement group, and 30 beams for the 20% replacement group. The beams were divided into six groups based on the TPM experimental procedure recommendation by (Rafai and Swartz, 1987) for three-point bending testing.

The beams were subjected to load according to standard three-point bending test and the peak load responsible for each beam were recorded and shown in Figure 20 and 21 in the Appendix. The beams were further classified into A, B and C to correspond to the 10%, 20%, and the control respectively.

After considering the average peak load data mentioned earlier, it was observed that the first three beam classes exhibited statistical significance. Hence, these classes were selected for further analysis in the subsequent stage. By calculating the average peak loads for each class, as depicted above, the derived average loads were utilized in conjunction with the Linear Elastic Fracture Mechanics (LEFM) equations displayed below for the subsequent analysis. Part of the steps is the Calculation the $\boldsymbol{K_{IC}^{S}}$ also the$\boldsymbol{CTOD_c}$from asequence of presumedvalue for $\boldsymbol{a_c}$ (see Table 4.2)

Table 4.1: Beam peak load

Sample Classification	P_{max} (N) 1	2	3	4	5	P_{max} (N)Avg
A1	2567.49	2576.81	2593.43	2425.37	2526.95	2538.01
A2	2569.67	2664.60	2528.04	2580.24	2527.61	2574.03
A3	1689.53	1405.58	1371.80	1550.05	1417.27	1486.84
A4	1027.40	969.31	938.87	900.84	925.43	952.37
A5	775.01	783.59	752.01	814.93	674.69	760.05
A6	281.18	409.91	352.76	297.72	390.05	346.32
B1	2484.84	2360.14	2517.22	2328.24	2481.28	2434.34
B2	2437.33	2493.70	2537.11	2394.55	2552.28	2482.99
B3	1370.98	1440.91	1493.69	1462.61	1342.14	1422.07
B4	765.93	706.21	699.75	715.49	706.04	718.68
B5	632.16	597.48	541.77	671.49	505.57	589.69
B6	270.12	297.38	299.88	340.90	257.76	293.21
C1	-	-	2416.07	2346.89	2377.27	2380.08
C2	-	-	2485.95	2491.73	2365.28	2447.65
C3	-	-	1421.28	1412.53	1437.96	1423.92
C4	-	-	1005.96	971.10	1013.09	996.71
C5	-	-	695.04	719.31	743.60	719.32
C6	-	-	341.23	372.58	300.30	338.04

Table 4.2: K_{IC}^{s} and $CTOD_c$ based on presumeda_c (Class A1)

S/N	W(m)	S(m)	B(m)	f'c (MPa)	a0 (m)	ac (m)	Pmax (N)Avg	K^{s}_{IC} (MPa)	$CTOD_C$ (mm)
1	0.102000	0.381000	0.07600	60.15	0.029580	0.056100	2380.08	1.150960	0.019522
2	0.102000	0.381000	0.07600	60.15	0.029580	0.056233	2380.08	1.156167	0.019696
3	0.102000	0.381000	0.07600	60.15	0.029580	0.056365	2380.08	1.161410	0.019872
4	0.102000	0.381000	0.07600	60.15	0.029580	0.056498	2380.08	1.166691	0.020050
5	0.102000	0.381000	0.07600	60.15	0.029580	0.056630	2380.08	1.172009	0.020229
6	0.102000	0.381000	0.07600	60.15	0.029580	0.056763	2380.08	1.177365	0.020410
7	0.102000	0.381000	0.07600	60.15	0.029580	0.056896	2380.08	1.182759	0.020593
8	0.102000	0.381000	0.07600	60.15	0.029580	0.057028	2380.08	1.188192	0.020777
9	0.102000	0.381000	0.07600	60.15	0.029580	0.057161	2380.08	1.193665	0.020963
10	0.102000	0.381000	0.07600	60.15	0.029580	0.057293	2380.08	1.199176	0.021151

NB: See full table in the appendix section

According to Tang, Ouyang, and Shah, (1996), the values of X and Y are utilized in a simple linear regression model to establish the relationship between X and Y. The resulting function is presented:

$$y = \boldsymbol{a} + \boldsymbol{bx} \tag{4.1}$$

$$\boldsymbol{b} = \frac{\boldsymbol{N}\sum \boldsymbol{xy} - (\sum \boldsymbol{x})(\sum \boldsymbol{y})}{\boldsymbol{N}\sum \boldsymbol{x^2} - (\sum \boldsymbol{x})^2} \tag{4.2}$$

$$a = \frac{\sum \boldsymbol{y} - \boldsymbol{b}\sum \boldsymbol{x}}{\boldsymbol{N}} \tag{4.3}$$

Using$\boldsymbol{K_{IC}^s}$as **x** and $\boldsymbol{CTOD_c}$as **y**, the purpose of$\boldsymbol{CTOD_c}(\boldsymbol{K_{IC}^s})$for the corresponding classes were shown as follows.

$$\boldsymbol{CTOD_c}(\boldsymbol{K_{IC}^s}) = \boldsymbol{0.0382K_{IC}^s - 0.0250} \tag{4.4}$$

$$\boldsymbol{CTOD_c}(\boldsymbol{K_{IC}^s}) = \boldsymbol{0.0364K_{IC}^s - 0.0251} \tag{4.5}$$

$$\boldsymbol{CTOD_c}(\boldsymbol{K_{IC}^s}) = \boldsymbol{0.0282K_{IC}^s - 0.0136} \tag{4.6}$$

In Eqs. (4.4), (4.5) and (4.6), similar values of $\boldsymbol{K_{IC}^s}$altered in the equations. The mean of the equivalent$\boldsymbol{CTOD_c}$ and the revised $\boldsymbol{(s^2)}$ (see Table 4.3 below).

Table 4.3: Calculated Average $CTOD_c$ and variance S^2 (Partial table)

K_{IC}^s (MPa)	$CTOD_c$ (Group 1)	$CTOD_c$ (Group 2)	$CTOD_c$ (Group 3)	Average	S^2
0.6700000	0.0005940	-0.0007120	0.0052940	0.0017253	0.997794533
0.6850000	0.0011670	-0.0001660	0.0057170	0.0022393	0.951484633
0.7000000	0.0017400	0.0003800	0.0061400	0.0027533	0.906453333
0.7150000	0.0023130	0.0009260	0.0065630	0.0032673	0.862700633
0.7300000	0.0028860	0.0014720	0.0069860	0.0037813	0.820226533
0.7450000	0.0034590	0.0020180	0.0074090	0.0042953	0.779031033
0.7600000	0.0040320	0.0025640	0.0078320	0.0048093	0.739114133
0.7750000	0.0046050	0.0031100	0.0082550	0.0053233	0.700475833
0.7900000	0.0051780	0.0036560	0.0086780	0.0058373	0.663116133
0.8050000	0.0057510	0.0042020	0.0091010	0.0063513	0.627035033

NB: See full table in the appendix section

By employing a multiple linear regression model, we can establish a function to describe the relationship between various variables. $\boldsymbol{S^2}(\boldsymbol{K_{IC}^s})$ can be developed utilizing the$\boldsymbol{K_{IC}^s}$, S^2 of$\boldsymbol{K_{IC}^s}$as variables. As such, the Eq (4.7) beneath was acquired proving a nonlinear connection linking $\boldsymbol{S^2}$and$\boldsymbol{K_{IC}^s}$ **(group A)**

$$\boldsymbol{S^2}(\boldsymbol{K_{IC}^s}) = \mathbf{2.8413}(\boldsymbol{K_{IC}^s})^{\mathbf{2}} - \mathbf{6.9373}(\boldsymbol{K_{IC}^s}) + \mathbf{4.3703} \quad (4.7)$$

From this relationship above, the minimum of the curve $\boldsymbol{S^2} - \boldsymbol{K_{IC}^s}$. The variable "matches to the $\boldsymbol{K_{IC}^s}$that characterizes the entire material. The following equation represents the linear regression model involving the average value of the variable. $\boldsymbol{CTOD_c}$ and $\boldsymbol{K_{IC}^s}$when used it can find the $\boldsymbol{CTOD_c}$ for the material.

To ensure the creation of precise models, an R-programming code was utilized to develop and solve the linear regression relationships. Based on the findings presented in Appendix, it was observed that both the $\boldsymbol{CTOD_c}$ and $\boldsymbol{K_{IC}^s}$ increase as the percentage of RHA increases, with 20% RHA demonstrating the highest values.

CHAPTER FIVE

CONCLUSION AND RECOMMENDATIONS

5.1 Conclusion

Referring to the research questions in chapter one

1. Is the efficacy of the fracture parameter of concrete produced from a rice husk ash–cement mixture in relation to accepted standards worthy of consideration?
2. What are the economic and environmental implications of utilizing rice husk ash in concrete fabrication?
3. Is it possible to gain a more comprehensive understanding of the structural characteristics of high-strength concrete formulated from rice husk ash?

The compressive testing process was conducted to analyse the effects of different percentages of RHA on the compressive strength of the material, with the percentages of RHA ranging from 0% to 50%. Data was then collected and analysed to determine the compressive strength of the material at each RHA percentage. The following conclusions were deduced from the results:

A. Investigation of RHA in HSC blends:

- The study showcased that incorporating RHA as a replacement in concrete enhances the compressive strength. The concrete realized its pinnacle strength at 63.70MPa with a 10% RHA substitution.

B. Fracture mechanics parameters:

- Analysis revealed a direct correlation between RHA percentage and the compressive strength of the beam. The highest of average compressive strength was attained with 10% RHA.
- Exploration of fracture parameters in HSC with RHA replacements of 0%, 10%, and 20% showcased a positive correlation, especially in the Critical Stress Intensity Factor and Crack Tip Opening Displacement (CTOD). The modified Three-Point Method (TPM) from Tang, Yang, and Zollinger (1999) was instrumental in this assessment.

C. Ecological outlook

- The upward trend in CTOD with increased RHA percentage underscores the potential economic viability of RHA as a cement substitute, given its performance benefits.
- Additionally, using RHA, an agricultural waste product, in cementitious materials not only offers strength benefits but also promotes sustainable and eco-friendly construction practices.

5.2 Recommendations

Based on the research findings, below are the recommendations:

- Further research to determine the optimal percentage of RHA in HSC blends to achieve the target strength and other desirable properties.
- Implement stringent quality control measures during HSC production to ensure consistency and predictability of RHA-based concrete properties.
- Consider exploring other replacement percentages beyond 0%, 10%, and 20% to understand the full spectrum of performance variations.
- Dive deeper into the mechanisms by which RHA improves crack resistance to develop even more resilient concrete blends.
- Conduct a cost-benefit analysis to understand the economic implications of adopting RHA in HSC blends on a large scale.
- Investigate different methods of processing Rice Husk Ash to determine if variations in processing can impact the properties of the resulting HSC.

5.3 Contributions to knowledge

The following are the contribution to knowledge:

- Sustainable utilization of Rice Husk Ash (RHA) in High-Strength Concrete (HSC) promotes eco-friendly construction
- Detailed analysis of fracture parameters, such as KIC and CTOD, in HSC with RHA blends enhances understanding of its mechanical behavior.
- Exploration of strength variations with RHA replacements provides a foundation for future optimizations.
- A model for the prediction of CTOD and Kic for RHA HSC was developed.

- Comparative study of 0%, 10%, and 20% RHA replacements offers a comprehensive view of RHA's effect on concrete performance.

5.4 Further research

Given the promising findings from this study related to the fracture mechanics of High-Strength Concrete (HSC) with Rice Husk Ash (RHA) blends, the following areas are suggested for further investigation:

- **Microscopic analysis**: Utilize advanced microscopic techniques to observe the fracture process zone and micro-cracks within the RHA-HSC matrix. This could provide a deeper understanding of the initiation and propagation of fractures at the micro-level.
- **Dynamic loading**: Investigate the response of RHA-HSC under dynamic or cyclic loading conditions to understand fatigue and its implications on fracture behavior.
- **Temperature effects**: Explore how different temperature conditions, including freeze-thaw cycles, impact the fracture toughness and resistance of RHA-HSC.
- **Interaction with other admixtures**: While this study focused on RHA, it would be interesting to see how the fracture mechanics parameters behave when RHA is used in conjunction with other admixtures or supplementary cementitious materials.
- **Size effect on fracture**: Examine the size effect on fracture to determine if there's a scale dependency on the fracture mechanics of RHA-HSC.
- **Numerical modeling**: Develop advanced numerical models to simulate the fracture behavior of RHA-HSC, which can be validated against experimental results and used for predictive purposes in more complex structures.
- **Fracture toughness over time**: It would be beneficial to understand how the fracture toughness of RHA-HSC evolves over time, especially as the concrete ages and undergoes various environmental exposures.

REFERENCES

ACI Committee 211. 2008. Guide for Selecting Proportions for High-Strength Concrete with Portland Cement and Fly Ash. ACI 211.1-91. American Concrete Institute, Farmington Hills, MI.

ACI Committee 212. 2010. Report on Chemical Admixtures for Concrete. ACI 212.3R-10. American Concrete Institute, Farmington Hills, MI.

ACI Committee 232. 1996. Use of Fly Ash in Concrete. ACI 232.2R-96. American Concrete Institute, Farmington Hills, MI.

ACI Committee 232. 2012. Use of Raw or Processed Natural Pozzolans in Concrete. ACI 232.1R-12. American Concrete Institute, Farmington Hills, MI.

ACI Committee 234. 1996. Guide for the Use of Silica Fume in Concrete. ACI 234R-96. American Concrete Institute, Farmington Hills, MI.

ACI Committee 363. 2010. High-Strength Concrete. ACI 363R-10. American Concrete Institute, Farmington Hills, MI.

ACI Committee 363R. 1992. State-of-the-Art Report on High-Strength Concrete. ACI 363R-92. American Concrete Institute, Farmington Hills, MI.

Adesina, A. 2020. "Recent Advances in the Concrete Industry to Reduce its Carbon Dioxide Emissions." Environmental Challenges 1: 100004. ISSN 2667-0100. https://doi.org/10.1016/j.envc.2020.100004

National Food Security Programme (NFSP). October 2008. Report of 2007 Agricultural Production Survey (APS). Federal Ministry of Agriculture and Water Resources.

Akande, 'Tunji, 2013. "An Overview of the Nigerian Rice Economy." Institute for Agriculture and Trade Policy. Accessed July 16, 2013. https://www.iatp.org/sites/default/files/451_2_70045.pdf.

Akinluyi, M., and Adeleye, O. 2013. "The Building Industry in the Housing Programme: Technology, Materials, and Labour Towards Addressing Housing Shortage in Nigeria." European Centre for Research Training and Development UK

Akinyoade, A., and Uche, C.. 2016. "Dangote Cement: An African Success Story?" ASC Working Paper 131. African Studies Centre, Leiden. Accessed August 25, 2014. https://core.ac.uk/download/pdf/388662808.pdf.

Akpokodje, G., Lançon, F., and Erenstein, O. 2001. "Nigeria's Rice Economy: State of the Art." In The Nigerian Rice Economy in A Competitive World: Constraints and Opportunities, Project Report.

Ali, M. B., Rahman Saidur, and M. S. Hossain. "A review on emission analysis in cement industries." Renewable and Sustainable Energy Reviews 15, no. 5 (2011): 2252-2261.

ASTM C1602/C1602M. 2006. Standard Specification for. Mixing Water Used in the Production of Hydraulic Cement Concrete. ASTM.

Ayanwale, A., Akinyosoye, V., Yusuf, S., and Oni, A. 2011. Rice Supply Response in Nigeria; whither changing Policies and Climate.

Bajaber, M. A., and I. Y. Hakeem. 2021. "UHPC evolution, development, and utilization in construction: A review." Journal of Materials Research and Technology 10 (2021): 1058-1074.

Barua, D., Rahman, M. M., Chowdhury, M. W., Abul Hasan, M. D., and Mohiuddin, M. A. 2018. Effectiveness of rice husk ash (RHA) as a partial replacement of cement in concrete.

Barger, Gregory M., Allen J. Hulshizer, Sandor Popovics, Bayard M. Call, Tarif M. Jaber, Jan Prusinski, Ramon L. Carrasquillo et al. "Use of Raw or Processed Natural Pozzolans in Concrete." ACI Committee 232 (2001). Kesler, C., Naus, D., and Lott, J. 1972. Fracture mechanics: its applicability to concrete. Proceedings of the International Conference on Mechanical Behaviour of Materials,. The society of materials science, pp.113-124.

Bay-lynx. (n.d.). Admixtures in concrete. Retrieved from https://bay-lynx.com/education/admixtures-in-concrete/

Bažant, Zdenek P., Jia-Liang Le, and Marco Salviato. Quasibrittle fracture mechanics and size effect: A first course. Oxford University Press, 2021.

Beaumont , P. W. 2020. The Structural Integrity of Composite Materials and Long-Life Implementation of Composite Structures. The Structural Integrity of Composite Materials and Long-Life Implementation of Composite Structures.

Berntsson, L., Chandra, S., and Kutti, T. 1990. Principles and Factors Influencing High-Strength Concrete Production, Concrete International, December, pp.59-62.

Berto, F., and . Lazzarin, P. 2014. "Recent developments in brittle and quasi-brittle failure assessment of engineering materials by means of local approaches." Materials Science and Engineering: R: Reports 75 (2014): 1-48.

Béton, C. E.I. 1994. Fédération Internationale de la Précontrainte (CEB-FIP). Applications of High Performance Concrete", Bulletin d' Information, 65 pp.

Brown, D., Sadiq, R., and Hewage, K. N. 2014. An overview of air emission intensities and environmental performance of grey cement manufacturing in Canada.

Bucknor, A. O., Animashaun, F. M., Olutoge, F. A., Adetayo, O. A., Ajagbe, W. O., and Ikponmwosa, E. E. 2020. Investigating the fracture characteristics of Nigerian rice husk ash (rha) - based high strength concrete (hsc). International Journal of Civil and Structural Engineering Research, Vol. 8, Issue 1, pp: (122-129.

Carpinteri, Alberto. "Application of fracture mechanics to concrete structures." Journal of the Structural Division 108, no. 4 (1982): 833-848.

Carrasquillo, R. L. (1985. Production of High Strength Pastes, Mortars, and Concrete," Very High Strength Cement-Based Materials, Materials Research Society Symposia Proceedings, Vol. 42, pp.151-168.

Cervera, M., Barbat, G. B. Michele C., and Wu, J-Y.. 2022. "A comparative review of XFEM, mixed FEM and phase-field models for quasi-brittle cracking." Archives of Computational Methods in Engineering 29, no. 2 (2022): 1009-1083.

Chalee, W., T. Sasakul, P. Suwanmaneechot, and C. Jaturapitakkul. "Utilization of rice husk–bark ash to improve the corrosion resistance of concrete under 5-year exposure in a marine environment." Cement and concrete composites 37 (2013): 47-53.

Chauhan, Darshan R., Hridyesh R. Tewani, and J. S. Kalyana Rama. "Application of Principles of Linear Elastic Fracture Mechanics for Concrete Structures: A Numerical Study." Applied Mechanics and Materials 877 (2018): 282-288.

Chima, D. A., Elvis, M. M., and George, U. A. 2023. Evaluation of sisal fiber and aluminum waste concrete blend for sustainable construction using adaptive neuro-fuzzy inference system. Scientific Reports 13, no. 1 (2023): 2814.

Das, S., and Satyabrata C. 2019. "Influence of effective stiffness on the performance of RC frame buildings designed using displacement-based method and evaluation of column effective stiffness using ANN." Engineering Structures 197 (2019): 109354.

Das, Swagato, Purnachandra Saha, Swatee Prajna Jena, and Pratyush Panda. "Geopolymer concrete: Sustainable green concrete for reduced greenhouse gas emission–A review." Materials Today: Proceedings 60 (2022): 62-71.

Della, V., Kuhn, I., and Dachamir, H. 2002. Rice husk ash as an alternate source for active silica production. Materials Letters, 57(4), pp.818-821.

Denli, F. A., Osman G., Gerhard, A. H., and Hüsnü, D. 2020 "A phase-field model for fracture of unidirectional fiber-reinforced polymer matrix composites." Computational Mechanics 65 (2020): 1149-1166.

Dils, J., Boel, V., Aggoun, S., Kaci, A., and De Schutter, G. 2013. Effect of entrapped and entrained air on the workability and rheology of cementitious materials.

Etim, M.A., Babaremu , K., Lazarus, J., and Omole, D. 2021. Health Risk and Environmental Assessment of CementProduction in Nigeria.

"Fracture Mechanics." Wikipedia. Last modified August 25, 2023. Accessed May 25, 2023. https://en.wikipedia.org/wiki/Fracture_mechanics.

Fu, Le, Håkan, E., and Wei X. 2020 "Glass–ceramics in dentistry: A review." Materials 13, no. 5 (2020): 1049.

Gandage, A. S. 2020. "Admixtures in Concrete–A Review." In Construction Materials and Management, 67. NICMAR Publication, 2020.

Gdoutos, E. E. 2020. Fracture mechanics: an introduction. Vol. 263. Springer Nature, 2020.

George, T., and Komnitsas, K. 2004. Cement industry towards sustainability. Technical University of Crete, Hania, Greece, Department of Mineral Resources Engineering,. Meristem Security Limited,.

Habeeb, G. A., and Fayyadh, M. M. 2009. the Effect of RHA Average Particle Size on Mechanical Properties and Drying Shrinkage Australian. Journal of Basic and Applied Sciences, 3(3): 1616-1622,.

Heffer, K. 2015. "Percolation of the interacting elastic stress fields of aligned cracks as an alternative explanation of critical crack densities." Geological Society, London, Special Publications 409, no. 1 (2015): 31-47.

Hillerborg , A. 1985. Results of three comparative test series for determining the fracture energyG F of concrete. Materials and structures 18 (1985): 407-413.

Hillerborg, A. 1985. The theoretical basis of a method to determine the fracture energy G_f of concrete. . Mater Struct 18(4): 407-413.

Hiroshi, T., Paris, P. C., and George, R. I. (n.d.). The Stress Analysis Of Cracks Handbook. ASME PRESS.

https://mechanicalc.com/reference/fracture-mechanics. 2014. Retrieved from https://mechanicalc.com/reference/fracture-mechanics:

Hwang, C., and Wu, D. 1989. Properties of cement paste containing rice husk ash. Am. Concr.Inst. SP-114, pp.733–765.

ICE. 1990. CEB-FIP Model Code 1990. ICE. Design code. Thomas Telford Publishing, 1993.

Ighalo, J. O., & Adeniyi, A. G. (2020). A perspective on environmental sustainability in the cement industry. Waste Disposal & Sustainable Energy, 2(3), 161-164.

Initiative, T. C. 2002. Our agenda for action,. World Business Council for Sustainable Development, , page 20,.

IRRI, A. (2010). Global Rice Science Partnership (GRiSP). Council for Partnership on Rice Research in Asia: Metro Manila, Philippines.

Iskander, M., and Nigel, S. 2018. "Fracture of brittle and quasi-brittle materials in compression: A review of the current state of knowledge and a different approach." Theoretical and Applied Fracture Mechanics 97 (2018): 250-257.

Jamal, H. 2017. Types of Admixtures of Concrete and Cement. Chemical, Mineral. [online] Aboutcivil.org. Available at: https://www.aboutcivil.org/concrete-technology-admixtures.

Jenq, Y. S., and Shah. S. P. 1988. "Mixed-mode fracture of concrete." International Journal of Fracture 38 (1988): 123-142.

Jenq, Y., and Shah. S. 1985. Two Parameter Fracture Model for Concrete. Journal of Engineering Mechanics, 111(10),, pp.1227-1241.

Jenq, Y., and Shah, S. 1988a. Geometrical effects on mode I fracture parameters. Report to RILEM Committee 89-FMT.

Jin, H, and Shuo Y. 2022. "Study on corrosion-induced cracks for the concrete with transverse cracks using an improved CDM-XFEM." Construction and Building Materials 318 (2022): 126173.

Kanvinde, A. 2016. Predicting Fracture in Civil Engineering Steel Structures: State of the Art. ournal of Structural Engineering.

Kaplan, M. 1961. Crack propagation and the fracture of concrete." In Journal Proceedings, vol. 58, no. 11, pp. 591-610. 1961.

Karihaloo, Bhushan L. "Fracture mechanics & structural concrete." Longman Scientific and Technical (1995).

Khalaf, N., and Yousif, A. 1984. “Use of rice husk ash in concrete. International journal of cement composites and light weight composites,, Vol.6,, pp 241-248.

Krishnarao, R., and Mahajan, Y. 1996. Formation of SiC whiskers from raw rice husks in argon atmosphere. Ceramics International, 22(5),, pp.353-358.

Kumar, S., and Barai, S. V. 2012. Size-effect of fracture parameters for crack propagation in concrete: a comparative study. pp.1-19.

Lanh, H. S., and Huynh, T.P. 2023. Long-term mechanical properties and durability of high-strength concrete containing high-volume local fly ash as a partial cement substitution.

Larisch, M. D. 2011. Experience with high strength concrete for the foundation of a high rise building.

Li, Lin, Yuehua Liu, Wei Liu, Xiong Zhang, Jie Chen, Deyi Jiang, and Jinyang Fan. "Crack evolution and failure modes of shale containing a pre-existing fissure under compression." ACS omega 6, no. 39 (2021): 25461-25475. M. Nisbet; M. Marceau; M. VanGeem;. 2002. Environmental Life Cycle Inventory of Portland Cement Concrete.

Mahasenan, N., Smith, S., and Humphreys, K. 2003. The Cement Industry and Global Climate Change Current and Potential Future Cement Industry CO2 Emissions. Greenhouse Gas Control Technologies - 6th International Conference, , pp.995-1000.

Mahasenan, N., Smith, S., and Humphreys, K. (2003). The Cement Industry and Global Climate ChangeCurrent and Potential Future Cement Industry CO2 Emissions.

Malitckii, E., H. Remes, P. Lehto, Y. Yagodzinskyy, S. Bossuyt, and H. Hänninen. "Strain accumulation during microstructurally small fatigue crack propagation in bcc Fe-Cr ferritic stainless steel." Acta Materialia 144 (2018): 51-59.

Matouš, Karel, Marc GD Geers, Varvara G. Kouznetsova, and Andrew Gillman. "A review of predictive nonlinear theories for multiscale modeling of heterogeneous materials." Journal of Computational Physics 330 (2017): 192-220.

Mehta, P. (1979). chemistry and technology of cement made from rice husk ash. Proceedings UNIDO/ESCAP/RCTT Workshop on Rice Husk Ash Cements, Peshawar, Pakistan. Regional Centre for Technology Transfer, Bangalore (India), pp. 113–22.

Mehta, P. K. (1986). Concrete structure, properties, and materials, . Prentice-Hall, Englewood Cliffs, N.J., pp. 266, 273.

Mehta, P., and Aïtcin, P. (1990). “Principles Underlying Production of High-Performance Concrete,”. Cement, Concrete, and Aggregates, ASTM, Vol. 12, No. 2, Winter,, pp. 70-78.

Meng, Fanzhen, Wong, Louis Ngai Yuen, and Zhou, Hui. 2021. "Rock Brittleness Indices and Their Applications to Different Fields of Rock Engineering: A Review." Journal of Rock Mechanics and Geotechnical Engineering 13 (1): 221-247. ISSN 1674-7755. https://doi.org/10.1016/j.jrmge.2020.06.008

Mohamad , N., Muthusamy , K., Embong , R., Kusbiantoro, A., and Hashim , M. H. (2021). Environmental impact of cement production and Solutions: A review.

Mohammed, H. M., Azari, Z., Guy, P., and Matvienko, Y. G. (2011). Two Parameter Engineering Fracture Mechanics: Calculation of the Relevant Parameters and Investigation of Their Influence on the Surface Notch.

Morris, “. H., and Michael, D. A. (n.d.). Use of Fly Ash in Concrete. ACI Committee 232.

Murali, T., and Kandasamy, S. (2009). Mix Proportioning of High Performance Self-Compacting Concrete using Response Surface Methodology. The Open Civil Engineering Journal, 3(1),, pp.93-97.

Muthadhi, A. (2010). Studies on production of reactive rice husk ash and performance of RHA-concrete.

Newspaper, This Day. (2014, 05 03). Rice Demand Pushes Up Global Price. Reported by Abimbola Akosile 26th Jan 2009, Available at: All Africa.Com,.

Nicolas, Alexandre, Ezequiel E. Ferrero, Kirsten Martens, and Jean-Louis Barrat. "Deformation and flow of amorphous solids: Insights from elastoplastic models." Reviews of Modern Physics 90, no. 4 (2018): 045006.

Nigeria - Country Commercial Guide. (2023). Retrieved from Official Website of the International Trade Administration: https://www.trade.gov/country-commercial-guides/nigeria-construction-sector

Ninyio, N. N. (2019). Legal System Of Tax Income And Tariff Revenue In The Natural Resources And The Mining Sector In Nigeria: Obstacles And Challenges In Collecting Taxes And Duties, Parliamentary And Judicial Control.

Njoku, H., Bafuwa, O. R., Mgbemene, C. A., and Ekechukwu, V. (2017). Benchmarking energy utilization in cement manufacturing processes in Nigeria and estimation of savings opportunities.

Odigure, J. O. (2014). The cement quality/prices and the challenge of building collapse in Nigeria.

Ofosu-Adarkwa, Jeffrey, Naiming Xie, and Saad Ahmed Javed. "Forecasting CO2 emissions of China's cement industry using a hybrid Verhulst-GM (1, N) model and emissions' technical conversion." Renewable and Sustainable Energy Reviews 130 (2020): 109945.

Oguntade, Sodiq Solagbade, Abdullahi Tunde Aborode, Oluwatoni Honour Afinjuomo, Victor Akolade Kayode, Toyeeb Abidemi Atanda, Oluwayomi Dapo Amupitan, Olatomide Blessing Ojajune, Abeeb Babajide Ajagbe, and Michael Olamilekan Omonitan. "The Impact of Climate Change on the State of Carbon Footprint in Nigeria." In Climate Change Impacts on Nigeria: Environment and Sustainable Development, pp. 155-177. Cham: Springer International Publishing, 2023.

Ohno, Kentaro, Kimitaka Uji, Atsushi Ueno, and Masayasu Ohtsu. "Fracture process zone in notched concrete beam under three-point bending by acoustic emission." Construction and building materials 67 (2014): 139-145.

Ojosipe, D. ([Accessed 15 Jul. 2015]). Rice production: Olam to mill 200, 000 metric tonnes. [online] Peoplesdailyng.com. Available at: http://www.peoplesdailyng.com/rice-production-olam-to-mill-200-000-metric-tonnes.

Okpala, D. (1987). Rice husk ash (RHA) as partial replacement of cement in concrete. Proceedings of 1987 annual conference of Nigerian Society of Engineers, Port Harcourt, , pp.83 -90.

Olga, A., William, L. B., Stanley, G. B., Leonard, W. B., James, E. B., Mike, B., . . . Thomas. (September 1.1993.). Selecting Proportions for High-Strength Concrete with Portland Cement and Fly Ash. ACI Committee.

Olonade, K. (2013). Economy of RHA (Rice Husk Ash) in Concrete for Low-Cost Housing Delivery in Nigeria. Journal of Civil Engineering and Architecture, 7(11).

Pender, D. ([Accessed 15 Jul. 2015]). Greenies think concrete is green! [online] EPAW. Available at: http://www.epaw.org/documents.php?lang=enandarticle=in10.

Peterman, M. B., and Carrasquillo, R. L. (1986). “Production of High Strength Concrete,”. Noyes Publications, Park Ridge, 278 pp.

Petersen, Richard C. "Accurate critical stress intensity factor Griffith crack theory measurements by numerical techniques." SAMPE journal. Society for the Advancement of Material and Process Engineering 2013 (2013): 737.

Planas, J. E. (1990). Fracture Criteria for concrete:. Mathematical validations and experimental validations Eng fract Mech 35:87-97.

Plizzari, G. A., and V. E. Saouma. "Linear or nonlinear fracture mechanics of concrete?." In Proceedings of Second International Conference on Fracture Mechanics of Concrete Structures FraMCoS2, pp. 1377-1386. 1995.

Project Coordinating Unit (PCU). (2002). “Crop area yield survey (CAY)”. Abuja,: Fed. Min. Agric. Rural Dev.

Qureshi, M. A., M. Aslam, S. N. R. Shah, and S. H. Otho. "Influence of Aggregate Characteristics on the Compressive Strength of Normal Weight Concrete." Technical Journal of University of Engineering & Technology Taxila 20, no. 3 (2015).

Rafai, T., and Swartz, S. E. (1987). Fracture behaviour of concrete beams in three-point bending considering the influence of size effects. Kansas State Universi, , Engineering Experiment Station, .

Ramezanianpour, Ali Akbar. "Cement replacement materials." Springer Geochemistry/Mineralogy, DOI 10 (2014): 978-3.

Ramezanianpour, A. A., Mahdi, M., and Ahmadibeni, G. (2009). The Effect of Rice Husk Ash on Mechanical Properties and Durability of Sustainable Concretes. International Journal of Civil Engineering., 83-91.

Rani, Manjeet, Priyanka Choudhary, Venkata Krishnan, and Sunny Zafar. "A review on recycling and reuse methods for carbon fiber/glass fiber composites waste from wind turbine blades." Composites part B: engineering 215 (2021): 108768.

Rashid, M. A., and Mansur, M. A. (2009). Considerations in producing high strength concrete. Journal of civil engineering (IEB), 37(1),, 53-63.

Gettu, Ravindra, Zdenek P. Bazant, and Martha E. Karr. "Fracture properties and brittleness of high-strength concrete." ACI Materials Journal 87, no. 6 (1990): 608-618.

Rezaei, Masoud, and Mohsen A. Issa. "Specimen and aggregate size effect on the dynamic fracture parameters of concrete under high loading rates." Engineering Fracture Mechanics 260 (2022): 108184.

Rozainee, Mohd, Saik Peng Ngo, A. A. Salema, Kean Giap Tan, M. Ariffin, and Z. N. Zainura. "Effect of fluidising velocity on the combustion of rice husk in a bench-scale fluidised bed combustor for the production of amorphous rice husk ash." Bioresource Technology 99, no. 4 (2008): 703-713.

Russell, H. G. (1994). "Structural Design Considerations and Applications",. (S. P. Shah, S. H. Ahmad, and A. Edward, Eds.) In High Performance Concretes and Applications,.

S. Muralidhara; B.K. Raghu Prasad; Hamid Eskandari c; B.L. Karihaloo . (Accepted 16 October 2009). Construction and Building Materials. Fracture process zone size and true fracture energy of concrete using acoustic emission, 9.

S. Nagataki; E.Sakai;. (1994). Applications in Japan and South East Asia. (S. P. Shah, S. H. Ahmad, and A. Edward, Eds.) In High Performance Concretes and Applications, pp. 375-397.

Sandor, P. (1992, January 1). Concrete Materials:. (T. and. –, Ed.) Properties, Specifications, and Testing. , 661.

Chandrasekhar, S. A. T. H. Y., K. G. Satyanarayana, P. N. Pramada, P. Raghavan, and T. N. Gupta. "Review processing, properties and applications of reactive silica from rice husk—an overview." Journal of materials science 38 (2003): 3159-3168.

Shah, S. N. R., F. W. Akashah, and P. Shafigh. "Performance of high strength concrete subjected to elevated temperatures: a review." Fire Technology 55 (2019): 1571-1597.

Shah, Surendra, and Alberto Carpinteri, eds. Fracture mechanics test methods for concrete. Vol. 5. CRC Press, 1991.

Shaikeea, Angkur Jyoti Dipanka, Huachen Cui, Mark O'Masta, Xiaoyu Rayne Zheng, and Vikram Sudhir Deshpande. "The toughness of mechanical metamaterials." Nature materials 21, no. 3 (2022): 297-304.

Shemirani, Alireza Bagher, Hadi Haeri, Vahab Sarfarazi, and Ahmadreza Hedayat. "A review paper about experimental investigations on failure behaviour of non-persistent joint." Geomechanics & engineering 13, no. 4 (2017): 535-570.

Silva, B. A., Pinto, A. P., Gomes, A., and Candeias, A. (2020). Admixtures potential role on the improvement of the freeze-thaw resistance of lime mortars.

Siriluk, C., Thanita, A., and Nurak, G. (2007, January). Influence of functional silanes on hydrophobicity of MCM-41 synthesized from rice husk. Science and Technology of Advanced Materials,, vol. 8, no. 1-2, pp. 110–115.

Siva Rama Prasad, C. V. (2021). Impact of Admixtures on Strength Properties of Concrete.

Steven, H. K., Beatrix, K., and William, C. P. (2002, January). Design and Control of Concrete Mixtures, 66 pp.

Sun News. (2015). Olam increases local rice production by 200,000MT. Retrieved from Olam increases local rice production by 200,000MT: https://m.facebook.com/9jafood/posts/olam-increases-local-rice-production-by-200000mtthe-federal-governments-efforts-/958272247518490/?_se_imp=06rxti71ichnBGS7r

Sun, C. T., and Z. H. Jin. "Griffith theory of fracture." Fracture Mechanics (2012): 11-24.

Swartz, S. E., and C. G. Go. "Validity of compliance calibration to cracked concrete beams in bending: The suitability of the compliance calibration technique to monitoring cracking in plain concrete beams was evaluated by using dye penetrant to determine average crack length. This was found to be less than that estimated by the compliance-calibration method." *Experimental Mechanics* 24 (1984): 129-134.

Tang, Tianxi, Chengsheng Ouyang, and Surendra P. Shah. "Simple method for determining material fracture parameters from peak loads." Materials Journal 93, no. 2 (1996): 147-157.

Tang, T., Yang, S., and Zollinger, D. G. (1999). Determination of fracture energy and process zone length using variable-notch one-size specimens. American Concrete Institute (ACI).

Tang, Y., and Chen, H. N. (2019). Characterizations on fracture process zone of plain concrete.

Terence, C. H., Rachel, D., Pierre-Claude, A., Allen, J. H., H. Celik, O., Dennis, O. A., . . . Na. (Reapproved 2000). Guide for the Use of Silica Fume in Concrete. ACI Committee.

Tijani, M. A., W. O. Ajagbe, and O. A. Agbede. "Modelling the Effect of burning temperature and time on chemical composition of sorghum husk ash for optimum pozzolanic activity." FUTA Journal Of Engineering And Engineering Technology 12, no. 2 (2018): 273-281.

Tijani, Murtadha Adekilekun, Wasiu Olabamiji Ajagbe, and Oluwole Akinyele Agbede. "Combined reusing of sorghum husk ash and recycled concrete aggregate for sustainable pervious concrete production." Journal of Cleaner Production 343 (2022): 131015.

U.S. Department of Energy. Office of Integrated Analysis and Forecasting. "Emissions of Greenhouse Gases in the United States 2006." November 2007. Washington, DC: Energy Information Administration.

Monogbe, Tunde G., and O. John Okah. "Export Promotion, Import Substitution and Economic Integration in Nigeria." iBusiness 9, no. 4 (2017): 134-148.

V. Saraswathy; H. Song. (2007). Corrosion performance of rice husk ash blended concrete. Construction and Building Materials,, 21(8),, pp.1779-1784.

Vatan, Meltem. "Evolution of construction systems: Cultural effects on traditional structures and their reflection on modern building construction." In Cultural Influences on Architecture, pp. 35-57. IGI Global, 2017.

Wang, Yusuo, Xiaozhi Hu, Li Liang, and Wancheng Zhu. "Determination of tensile strength and fracture toughness of concrete using notched 3-pb specimens." Engineering Fracture Mechanics 160 (2016): 67-77.

Wang, Bo, Libo Yan, Qiuni Fu, and Bohumil Kasal. "A comprehensive review on recycled aggregate and recycled aggregate concrete." Resources, Conservation and Recycling 171 (2021): 105565.

Wang, Lei, Nazaib Ur Rehman, Iurie Curosu, Zhou Zhu, Mirza Abdul Basit Beigh, Marco Liebscher, Liang Chen, Daniel CW Tsang, Simone Hempel, and Viktor Mechtcherine. "On the use of limestone calcined clay cement (LC3) in high-strength strain-hardening cement-based composites (HS-SHCC)." Cement and Concrete Research 144 (2021): 10642

Wciślik, W., and Lipiec, S. (2022). Void-Induced Ductile Fracture of Metals: Experimental Observations. Void-Induced Ductile Fracture of Metals: Experimental Observations.

Wei, Ming-Dong, Feng Dai, Nu-Wen Xu, Tao Zhao, and Yi Liu. "An experimental and theoretical assessment of semi-circular bend specimens with chevron and straight-through notches for mode I fracture toughness testing of rocks." International Journal of Rock Mechanics and Mining Sciences 99 (2017): 28-38.

Xie, Chaopeng, Mingli Cao, Mehran Khan, Hong Yin, and Junfeng Guan. "Review on different testing methods and factors affecting fracture properties of fiber reinforced cementitious composites." Construction and Building Materials 273 (2021): 121766.

Xu, S. L., and H.W. Reinhardt. (1999b). .Determination of double-K criterion for crack propagation in quasi-brittle fracture, Part III: Compact tension specimens and wedge splitting specimens,. International Journal of Fracture, 98(2):, 179-193.

Xu, S., and Reinhard, H. (1999a.). Determination of double K criterion for crack propagation in quasi-brittle materials, part II: analytical evaluating and practical measuring methods for three-point bending notched beams. International Journal of Fracture :, 98(2), 151-177.

Xu, S., and Reinhardt, H. (1999). Determination of double-K criterion for crack propagation in quasibrittle materials, Part II: Analytical.

Xu, S., and Zhang, X. (2008). Determination of fracture parameters for crack propagation in concrete using an energy approach.

Xu, S., Zhao, Y., and Wu, Z. (2006). Study on the Average Fracture Energy for Crack Propagation in Concrete.

Yeoh, A. K., Bidin, R., Chong, C., and Tay, C. (1979). The relationship between temperature and duration of burning of rice-husk in the development of amorphous rice-husk ash silica,. Proceedings of UNIDO/ESCAP/ RCTT Follow-up Meeting on Rice-Husk Ash Cement.

Zhang, Shizhe, Zhenming Li, Bahman Ghiassi, Suhong Yin, and Guang Ye. "Fracture properties and microstructure formation of hardened alkali-activated slag/fly ash pastes." Cement and Concrete Research 144 (2021): 106447.

Zhang, M., Li, D., Yang, L., Chen, L., Shen, M., Huo, J., and Li, Y. (2022). An ultrafast time-resolution method based on picosecond pulsed laser for determining rock fracture toughness at multipoint during the crack propagation. Scientifc Reports.

Zhang, X., and Xu, S. (2007). Fracture resistance on aggregate bridging crack in concrete. Front Archit Civ Eng China 1(1):, 63–70.

Zhao, Y., and Xu, S. (2004). An analytical and computational study on energy dissipation along fracture process zone in concrete. Comput Concr 1(1):, 47–60.

APPENDIX

Appendix A: Fracture Mechanics Literature Review

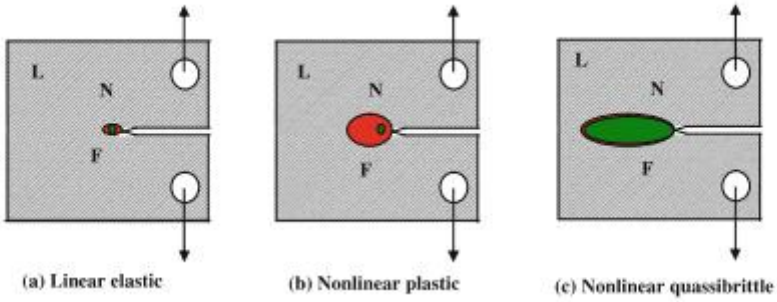

Figure 11:Different materials exhibit varying types of nonlinear zones: L (linear elastic), N (nonlinear due to plasticity), and F (fracture process zone, FPZ).

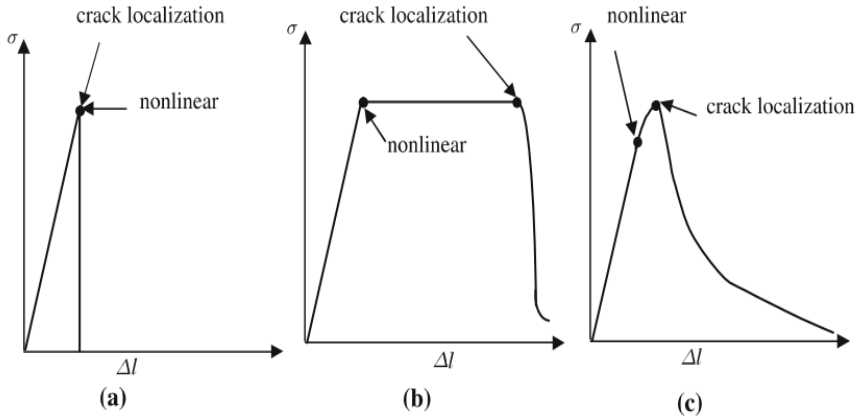

Figure 12: Stress-displacement behaviour under uniaxial tension: (a) brittle, (b) ductile, and (c) quasi-brittle materials

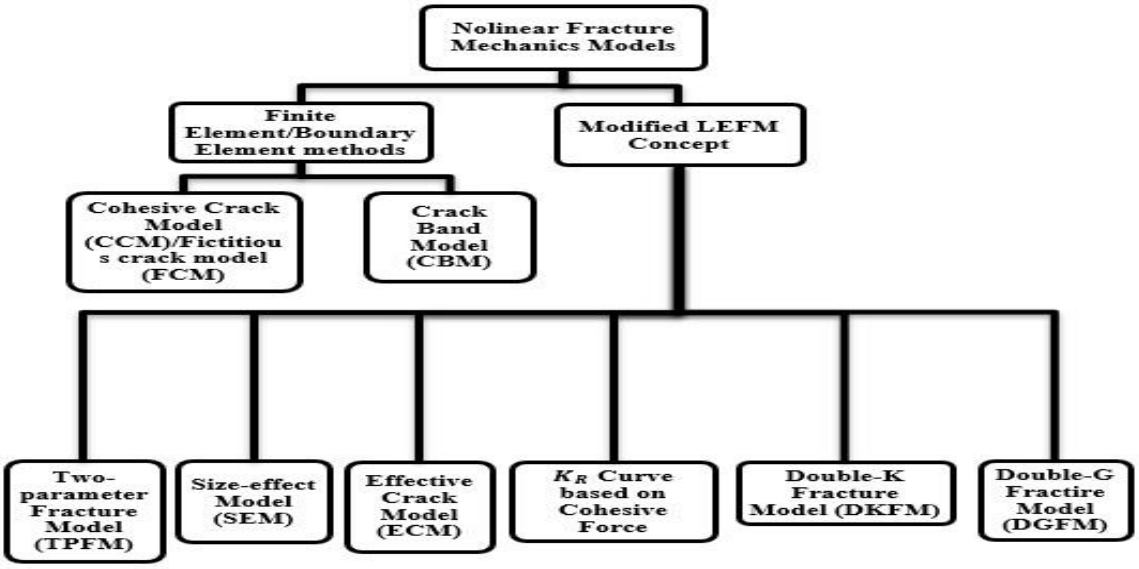

Figure 13: Classification of nonlinear Fracture Models for concrete

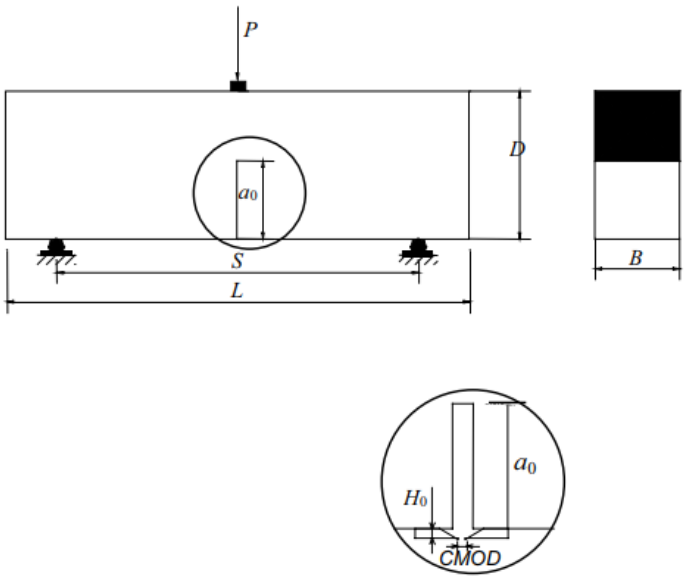

Figure 14: Typical Three-point Bending Test Set-up

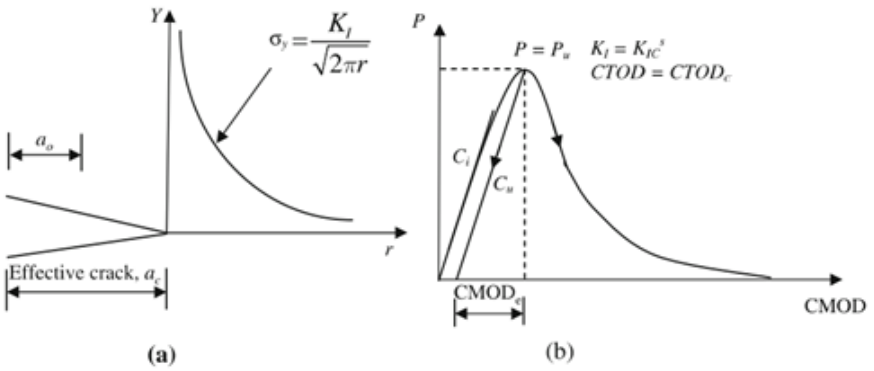

Figure 15: (a) Equivalent Griffith Crack; (b) Typical Load-CMOD curve for TPFM Source: (Jenq and S. Shah, 1985).

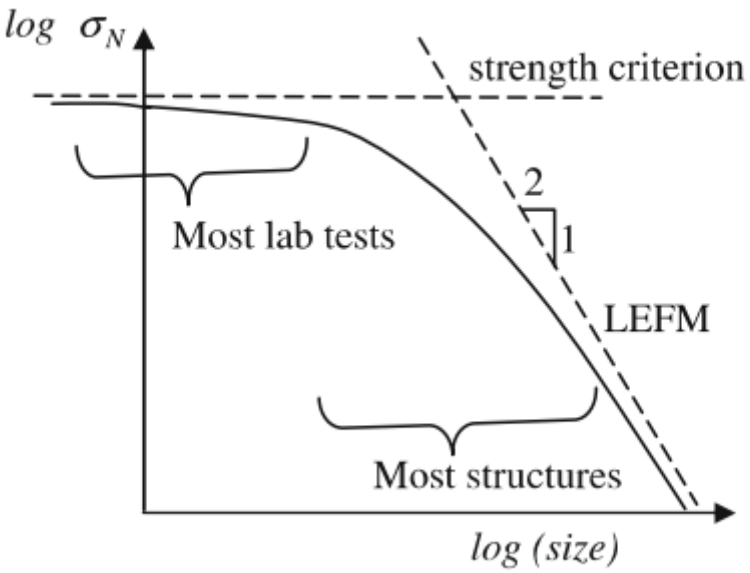

Figure 16: Size effects as a plot of normal strength vs size on a bi-logarithmic scale. Source: (Bažant and Kazemi, 1986).

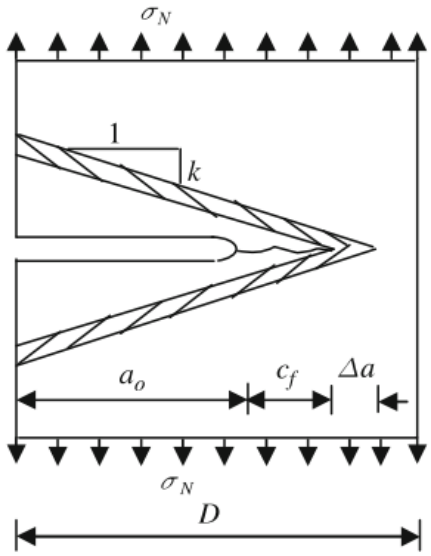

Figure 17:Energy Transfer during infinitesimal crack extension in slit-like process zone. Source: (Bazant and Jaime, 1997).

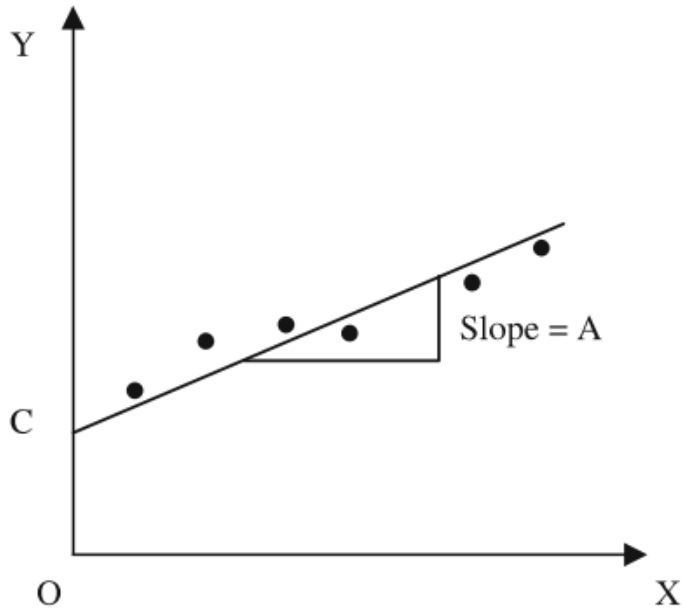

Figure 18:Linear Regression for test data. Source: (Kumar and Barai, 2012).

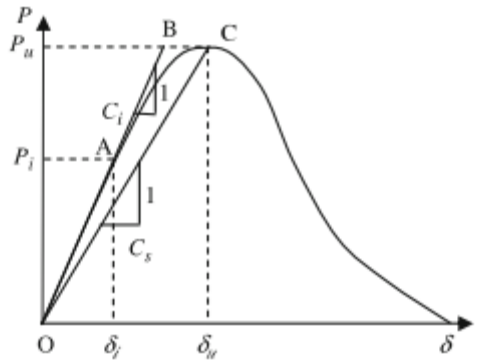

Figure 19:Determination of ac using CMOD measured at the pint D (P = 0.95P_u) on the P-CMOD curve by (Swartz and Go, 1984)

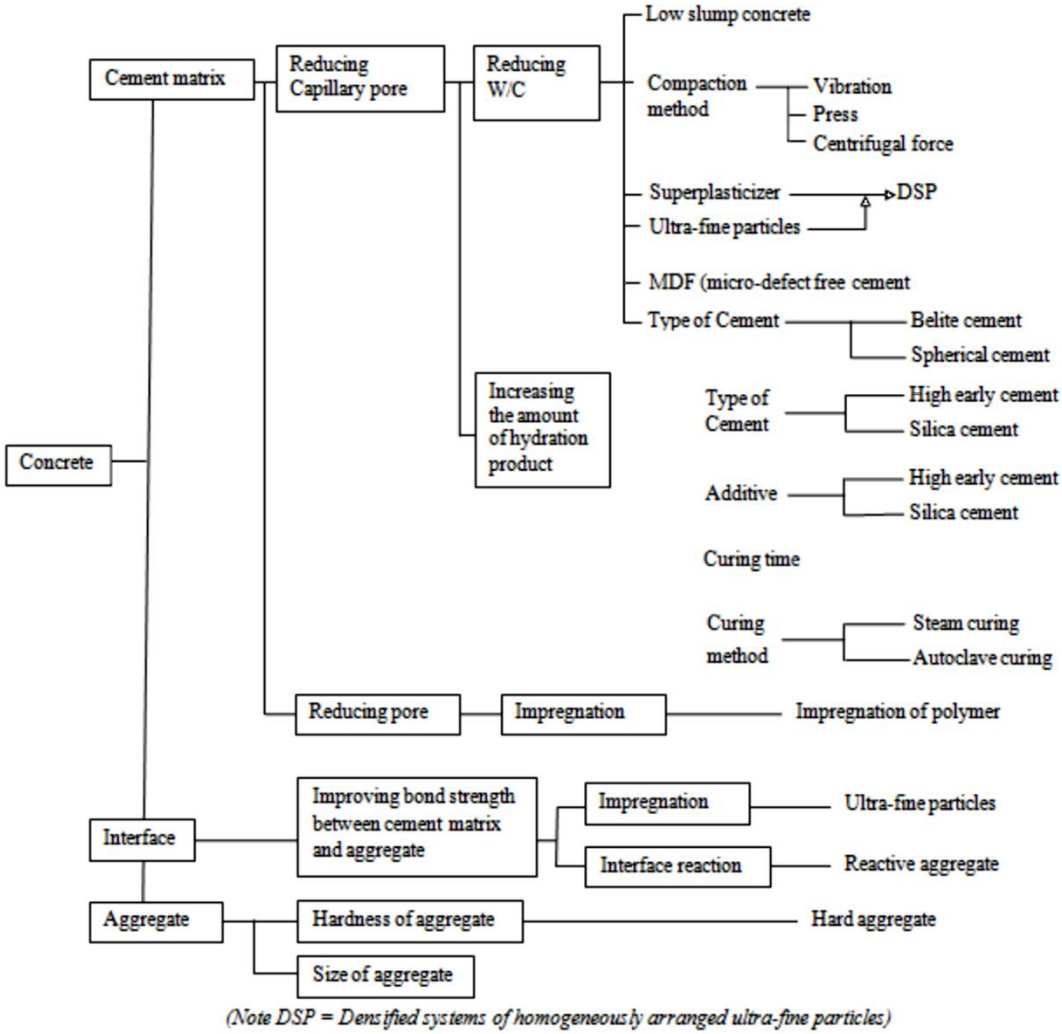

Figure 20:Various techniques for achieving high strength concrete (Nagataki and Sakai, 1994)

Appendix F: Cube test Results

Table 6.1: #1 7 days Cube Test

%	Weight 1 (kg)	Weight 2 (kg)	Weight 3 (kg)	Load 1 (kN)	Load 2 (kN)	Load 3 (kN)	Avg Weight (kg)	Avg Load (kN)	Compressive stress (MPa)
0	8.16	8.35	8.14	725	740	740	8.22	735.00	32.67
10	7.31	7.67	8.35	520	470	400	7.78	463.33	20.59
20	7.44	7.22	8.03	215	205	215	7.56	211.67	9.41
30	7.36	6.53	6.85	110	80	75	6.91	88.33	3.93
40	6.1	6.38	6.29	65	85	80	6.26	76.67	3.41
50	7.76	5.34	5.6	10	10	15	6.23	11.67	0.52

Table 6.2: #1 14 days Cube Test

%	Weight 1 (kg)	Weight 2 (kg)	Weight 3 (kg)	Load 1 (kN)	Load 2 (kN)	Load 3 (kN)	Avg Weight (kg)	Avg Load (kN)	Compressive stress (MPa)
0	8.06	8.11	8.36	780	680	830	8.18	763.33	33.93
10	8.26	7.8	7.84	610	550	615	7.97	591.67	26.30
20	7.1	7.39	7.08	285	330	280	7.19	298.33	13.26
30	6.73	6.61	6.98	110	110	115	6.77	111.67	4.96
40	6.54	7.13	6.72	110	110	115	6.80	111.67	4.96
50	6.36	6.28	6.88	90	95	95	6.51	93.33	4.15

Table 6.3: #1 21 days Cube Test

%	Weight 1 (kg)	Weight 2 (kg)	Weight 3 (kg)	Load 1 (kN)	Load 2 (kN)	Load 3 (kN)	Avg Weight (kg)	Avg Load (kN)	Compressive stress (MPa)
0	8.33	8.29	8.33	920	850	950	8.32	906.67	40.30
10	7.88	8.21	7.78	660	630	640	7.96	643.33	28.59
20	7.24	8.03	7.22	320	360	340	7.50	340.00	15.11
30	6.79	6.71	6.77	160	165	150	6.76	158.33	7.04
40	6.88	6.02	6.33	135	165	155	6.41	151.67	6.74
50	6.81	6.35	6.19	130	125	115	6.45	123.33	5.48

Table 6.4: #1 28 days Cube Test

%	Weight 1 (kg)	Weight 2 (kg)	Weight 3 (kg)	Load 1 (kN)	Load 2 (kN)	Load 3 (kN)	Avg Weight (kg)	Avg Load (kN)	Compressive stress (MPa)
0	8.14	8.2	-	920	925	-	8.17	922.50	41.00
10	8.08	7.63	7.77	700	640	550	7.83	630.00	28.00
20	7.06	7.44	7.76	365	360	345	7.42	356.67	15.85
30	-	-	-	-	-	-	-	-	-
40	-	-	-	-	-	-	-	-	-
50	-	-	-	-	-	-	-	-	-

Table 6.5: #1 Data Summary

#1 Cube weight					#1 Compressive Strength			
%	**7**	**14**	**21**	**28**	**7**	**14**	**21**	**28**
0	8.22	8.18	8.32	8.21	32.67	33.93	40.30	43.95
10	7.78	7.97	7.96	7.81	20.59	26.30	28.59	37.40
20	7.56	7.19	7.50	7.41	9.41	13.26	15.11	30.87
30	6.91	6.77	6.76	7.01	3.93	4.96	7.04	24.33
40	6.26	6.80	6.41	6.61	3.41	4.96	6.74	17.79
50	6.23	6.51	6.45	6.21	0.52	4.15	5.48	11.25

Table 6.6: #2 7 days Cube Test

%	Weight 1 (kg)	Weight 2 (kg)	Weight 3 (kg)	Load 1 (kN)	Load 2 (kN)	Load 3 (kN)	Avg Weight (kg)	Avg Load (kN)	Compressive stress (MPa)
0	8.38	8.29	8.38	1030	1070	1010	8.35	1036.67	46.07
10	7.87	7.8	7.87	1065	1005	1115	7.85	1061.67	47.19
20	7.57	7.63	7.56	1050	1020	1055	7.59	1041.67	46.30
30	6.9	6.93	6.91	1050	1015	960	6.91	1008.33	44.81
40	6.35	6.23	6.28	1030	1030	995	6.29	1018.33	45.26
50	6.23	6.16	6.22	995	970	1000	6.20	988.33	43.93

Table 6.7: #2 14 days Cube Test

%	Weight 1 (kg)	Weight 2 (kg)	Weight 3 (kg)	Load 1 (kN)	Load 2 (kN)	Load 3 (kN)	Avg Weight (kg)	Avg Load (kN)	Compressive stress (MPa)
0	8.61	8.84	8.52	1210	1125	1250	8.66	1195.00	53.11
10	7.77	7.87	7.8	1245	1240	1245	7.81	1243.33	55.26
20	7.04	7.34	7.15	1205	1200	1200	7.18	1201.67	53.41
30	6.71	6.52	6.81	1190	1200	1205	6.68	1198.33	53.26
40	6.95	6.83	6.73	1185	1190	1185	6.84	1186.67	52.74
50	6.43	6.65	6.49	1180	1175	1190	6.52	1181.67	52.52

Table 6.8: #2 21 days Cube Test

%	Weight 1 (kg)	Weight 2 (kg)	Weight 3 (kg)	Load 1 (kN)	Load 2 (kN)	Load 3 (kN)	Avg Weight (kg)	Avg Load (kN)	Compressive stress (MPa)
0	8.57	8.51	8.37	1235	1250	1335	8.48	1273.33	56.59
10	7.87	7.88	7.97	1400	1305	1360	7.91	1355.00	60.22
20	7.44	7.57	7.52	1320	1315	1135	7.51	1256.67	55.85
30	6.93	6.67	6.8	1270	1210	1245	6.80	1241.67	55.19
40	6.5	6.45	6.51	1255	1205	1265	6.49	1241.67	55.19
50	6.46	6.45	6.46	1225	1240	1215	6.46	1226.67	54.52

Table 6.9: #2 28 days Cube Test

%	Weight 1 (kg)	Weight 2 (kg)	Weight 3 (kg)	Load 1 (kN)	Load 2 (kN)	Load 3 (kN)	Avg Weight (kg)	Avg Load (kN)	Compressive stress (MPa)
0	8.45	8.47	8.2	1245	1445	1370	8.37	1353.33	60.15
10	7.91	7.92	7.89	1450	1460	1390	7.91	1433.33	63.70
20	7.64	7.55	7.16	1475	1265	1300	7.45	1346.67	59.85
30	6.87	6.97	6.68	1340	1255	1295	6.84	1296.67	57.63
40	6.57	6.42	6.45	1200	1375	1140	6.48	1238.33	55.04
50	6.5	6.46	6.5	1100	1180	1375	6.49	1218.33	54.15

Table 6.10: #2 Data Summary

#1 Cube weight					#1 Compressive Strength			
%	**7**	**14**	**21**	**28**	**7**	**14**	**21**	**28**
0	8.35	8.66	8.48	8.37	46.07	53.11	56.59	60.15
10	7.85	7.81	7.91	7.91	53.11	55.26	60.22	63.70
20	7.59	7.18	7.51	7.45	53.41	53.41	55.85	59.85
30	6.91	6.68	6.80	6.84	44.81	44.81	55.19	57.63
40	6.29	6.84	6.49	6.48	45.26	45.26	55.19	55.04
50	6.20	6.52	6.46	6.49	43.93	43.93	54.52	54.15

Appendix G: Three-Point Bending Test (TPBT) and Result

Table 6.11: TPBT Peak load Results

Sample Classification	P_{max} (N) 1	2	3	4	5	P_{max} (N)Avg
A1	2567.49	2576.81	2593.43	2425.37	2526.95	2538.01
A2	2569.67	2664.60	2528.04	2580.24	2527.61	2574.03
A3	1689.53	1405.58	1371.80	1550.05	1417.27	1486.84
A4	1027.40	969.31	938.87	900.84	925.43	952.37
A5	775.01	783.59	752.01	814.93	674.69	760.05
A6	281.18	409.91	352.76	297.72	390.05	346.32
B1	2484.84	2360.14	2517.22	2328.24	2481.28	2434.34
B2	2437.33	2493.70	2537.11	2394.55	2552.28	2482.99
B3	1370.98	1440.91	1493.69	1462.61	1342.14	1422.07
B4	765.93	706.21	699.75	715.49	706.04	718.68
B5	632.16	597.48	541.77	671.49	505.57	589.69
B6	270.12	297.38	299.88	340.90	257.76	293.21
C1	-	-	2416.07	2346.89	2377.27	2380.08
C2	-	-	2485.95	2491.73	2365.28	2447.65
C3	-	-	1421.28	1412.53	1437.96	1423.92
C4	-	-	1005.96	971.10	1013.09	996.71
C5	-	-	695.04	719.31	743.60	719.32
C6	-	-	341.23	372.58	300.30	338.04

Appendix H: Fracture Parameters Results

Table 6.12: Fracture Parameters for C1 Peak Load

S/N	W(m)	S(m)	B(m)	f'_c (MPa)	W (kg/m^3)	E (GPa)	a_0 (m)	a_c (m)	α_c	β	$F(\alpha_c)$	$V(\alpha_c)$	N (α_c, β)	Pmax (N)Avg	K^s_{IC} (MPa)	$CTOD_C$ (mm)
1	0.102000	0.381000	0.07600	60.15	2480.00	41.19	0.029580	0.056100	0.550000	0.527273	1.593713	3.596529	0.579137	2380.08	1.150960	0.019522
2	0.102000	0.381000	0.07600	60.15	2480.00	41.19	0.029580	0.056233	0.551300	0.526029	1.599034	3.615607	0.579857	2380.08	1.156167	0.019696
3	0.102000	0.381000	0.07600	60.15	2480.00	41.19	0.029580	0.056365	0.552600	0.524792	1.604395	3.634851	0.580572	2380.08	1.161410	0.019872
4	0.102000	0.381000	0.07600	60.15	2480.00	41.19	0.029580	0.056498	0.553900	0.523560	1.609798	3.654264	0.581283	2380.08	1.166691	0.020050
5	0.102000	0.381000	0.07600	60.15	2480.00	41.19	0.029580	0.056630	0.555200	0.522334	1.615241	3.673847	0.581990	2380.08	1.172009	0.020229
6	0.102000	0.381000	0.07600	60.15	2480.00	41.19	0.029580	0.056763	0.556500	0.521114	1.620726	3.693603	0.582692	2380.08	1.177365	0.020410
7	0.102000	0.381000	0.07600	60.15	2480.00	41.19	0.029580	0.056896	0.557800	0.519900	1.626254	3.713534	0.583390	2380.08	1.182759	0.020593
8	0.102000	0.381000	0.07600	60.15	2480.00	41.19	0.029580	0.057028	0.559100	0.518691	1.631823	3.733641	0.584084	2380.08	1.188192	0.020777
9	0.102000	0.381000	0.07600	60.15	2480.00	41.19	0.029580	0.057161	0.560400	0.517488	1.637436	3.753927	0.584773	2380.08	1.193665	0.020963
10	0.102000	0.381000	0.07600	60.15	2480.00	41.19	0.029580	0.057293	0.561700	0.516290	1.643092	3.774394	0.585458	2380.08	1.199176	0.021151
11	0.102000	0.381000	0.07600	60.15	2480.00	41.19	0.029580	0.057426	0.563000	0.515098	1.648792	3.795043	0.586140	2380.08	1.204728	0.021341
12	0.102000	0.381000	0.07600	60.15	2480.00	41.19	0.029580	0.057559	0.564300	0.513911	1.654536	3.815877	0.586816	2380.08	1.210319	0.021533
13	0.102000	0.381000	0.07600	60.15	2480.00	41.19	0.029580	0.057691	0.565600	0.512730	1.660324	3.836899	0.587489	2380.08	1.215952	0.021726
14	0.102000	0.381000	0.07600	60.15	2480.00	41.19	0.029580	0.057824	0.566900	0.511554	1.666158	3.858110	0.588158	2380.08	1.221626	0.021921
15	0.102000	0.381000	0.07600	60.15	2480.00	41.19	0.029580	0.057956	0.568200	0.510384	1.672037	3.879512	0.588823	2380.08	1.227341	0.022118
16	0.102000	0.381000	0.07600	60.15	2480.00	41.19	0.029580	0.058089	0.569500	0.509219	1.677962	3.901108	0.589484	2380.08	1.233099	0.022317
17	0.102000	0.381000	0.07600	60.15	2480.00	41.19	0.029580	0.058222	0.570800	0.508059	1.683933	3.922900	0.590141	2380.08	1.238899	0.022518
18	0.102000	0.381000	0.07600	60.15	2480.00	41.19	0.029580	0.058354	0.572100	0.506904	1.689952	3.944891	0.590794	2380.08	1.244741	0.022721
19	0.102000	0.381000	0.07600	60.15	2480.00	41.19	0.029580	0.058487	0.573400	0.505755	1.696018	3.967083	0.591443	2380.08	1.250628	0.022926
20	0.102000	0.381000	0.07600	60.15	2480.00	41.19	0.029580	0.058619	0.574700	0.504611	1.702131	3.989478	0.592088	2380.08	1.256558	0.023133
21	0.102000	0.381000	0.07600	60.15	2480.00	41.19	0.029580	0.058752	0.576000	0.503472	1.708293	4.012078	0.592730	2380.08	1.262532	0.023342
22	0.102000	0.381000	0.07600	60.15	2480.00	41.19	0.029580	0.058885	0.577300	0.502338	1.714504	4.034887	0.593368	2380.08	1.268552	0.023553

23	0.102000	0.381000	0.07600	60.15	2480.00	41.19	0.029580	0.059017	0.578600	0.501210	1.720765	4.057907	0.594002	2380.08	1.274617	0.023766
24	0.102000	0.381000	0.07600	60.15	2480.00	41.19	0.029580	0.059150	0.579900	0.500086	1.727075	4.081140	0.594632	2380.08	1.280727	0.023981
25	0.102000	0.381000	0.07600	60.15	2480.00	41.19	0.029580	0.059282	0.581200	0.498968	1.733436	4.104589	0.595259	2380.08	1.286884	0.024199
26	0.102000	0.381000	0.07600	60.15	2480.00	41.19	0.029580	0.059415	0.582500	0.497854	1.739848	4.128257	0.595882	2380.08	1.293088	0.024418
27	0.102000	0.381000	0.07600	60.15	2480.00	41.19	0.029580	0.059548	0.583800	0.496745	1.746311	4.152146	0.596502	2380.08	1.299339	0.024640
28	0.102000	0.381000	0.07600	60.15	2480.00	41.19	0.029580	0.059680	0.585100	0.495642	1.752826	4.176259	0.597118	2380.08	1.305638	0.024864
29	0.102000	0.381000	0.07600	60.15	2480.00	41.19	0.029580	0.059813	0.586400	0.494543	1.759394	4.200598	0.597730	2380.08	1.311985	0.025090
30	0.102000	0.381000	0.07600	60.15	2480.00	41.19	0.029580	0.059945	0.587700	0.493449	1.766015	4.225168	0.598339	2380.08	1.318381	0.025318
31	0.102000	0.381000	0.07600	60.15	2480.00	41.19	0.029580	0.060078	0.589000	0.492360	1.772690	4.249970	0.598945	2380.08	1.324827	0.025549
32	0.102000	0.381000	0.07600	60.15	2480.00	41.19	0.029580	0.060211	0.590300	0.491276	1.779419	4.275007	0.599547	2380.08	1.331323	0.025782
33	0.102000	0.381000	0.07600	60.15	2480.00	41.19	0.029580	0.060343	0.591600	0.490196	1.786203	4.300283	0.600145	2380.08	1.337870	0.026018
34	0.102000	0.381000	0.07600	60.15	2480.00	41.19	0.029580	0.060476	0.592900	0.489121	1.793043	4.325800	0.600741	2380.08	1.344467	0.026256
35	0.102000	0.381000	0.07600	60.15	2480.00	41.19	0.029580	0.060608	0.594200	0.488051	1.799938	4.351562	0.601333	2380.08	1.351116	0.026496
36	0.102000	0.381000	0.07600	60.15	2480.00	41.19	0.029580	0.060741	0.595500	0.486986	1.806891	4.377571	0.601921	2380.08	1.357818	0.026739
37	0.102000	0.381000	0.07600	60.15	2480.00	41.19	0.029580	0.060874	0.596800	0.485925	1.813900	4.403831	0.602506	2380.08	1.364573	0.026984
38	0.102000	0.381000	0.07600	60.15	2480.00	41.19	0.029580	0.061006	0.598100	0.484869	1.820968	4.430345	0.603089	2380.08	1.371381	0.027232
39	0.102000	0.381000	0.07600	60.15	2480.00	41.19	0.029580	0.061139	0.599400	0.483817	1.828094	4.457116	0.603667	2380.08	1.378243	0.027483
40	0.102000	0.381000	0.07600	60.15	2480.00	41.19	0.029580	0.061271	0.600700	0.482770	1.835280	4.484148	0.604243	2380.08	1.385160	0.027736
41	0.102000	0.381000	0.07600	60.15	2480.00	41.19	0.029580	0.061404	0.602000	0.481728	1.842526	4.511444	0.604816	2380.08	1.392133	0.027991
42	0.102000	0.381000	0.07600	60.15	2480.00	41.19	0.029580	0.061537	0.603300	0.480690	1.849832	4.539007	0.605385	2380.08	1.399161	0.028250
43	0.102000	0.381000	0.07600	60.15	2480.00	41.19	0.029580	0.061669	0.604600	0.479656	1.857199	4.566841	0.605951	2380.08	1.406246	0.028511
44	0.102000	0.381000	0.07600	60.15	2480.00	41.19	0.029580	0.061802	0.605900	0.478627	1.864629	4.594949	0.606514	2380.08	1.413389	0.028775
45	0.102000	0.381000	0.07600	60.15	2480.00	41.19	0.029580	0.061934	0.607200	0.477602	1.872121	4.623335	0.607074	2380.08	1.420589	0.029042
46	0.102000	0.381000	0.07600	60.15	2480.00	41.19	0.029580	0.062067	0.608500	0.476582	1.879676	4.652003	0.607631	2380.08	1.427849	0.029311
47	0.102000	0.381000	0.07600	60.15	2480.00	41.19	0.029580	0.062200	0.609800	0.475566	1.887296	4.680956	0.608185	2380.08	1.435167	0.029583
48	0.102000	0.381000	0.07600	60.15	2480.00	41.19	0.029580	0.062332	0.611100	0.474554	1.894980	4.710199	0.608736	2380.08	1.442546	0.029859
49	0.102000	0.381000	0.07600	60.15	2480.00	41.19	0.029580	0.062465	0.612400	0.473547	1.902730	4.739734	0.609284	2380.08	1.449986	0.030137

50	0.102000	0.381000	0.07600	60.15	2480.00	41.19	0.029580	0.062597	0.613700	0.472544	1.910547	4.769567	0.609829	2380.08	1.457487	0.030418
51	0.102000	0.381000	0.07600	60.15	2480.00	41.19	0.029580	0.062730	0.615000	0.471545	1.918430	4.799700	0.610371	2380.08	1.465050	0.030702
52	0.102000	0.381000	0.07600	60.15	2480.00	41.19	0.029580	0.062863	0.616300	0.470550	1.926382	4.830138	0.610911	2380.08	1.472676	0.030990
53	0.102000	0.381000	0.07600	60.15	2480.00	41.19	0.029580	0.062995	0.617600	0.469560	1.934402	4.860885	0.611447	2380.08	1.480366	0.031280
54	0.102000	0.381000	0.07600	60.15	2480.00	41.19	0.029580	0.063128	0.618900	0.468573	1.942492	4.891946	0.611980	2380.08	1.488121	0.031574
55	0.102000	0.381000	0.07600	60.15	2480.00	41.19	0.029580	0.063260	0.620200	0.467591	1.950652	4.923324	0.612511	2380.08	1.495941	0.031871
56	0.102000	0.381000	0.07600	60.15	2480.00	41.19	0.029580	0.063393	0.621500	0.466613	1.958883	4.955024	0.613039	2380.08	1.503827	0.032171
57	0.102000	0.381000	0.07600	60.15	2480.00	41.19	0.029580	0.063526	0.622800	0.465639	1.967186	4.987051	0.613564	2380.08	1.511780	0.032475
58	0.102000	0.381000	0.07600	60.15	2480.00	41.19	0.029580	0.063658	0.624100	0.464669	1.975562	5.019408	0.614086	2380.08	1.519800	0.032781
59	0.102000	0.381000	0.07600	60.15	2480.00	41.19	0.029580	0.063791	0.625400	0.463703	1.984011	5.052100	0.614606	2380.08	1.527890	0.033092
60	0.102000	0.381000	0.07600	60.15	2480.00	41.19	0.029580	0.063923	0.626700	0.462741	1.992536	5.085133	0.615123	2380.08	1.536048	0.033405
61	0.102000	0.381000	0.07600	60.15	2480.00	41.19	0.029580	0.064056	0.628000	0.461783	2.001136	5.118510	0.615637	2380.08	1.544277	0.033722
62	0.102000	0.381000	0.07600	60.15	2480.00	41.19	0.029580	0.064189	0.629300	0.460829	2.009812	5.152237	0.616149	2380.08	1.552577	0.034043
63	0.102000	0.381000	0.07600	60.15	2480.00	41.19	0.029580	0.064321	0.630600	0.459879	2.018565	5.186319	0.616658	2380.08	1.560949	0.034367
64	0.102000	0.381000	0.07600	60.15	2480.00	41.19	0.029580	0.064454	0.631900	0.458933	2.027397	5.220759	0.617164	2380.08	1.569394	0.034695
65	0.102000	0.381000	0.07600	60.15	2480.00	41.19	0.029580	0.064586	0.633200	0.457991	2.036308	5.255565	0.617667	2380.08	1.577912	0.035027
66	0.102000	0.381000	0.07600	60.15	2480.00	41.19	0.029580	0.064719	0.634500	0.457053	2.045300	5.290740	0.618169	2380.08	1.586506	0.035363
67	0.102000	0.381000	0.07600	60.15	2480.00	41.19	0.029580	0.064852	0.635800	0.456118	2.054372	5.326290	0.618667	2380.08	1.595175	0.035702
68	0.102000	0.381000	0.07600	60.15	2480.00	41.19	0.029580	0.064984	0.637100	0.455188	2.063527	5.362220	0.619163	2380.08	1.603920	0.036045
69	0.102000	0.381000	0.07600	60.15	2480.00	41.19	0.029580	0.065117	0.638400	0.454261	2.072765	5.398536	0.619656	2380.08	1.612744	0.036392
70	0.102000	0.381000	0.07600	60.15	2480.00	41.19	0.029580	0.065249	0.639700	0.453338	2.082087	5.435244	0.620147	2380.08	1.621645	0.036743
71	0.102000	0.381000	0.07600	60.15	2480.00	41.19	0.029580	0.065382	0.641000	0.452418	2.091495	5.472348	0.620636	2380.08	1.630627	0.037099
72	0.102000	0.381000	0.07600	60.15	2480.00	41.19	0.029580	0.065515	0.642300	0.451502	2.100989	5.509855	0.621122	2380.08	1.639689	0.037458
73	0.102000	0.381000	0.07600	60.15	2480.00	41.19	0.029580	0.065647	0.643600	0.450590	2.110570	5.547771	0.621605	2380.08	1.648833	0.037822
74	0.102000	0.381000	0.07600	60.15	2480.00	41.19	0.029580	0.065780	0.644900	0.449682	2.120240	5.586101	0.622086	2380.08	1.658059	0.038189
75	0.102000	0.381000	0.07600	60.15	2480.00	41.19	0.029580	0.065912	0.646200	0.448777	2.130000	5.624852	0.622565	2380.08	1.667370	0.038561
76	0.102000	0.381000	0.07600	60.15	2480.00	41.19	0.029580	0.066045	0.647500	0.447876	2.139850	5.664030	0.623041	2380.08	1.676765	0.038938

77	0.102000	0.381000	0.07600	60.15	2480.00	41.19	0.029580	0.066178	0.648800	0.446979	2.149793	5.703641	0.623515	2380.08	1.686246	0.039319
78	0.102000	0.381000	0.07600	60.15	2480.00	41.19	0.029580	0.066310	0.650100	0.446085	2.159829	5.743692	0.623987	2380.08	1.695814	0.039704
79	0.102000	0.381000	0.07600	60.15	2480.00	41.19	0.029580	0.066443	0.651400	0.445195	2.169959	5.784188	0.624456	2380.08	1.705471	0.040094
80	0.102000	0.381000	0.07600	60.15	2480.00	41.19	0.029580	0.066575	0.652700	0.444308	2.180185	5.825138	0.624923	2380.08	1.715217	0.040489
81	0.102000	0.381000	0.07600	60.15	2480.00	41.19	0.029580	0.066708	0.654000	0.443425	2.190508	5.866547	0.625387	2380.08	1.725054	0.040888
82	0.102000	0.381000	0.07600	60.15	2480.00	41.19	0.029580	0.066841	0.655300	0.442545	2.200929	5.908422	0.625850	2380.08	1.734982	0.041293
83	0.102000	0.381000	0.07600	60.15	2480.00	41.19	0.029580	0.066973	0.656600	0.441669	2.211450	5.950772	0.626310	2380.08	1.745004	0.041702
84	0.102000	0.381000	0.07600	60.15	2480.00	41.19	0.029580	0.067106	0.657900	0.440796	2.222071	5.993602	0.626767	2380.08	1.755120	0.042116
85	0.102000	0.381000	0.07600	60.15	2480.00	41.19	0.029580	0.067238	0.659200	0.439927	2.232794	6.036920	0.627223	2380.08	1.765331	0.042535
86	0.102000	0.381000	0.07600	60.15	2480.00	41.19	0.029580	0.067371	0.660500	0.439061	2.243621	6.080733	0.627676	2380.08	1.775640	0.042959
87	0.102000	0.381000	0.07600	60.15	2480.00	41.19	0.029580	0.067504	0.661800	0.438199	2.254553	6.125050	0.628127	2380.08	1.786046	0.043388
88	0.102000	0.381000	0.07600	60.15	2480.00	41.19	0.029580	0.067636	0.663100	0.437340	2.265591	6.169878	0.628576	2380.08	1.796552	0.043823
89	0.102000	0.381000	0.07600	60.15	2480.00	41.19	0.029580	0.067769	0.664400	0.436484	2.276737	6.215224	0.629023	2380.08	1.807159	0.044263
90	0.102000	0.381000	0.07600	60.15	2480.00	41.19	0.029580	0.067901	0.665700	0.435632	2.287991	6.261098	0.629468	2380.08	1.817869	0.044709
91	0.102000	0.381000	0.07600	60.15	2480.00	41.19	0.029580	0.068034	0.667000	0.434783	2.299357	6.307507	0.629910	2380.08	1.828682	0.045160
92	0.102000	0.381000	0.07600	60.15	2480.00	41.19	0.029580	0.068167	0.668300	0.433937	2.310834	6.354459	0.630350	2380.08	1.839600	0.045617
93	0.102000	0.381000	0.07600	60.15	2480.00	41.19	0.029580	0.068299	0.669600	0.433094	2.322425	6.401963	0.630789	2380.08	1.850625	0.046079
94	0.102000	0.381000	0.07600	60.15	2480.00	41.19	0.029580	0.068432	0.670900	0.432255	2.334132	6.450029	0.631225	2380.08	1.861757	0.046547
95	0.102000	0.381000	0.07600	60.15	2480.00	41.19	0.029580	0.068564	0.672200	0.431419	2.345955	6.498664	0.631659	2380.08	1.873000	0.047021
96	0.102000	0.381000	0.07600	60.15	2480.00	41.19	0.029580	0.068697	0.673500	0.430586	2.357896	6.547877	0.632091	2380.08	1.884354	0.047502
97	0.102000	0.381000	0.07600	60.15	2480.00	41.19	0.029580	0.068830	0.674800	0.429757	2.369958	6.597679	0.632521	2380.08	1.895820	0.047988
98	0.102000	0.381000	0.07600	60.15	2480.00	41.19	0.029580	0.068962	0.676100	0.428931	2.382141	6.648079	0.632949	2380.08	1.907400	0.048480
99	0.102000	0.381000	0.07600	60.15	2480.00	41.19	0.029580	0.069095	0.677400	0.428107	2.394448	6.699085	0.633375	2380.08	1.919097	0.048979
100	0.102000	0.381000	0.07600	60.15	2480.00	41.19	0.029580	0.069227	0.678700	0.427287	2.406880	6.750709	0.633799	2380.08	1.930911	0.049484

Table 6.13: Fracture Parameters for C2 Peak Load

S/N	W(m)	S(m)	B(m)	f'_c (MPa)	W (kg/m^3)	E (GPa)	a_0 (m)	a_c (m)	α_c	β	$F(\alpha_c)$	$V(\alpha_c)$	N (α_c, β)	Pmax (N)Avg	K^s_{IC} (MPa)	$CTOD_C$ (mm)
1	0.102000	0.381000	0.07600	60.15	2480.00	41.19	0.032640	0.056100	0.550000	0.581818	1.593713	3.596529	0.533041	2447.65	1.183637	0.018478
2	0.102000	0.381000	0.07600	60.15	2480.00	41.19	0.032640	0.056233	0.551300	0.580446	1.599034	3.615607	0.533871	2447.65	1.188991	0.018649
3	0.102000	0.381000	0.07600	60.15	2480.00	41.19	0.032640	0.056365	0.552600	0.579081	1.604395	3.634851	0.534695	2447.65	1.194384	0.018821
4	0.102000	0.381000	0.07600	60.15	2480.00	41.19	0.032640	0.056498	0.553900	0.577722	1.609798	3.654264	0.535514	2447.65	1.199814	0.018996
5	0.102000	0.381000	0.07600	60.15	2480.00	41.19	0.032640	0.056630	0.555200	0.576369	1.615241	3.673847	0.536328	2447.65	1.205283	0.019171
6	0.102000	0.381000	0.07600	60.15	2480.00	41.19	0.032640	0.056763	0.556500	0.575022	1.620726	3.693603	0.537137	2447.65	1.210791	0.019349
7	0.102000	0.381000	0.07600	60.15	2480.00	41.19	0.032640	0.056896	0.557800	0.573682	1.626254	3.713534	0.537940	2447.65	1.216339	0.019528
8	0.102000	0.381000	0.07600	60.15	2480.00	41.19	0.032640	0.057028	0.559100	0.572348	1.631823	3.733641	0.538738	2447.65	1.221926	0.019708
9	0.102000	0.381000	0.07600	60.15	2480.00	41.19	0.032640	0.057161	0.560400	0.571021	1.637436	3.753927	0.539531	2447.65	1.227554	0.019891
10	0.102000	0.381000	0.07600	60.15	2480.00	41.19	0.032640	0.057293	0.561700	0.569699	1.643092	3.774394	0.540319	2447.65	1.233222	0.020075
11	0.102000	0.381000	0.07600	60.15	2480.00	41.19	0.032640	0.057426	0.563000	0.568384	1.648792	3.795043	0.541102	2447.65	1.238931	0.020261
12	0.102000	0.381000	0.07600	60.15	2480.00	41.19	0.032640	0.057559	0.564300	0.567074	1.654536	3.815877	0.541879	2447.65	1.244681	0.020448
13	0.102000	0.381000	0.07600	60.15	2480.00	41.19	0.032640	0.057691	0.565600	0.565771	1.660324	3.836899	0.542652	2447.65	1.250474	0.020638
14	0.102000	0.381000	0.07600	60.15	2480.00	41.19	0.032640	0.057824	0.566900	0.564473	1.666158	3.858110	0.543420	2447.65	1.256309	0.020829
15	0.102000	0.381000	0.07600	60.15	2480.00	41.19	0.032640	0.057956	0.568200	0.563182	1.672037	3.879512	0.544183	2447.65	1.262186	0.021022
16	0.102000	0.381000	0.07600	60.15	2480.00	41.19	0.032640	0.058089	0.569500	0.561896	1.677962	3.901108	0.544942	2447.65	1.268107	0.021217
17	0.102000	0.381000	0.07600	60.15	2480.00	41.19	0.032640	0.058222	0.570800	0.560617	1.683933	3.922900	0.545695	2447.65	1.274072	0.021414
18	0.102000	0.381000	0.07600	60.15	2480.00	41.19	0.032640	0.058354	0.572100	0.559343	1.689952	3.944891	0.546444	2447.65	1.280081	0.021612
19	0.102000	0.381000	0.07600	60.15	2480.00	41.19	0.032640	0.058487	0.573400	0.558075	1.696018	3.967083	0.547188	2447.65	1.286134	0.021813
20	0.102000	0.381000	0.07600	60.15	2480.00	41.19	0.032640	0.058619	0.574700	0.556812	1.702131	3.989478	0.547928	2447.65	1.292233	0.022016
21	0.102000	0.381000	0.07600	60.15	2480.00	41.19	0.032640	0.058752	0.576000	0.555556	1.708293	4.012078	0.548663	2447.65	1.298377	0.022220
22	0.102000	0.381000	0.07600	60.15	2480.00	41.19	0.032640	0.058885	0.577300	0.554305	1.714504	4.034887	0.549394	2447.65	1.304567	0.022427
23	0.102000	0.381000	0.07600	60.15	2480.00	41.19	0.032640	0.059017	0.578600	0.553059	1.720765	4.057907	0.550120	2447.65	1.310804	0.022635

24	0.102000	0.381000	0.07600	60.15	2480.00	41.19	0.032640	0.059150	0.579900	0.551819	1.727075	4.081140	0.550841	2447.65	1.317088	0.022846
25	0.102000	0.381000	0.07600	60.15	2480.00	41.19	0.032640	0.059282	0.581200	0.550585	1.733436	4.104589	0.551559	2447.65	1.323420	0.023059
26	0.102000	0.381000	0.07600	60.15	2480.00	41.19	0.032640	0.059415	0.582500	0.549356	1.739848	4.128257	0.552271	2447.65	1.329800	0.023274
27	0.102000	0.381000	0.07600	60.15	2480.00	41.19	0.032640	0.059548	0.583800	0.548133	1.746311	4.152146	0.552980	2447.65	1.336228	0.023491
28	0.102000	0.381000	0.07600	60.15	2480.00	41.19	0.032640	0.059680	0.585100	0.546915	1.752826	4.176259	0.553684	2447.65	1.342706	0.023710
29	0.102000	0.381000	0.07600	60.15	2480.00	41.19	0.032640	0.059813	0.586400	0.545703	1.759394	4.200598	0.554384	2447.65	1.349233	0.023931
30	0.102000	0.381000	0.07600	60.15	2480.00	41.19	0.032640	0.059945	0.587700	0.544495	1.766015	4.225168	0.555080	2447.65	1.355811	0.024155
31	0.102000	0.381000	0.07600	60.15	2480.00	41.19	0.032640	0.060078	0.589000	0.543294	1.772690	4.249970	0.555772	2447.65	1.362440	0.024381
32	0.102000	0.381000	0.07600	60.15	2480.00	41.19	0.032640	0.060211	0.590300	0.542097	1.779419	4.275007	0.556460	2447.65	1.369120	0.024609
33	0.102000	0.381000	0.07600	60.15	2480.00	41.19	0.032640	0.060343	0.591600	0.540906	1.786203	4.300283	0.557143	2447.65	1.375853	0.024839
34	0.102000	0.381000	0.07600	60.15	2480.00	41.19	0.032640	0.060476	0.592900	0.539720	1.793043	4.325800	0.557823	2447.65	1.382638	0.025072
35	0.102000	0.381000	0.07600	60.15	2480.00	41.19	0.032640	0.060608	0.594200	0.538539	1.799938	4.351562	0.558499	2447.65	1.389476	0.025307
36	0.102000	0.381000	0.07600	60.15	2480.00	41.19	0.032640	0.060741	0.595500	0.537364	1.806891	4.377571	0.559170	2447.65	1.396368	0.025545
37	0.102000	0.381000	0.07600	60.15	2480.00	41.19	0.032640	0.060874	0.596800	0.536193	1.813900	4.403831	0.559838	2447.65	1.403314	0.025785
38	0.102000	0.381000	0.07600	60.15	2480.00	41.19	0.032640	0.061006	0.598100	0.535028	1.820968	4.430345	0.560502	2447.65	1.410315	0.026028
39	0.102000	0.381000	0.07600	60.15	2480.00	41.19	0.032640	0.061139	0.599400	0.533867	1.828094	4.457116	0.561161	2447.65	1.417373	0.026273
40	0.102000	0.381000	0.07600	60.15	2480.00	41.19	0.032640	0.061271	0.600700	0.532712	1.835280	4.484148	0.561818	2447.65	1.424486	0.026520
41	0.102000	0.381000	0.07600	60.15	2480.00	41.19	0.032640	0.061404	0.602000	0.531561	1.842526	4.511444	0.562470	2447.65	1.431656	0.026771
42	0.102000	0.381000	0.07600	60.15	2480.00	41.19	0.032640	0.061537	0.603300	0.530416	1.849832	4.539007	0.563118	2447.65	1.438884	0.027024
43	0.102000	0.381000	0.07600	60.15	2480.00	41.19	0.032640	0.061669	0.604600	0.529276	1.857199	4.566841	0.563763	2447.65	1.446171	0.027279
44	0.102000	0.381000	0.07600	60.15	2480.00	41.19	0.032640	0.061802	0.605900	0.528140	1.864629	4.594949	0.564404	2447.65	1.453516	0.027537
45	0.102000	0.381000	0.07600	60.15	2480.00	41.19	0.032640	0.061934	0.607200	0.527009	1.872121	4.623335	0.565042	2447.65	1.460921	0.027798
46	0.102000	0.381000	0.07600	60.15	2480.00	41.19	0.032640	0.062067	0.608500	0.525883	1.879676	4.652003	0.565676	2447.65	1.468386	0.028062
47	0.102000	0.381000	0.07600	60.15	2480.00	41.19	0.032640	0.062200	0.609800	0.524762	1.887296	4.680956	0.566306	2447.65	1.475913	0.028328
48	0.102000	0.381000	0.07600	60.15	2480.00	41.19	0.032640	0.062332	0.611100	0.523646	1.894980	4.710199	0.566933	2447.65	1.483501	0.028598
49	0.102000	0.381000	0.07600	60.15	2480.00	41.19	0.032640	0.062465	0.612400	0.522534	1.902730	4.739734	0.567556	2447.65	1.491152	0.028870

50	0.102000	0.381000	0.07600	60.15	2480.00	41.19	0.032640	0.062597	0.613700	0.521427	1.910547	4.769567	0.568176	2447.65	1.498866	0.029145
51	0.102000	0.381000	0.07600	60.15	2480.00	41.19	0.032640	0.062730	0.615000	0.520325	1.918430	4.799700	0.568792	2447.65	1.506644	0.029423
52	0.102000	0.381000	0.07600	60.15	2480.00	41.19	0.032640	0.062863	0.616300	0.519228	1.926382	4.830138	0.569405	2447.65	1.514487	0.029704
53	0.102000	0.381000	0.07600	60.15	2480.00	41.19	0.032640	0.062995	0.617600	0.518135	1.934402	4.860885	0.570014	2447.65	1.522395	0.029989
54	0.102000	0.381000	0.07600	60.15	2480.00	41.19	0.032640	0.063128	0.618900	0.517046	1.942492	4.891946	0.570620	2447.65	1.530370	0.030276
55	0.102000	0.381000	0.07600	60.15	2480.00	41.19	0.032640	0.063260	0.620200	0.515963	1.950652	4.923324	0.571223	2447.65	1.538412	0.030566
56	0.102000	0.381000	0.07600	60.15	2480.00	41.19	0.032640	0.063393	0.621500	0.514883	1.958883	4.955024	0.571823	2447.65	1.546522	0.030860
57	0.102000	0.381000	0.07600	60.15	2480.00	41.19	0.032640	0.063526	0.622800	0.513809	1.967186	4.987051	0.572419	2447.65	1.554700	0.031157
58	0.102000	0.381000	0.07600	60.15	2480.00	41.19	0.032640	0.063658	0.624100	0.512738	1.975562	5.019408	0.573011	2447.65	1.562949	0.031457
59	0.102000	0.381000	0.07600	60.15	2480.00	41.19	0.032640	0.063791	0.625400	0.511673	1.984011	5.052100	0.573601	2447.65	1.571268	0.031761
60	0.102000	0.381000	0.07600	60.15	2480.00	41.19	0.032640	0.063923	0.626700	0.510611	1.992536	5.085133	0.574187	2447.65	1.579658	0.032067
61	0.102000	0.381000	0.07600	60.15	2480.00	41.19	0.032640	0.064056	0.628000	0.509554	2.001136	5.118510	0.574771	2447.65	1.588120	0.032378
62	0.102000	0.381000	0.07600	60.15	2480.00	41.19	0.032640	0.064189	0.629300	0.508502	2.009812	5.152237	0.575351	2447.65	1.596656	0.032691
63	0.102000	0.381000	0.07600	60.15	2480.00	41.19	0.032640	0.064321	0.630600	0.507453	2.018565	5.186319	0.575928	2447.65	1.605265	0.033009
64	0.102000	0.381000	0.07600	60.15	2480.00	41.19	0.032640	0.064454	0.631900	0.506409	2.027397	5.220759	0.576502	2447.65	1.613950	0.033330
65	0.102000	0.381000	0.07600	60.15	2480.00	41.19	0.032640	0.064586	0.633200	0.505370	2.036308	5.255565	0.577072	2447.65	1.622710	0.033654
66	0.102000	0.381000	0.07600	60.15	2480.00	41.19	0.032640	0.064719	0.634500	0.504334	2.045300	5.290740	0.577640	2447.65	1.631548	0.033982
67	0.102000	0.381000	0.07600	60.15	2480.00	41.19	0.032640	0.064852	0.635800	0.503303	2.054372	5.326290	0.578205	2447.65	1.640463	0.034314
68	0.102000	0.381000	0.07600	60.15	2480.00	41.19	0.032640	0.064984	0.637100	0.502276	2.063527	5.362220	0.578766	2447.65	1.649457	0.034650
69	0.102000	0.381000	0.07600	60.15	2480.00	41.19	0.032640	0.065117	0.638400	0.501253	2.072765	5.398536	0.579325	2447.65	1.658531	0.034990
70	0.102000	0.381000	0.07600	60.15	2480.00	41.19	0.032640	0.065249	0.639700	0.500234	2.082087	5.435244	0.579881	2447.65	1.667685	0.035333
71	0.102000	0.381000	0.07600	60.15	2480.00	41.19	0.032640	0.065382	0.641000	0.499220	2.091495	5.472348	0.580434	2447.65	1.676922	0.035681
72	0.102000	0.381000	0.07600	60.15	2480.00	41.19	0.032640	0.065515	0.642300	0.498210	2.100989	5.509855	0.580984	2447.65	1.686241	0.036032
73	0.102000	0.381000	0.07600	60.15	2480.00	41.19	0.032640	0.065647	0.643600	0.497203	2.110570	5.547771	0.581531	2447.65	1.695645	0.036388
74	0.102000	0.381000	0.07600	60.15	2480.00	41.19	0.032640	0.065780	0.644900	0.496201	2.120240	5.586101	0.582075	2447.65	1.705133	0.036748
75	0.102000	0.381000	0.07600	60.15	2480.00	41.19	0.032640	0.065912	0.646200	0.495203	2.130000	5.624852	0.582616	2447.65	1.714708	0.037112

76	0.102000	0.381000	0.07600	60.15	2480.00	41.19	0.032640	0.066045	0.647500	0.494208	2.139850	5.664030	0.583155	2447.65	1.724370	0.037480
77	0.102000	0.381000	0.07600	60.15	2480.00	41.19	0.032640	0.066178	0.648800	0.493218	2.149793	5.703641	0.583690	2447.65	1.734120	0.037852
78	0.102000	0.381000	0.07600	60.15	2480.00	41.19	0.032640	0.066310	0.650100	0.492232	2.159829	5.743692	0.584223	2447.65	1.743960	0.038230
79	0.102000	0.381000	0.07600	60.15	2480.00	41.19	0.032640	0.066443	0.651400	0.491250	2.169959	5.784188	0.584754	2447.65	1.753891	0.038611
80	0.102000	0.381000	0.07600	60.15	2480.00	41.19	0.032640	0.066575	0.652700	0.490271	2.180185	5.825138	0.585281	2447.65	1.763913	0.038997
81	0.102000	0.381000	0.07600	60.15	2480.00	41.19	0.032640	0.066708	0.654000	0.489297	2.190508	5.866547	0.585806	2447.65	1.774029	0.039388
82	0.102000	0.381000	0.07600	60.15	2480.00	41.19	0.032640	0.066841	0.655300	0.488326	2.200929	5.908422	0.586328	2447.65	1.784240	0.039783
83	0.102000	0.381000	0.07600	60.15	2480.00	41.19	0.032640	0.066973	0.656600	0.487359	2.211450	5.950772	0.586848	2447.65	1.794546	0.040184
84	0.102000	0.381000	0.07600	60.15	2480.00	41.19	0.032640	0.067106	0.657900	0.486396	2.222071	5.993602	0.587364	2447.65	1.804949	0.040589
85	0.102000	0.381000	0.07600	60.15	2480.00	41.19	0.032640	0.067238	0.659200	0.485437	2.232794	6.036920	0.587879	2447.65	1.815450	0.040999
86	0.102000	0.381000	0.07600	60.15	2480.00	41.19	0.032640	0.067371	0.660500	0.484481	2.243621	6.080733	0.588390	2447.65	1.826051	0.041414
87	0.102000	0.381000	0.07600	60.15	2480.00	41.19	0.032640	0.067504	0.661800	0.483530	2.254553	6.125050	0.588899	2447.65	1.836754	0.041834
88	0.102000	0.381000	0.07600	60.15	2480.00	41.19	0.032640	0.067636	0.663100	0.482582	2.265591	6.169878	0.589406	2447.65	1.847558	0.042259
89	0.102000	0.381000	0.07600	60.15	2480.00	41.19	0.032640	0.067769	0.664400	0.481638	2.276737	6.215224	0.589910	2447.65	1.858466	0.042689
90	0.102000	0.381000	0.07600	60.15	2480.00	41.19	0.032640	0.067901	0.665700	0.480697	2.287991	6.261098	0.590411	2447.65	1.869479	0.043125
91	0.102000	0.381000	0.07600	60.15	2480.00	41.19	0.032640	0.068034	0.667000	0.479760	2.299357	6.307507	0.590910	2447.65	1.880599	0.043567
92	0.102000	0.381000	0.07600	60.15	2480.00	41.19	0.032640	0.068167	0.668300	0.478827	2.310834	6.354459	0.591407	2447.65	1.891828	0.044013
93	0.102000	0.381000	0.07600	60.15	2480.00	41.19	0.032640	0.068299	0.669600	0.477897	2.322425	6.401963	0.591901	2447.65	1.903165	0.044466
94	0.102000	0.381000	0.07600	60.15	2480.00	41.19	0.032640	0.068432	0.670900	0.476971	2.334132	6.450029	0.592392	2447.65	1.914614	0.044924
95	0.102000	0.381000	0.07600	60.15	2480.00	41.19	0.032640	0.068564	0.672200	0.476049	2.345955	6.498664	0.592881	2447.65	1.926176	0.045388
96	0.102000	0.381000	0.07600	60.15	2480.00	41.19	0.032640	0.068697	0.673500	0.475130	2.357896	6.547877	0.593368	2447.65	1.937852	0.045858
97	0.102000	0.381000	0.07600	60.15	2480.00	41.19	0.032640	0.068830	0.674800	0.474215	2.369958	6.597679	0.593852	2447.65	1.949644	0.046333
98	0.102000	0.381000	0.07600	60.15	2480.00	41.19	0.032640	0.068962	0.676100	0.473303	2.382141	6.648079	0.594334	2447.65	1.961553	0.046815
99	0.102000	0.381000	0.07600	60.15	2480.00	41.19	0.032640	0.069095	0.677400	0.472394	2.394448	6.699085	0.594814	2447.65	1.973582	0.047303
100	0.102000	0.381000	0.07600	60.15	2480.00	41.19	0.032640	0.069227	0.678700	0.471490	2.406880	6.750709	0.595291	2447.65	1.985731	0.047798

Table 6.14: Fracture Parameters for C3 Peak Load

S/N	W(m)	S(m)	B(m)	f'_c (MPa)	W (kg/m^3)	E (GPa)	a_0 (m)	a_c (m)	α_c	β	$F(\alpha_c)$	$V(\alpha_c)$	N (α_c, β)	Pmax (N)Avg	K^s_{IC} (MPa)	$CTOD_C$ (mm)
1	0.102000	0.381000	0.07600	60.15	2480.00	41.19	0.046920	0.056100	0.550000	0.836364	1.593713	3.596529	0.297041	1423.92	0.688582	0.005990
2	0.102000	0.381000	0.07600	60.15	2480.00	41.19	0.046920	0.056233	0.551300	0.834391	1.599034	3.615607	0.298782	1423.92	0.691697	0.006072
3	0.102000	0.381000	0.07600	60.15	2480.00	41.19	0.046920	0.056365	0.552600	0.832429	1.604395	3.634851	0.300503	1423.92	0.694834	0.006154
4	0.102000	0.381000	0.07600	60.15	2480.00	41.19	0.046920	0.056498	0.553900	0.830475	1.609798	3.654264	0.302205	1423.92	0.697993	0.006236
5	0.102000	0.381000	0.07600	60.15	2480.00	41.19	0.046920	0.056630	0.555200	0.828530	1.615241	3.673847	0.303889	1423.92	0.701175	0.006319
6	0.102000	0.381000	0.07600	60.15	2480.00	41.19	0.046920	0.056763	0.556500	0.826595	1.620726	3.693603	0.305555	1423.92	0.704379	0.006403
7	0.102000	0.381000	0.07600	60.15	2480.00	41.19	0.046920	0.056896	0.557800	0.824668	1.626254	3.713534	0.307203	1423.92	0.707606	0.006487
8	0.102000	0.381000	0.07600	60.15	2480.00	41.19	0.046920	0.057028	0.559100	0.822751	1.631823	3.733641	0.308834	1423.92	0.710857	0.006573
9	0.102000	0.381000	0.07600	60.15	2480.00	41.19	0.046920	0.057161	0.560400	0.820842	1.637436	3.753927	0.310447	1423.92	0.714130	0.006658
10	0.102000	0.381000	0.07600	60.15	2480.00	41.19	0.046920	0.057293	0.561700	0.818942	1.643092	3.774394	0.312044	1423.92	0.717428	0.006745
11	0.102000	0.381000	0.07600	60.15	2480.00	41.19	0.046920	0.057426	0.563000	0.817052	1.648792	3.795043	0.313625	1423.92	0.720749	0.006832
12	0.102000	0.381000	0.07600	60.15	2480.00	41.19	0.046920	0.057559	0.564300	0.815169	1.654536	3.815877	0.315190	1423.92	0.724094	0.006919
13	0.102000	0.381000	0.07600	60.15	2480.00	41.19	0.046920	0.057691	0.565600	0.813296	1.660324	3.836899	0.316738	1423.92	0.727464	0.007008
14	0.102000	0.381000	0.07600	60.15	2480.00	41.19	0.046920	0.057824	0.566900	0.811431	1.666158	3.858110	0.318272	1423.92	0.730859	0.007097
15	0.102000	0.381000	0.07600	60.15	2480.00	41.19	0.046920	0.057956	0.568200	0.809574	1.672037	3.879512	0.319790	1423.92	0.734278	0.007187
16	0.102000	0.381000	0.07600	60.15	2480.00	41.19	0.046920	0.058089	0.569500	0.807726	1.677962	3.901108	0.321293	1423.92	0.737722	0.007277
17	0.102000	0.381000	0.07600	60.15	2480.00	41.19	0.046920	0.058222	0.570800	0.805886	1.683933	3.922900	0.322781	1423.92	0.741192	0.007369
18	0.102000	0.381000	0.07600	60.15	2480.00	41.19	0.046920	0.058354	0.572100	0.804055	1.689952	3.944891	0.324256	1423.92	0.744688	0.007461
19	0.102000	0.381000	0.07600	60.15	2480.00	41.19	0.046920	0.058487	0.573400	0.802232	1.696018	3.967083	0.325716	1423.92	0.748210	0.007554
20	0.102000	0.381000	0.07600	60.15	2480.00	41.19	0.046920	0.058619	0.574700	0.800418	1.702131	3.989478	0.327162	1423.92	0.751757	0.007647
21	0.102000	0.381000	0.07600	60.15	2480.00	41.19	0.046920	0.058752	0.576000	0.798611	1.708293	4.012078	0.328594	1423.92	0.755332	0.007742
22	0.102000	0.381000	0.07600	60.15	2480.00	41.19	0.046920	0.058885	0.577300	0.796813	1.714504	4.034887	0.330013	1423.92	0.758933	0.007837
23	0.102000	0.381000	0.07600	60.15	2480.00	41.19	0.046920	0.059017	0.578600	0.795022	1.720765	4.057907	0.331419	1423.92	0.762561	0.007933

24	0.102000	0.381000	0.07600	60.15	2480.00	41.19	0.046920	0.059150	0.579900	0.793240	1.727075	4.081140	0.332812	1423.92	0.766217	0.008030
25	0.102000	0.381000	0.07600	60.15	2480.00	41.19	0.046920	0.059282	0.581200	0.791466	1.733436	4.104589	0.334192	1423.92	0.769901	0.008128
26	0.102000	0.381000	0.07600	60.15	2480.00	41.19	0.046920	0.059415	0.582500	0.789700	1.739848	4.128257	0.335560	1423.92	0.773612	0.008227
27	0.102000	0.381000	0.07600	60.15	2480.00	41.19	0.046920	0.059548	0.583800	0.787941	1.746311	4.152146	0.336915	1423.92	0.777352	0.008326
28	0.102000	0.381000	0.07600	60.15	2480.00	41.19	0.046920	0.059680	0.585100	0.786190	1.752826	4.176259	0.338258	1423.92	0.781120	0.008427
29	0.102000	0.381000	0.07600	60.15	2480.00	41.19	0.046920	0.059813	0.586400	0.784447	1.759394	4.200598	0.339589	1423.92	0.784918	0.008528
30	0.102000	0.381000	0.07600	60.15	2480.00	41.19	0.046920	0.059945	0.587700	0.782712	1.766015	4.225168	0.340908	1423.92	0.788744	0.008630
31	0.102000	0.381000	0.07600	60.15	2480.00	41.19	0.046920	0.060078	0.589000	0.780985	1.772690	4.249970	0.342216	1423.92	0.792601	0.008733
32	0.102000	0.381000	0.07600	60.15	2480.00	41.19	0.046920	0.060211	0.590300	0.779265	1.779419	4.275007	0.343512	1423.92	0.796487	0.008838
33	0.102000	0.381000	0.07600	60.15	2480.00	41.19	0.046920	0.060343	0.591600	0.777552	1.786203	4.300283	0.344797	1423.92	0.800403	0.008943
34	0.102000	0.381000	0.07600	60.15	2480.00	41.19	0.046920	0.060476	0.592900	0.775848	1.793043	4.325800	0.346072	1423.92	0.804351	0.009049
35	0.102000	0.381000	0.07600	60.15	2480.00	41.19	0.046920	0.060608	0.594200	0.774150	1.799938	4.351562	0.347335	1423.92	0.808329	0.009156
36	0.102000	0.381000	0.07600	60.15	2480.00	41.19	0.046920	0.060741	0.595500	0.772460	1.806891	4.377571	0.348587	1423.92	0.812338	0.009264
37	0.102000	0.381000	0.07600	60.15	2480.00	41.19	0.046920	0.060874	0.596800	0.770777	1.813900	4.403831	0.349829	1423.92	0.816379	0.009373
38	0.102000	0.381000	0.07600	60.15	2480.00	41.19	0.046920	0.061006	0.598100	0.769102	1.820968	4.430345	0.351060	1423.92	0.820452	0.009484
39	0.102000	0.381000	0.07600	60.15	2480.00	41.19	0.046920	0.061139	0.599400	0.767434	1.828094	4.457116	0.352282	1423.92	0.824558	0.009595
40	0.102000	0.381000	0.07600	60.15	2480.00	41.19	0.046920	0.061271	0.600700	0.765773	1.835280	4.484148	0.353493	1423.92	0.828696	0.009707
41	0.102000	0.381000	0.07600	60.15	2480.00	41.19	0.046920	0.061404	0.602000	0.764120	1.842526	4.511444	0.354694	1423.92	0.832867	0.009821
42	0.102000	0.381000	0.07600	60.15	2480.00	41.19	0.046920	0.061537	0.603300	0.762473	1.849832	4.539007	0.355885	1423.92	0.837072	0.009935
43	0.102000	0.381000	0.07600	60.15	2480.00	41.19	0.046920	0.061669	0.604600	0.760834	1.857199	4.566841	0.357067	1423.92	0.841311	0.010051
44	0.102000	0.381000	0.07600	60.15	2480.00	41.19	0.046920	0.061802	0.605900	0.759201	1.864629	4.594949	0.358239	1423.92	0.845584	0.010168
45	0.102000	0.381000	0.07600	60.15	2480.00	41.19	0.046920	0.061934	0.607200	0.757576	1.872121	4.623335	0.359401	1423.92	0.849892	0.010286
46	0.102000	0.381000	0.07600	60.15	2480.00	41.19	0.046920	0.062067	0.608500	0.755957	1.879676	4.652003	0.360555	1423.92	0.854235	0.010405
47	0.102000	0.381000	0.07600	60.15	2480.00	41.19	0.046920	0.062200	0.609800	0.754346	1.887296	4.680956	0.361699	1423.92	0.858614	0.010526
48	0.102000	0.381000	0.07600	60.15	2480.00	41.19	0.046920	0.062332	0.611100	0.752741	1.894980	4.710199	0.362834	1423.92	0.863028	0.010647
49	0.102000	0.381000	0.07600	60.15	2480.00	41.19	0.046920	0.062465	0.612400	0.751143	1.902730	4.739734	0.363960	1423.92	0.867479	0.010770

50	0.102000	0.381000	0.07600	60.15	2480.00	41.19	0.046920	0.062597	0.613700	0.749552	1.910547	4.769567	0.365078	1423.92	0.871966	0.010894
51	0.102000	0.381000	0.07600	60.15	2480.00	41.19	0.046920	0.062730	0.615000	0.747967	1.918430	4.799700	0.366187	1423.92	0.876491	0.011020
52	0.102000	0.381000	0.07600	60.15	2480.00	41.19	0.046920	0.062863	0.616300	0.746390	1.926382	4.830138	0.367287	1423.92	0.881054	0.011147
53	0.102000	0.381000	0.07600	60.15	2480.00	41.19	0.046920	0.062995	0.617600	0.744819	1.934402	4.860885	0.368379	1423.92	0.885655	0.011275
54	0.102000	0.381000	0.07600	60.15	2480.00	41.19	0.046920	0.063128	0.618900	0.743254	1.942492	4.891946	0.369462	1423.92	0.890294	0.011404
55	0.102000	0.381000	0.07600	60.15	2480.00	41.19	0.046920	0.063260	0.620200	0.741696	1.950652	4.923324	0.370538	1423.92	0.894972	0.011535
56	0.102000	0.381000	0.07600	60.15	2480.00	41.19	0.046920	0.063393	0.621500	0.740145	1.958883	4.955024	0.371605	1423.92	0.899690	0.011667
57	0.102000	0.381000	0.07600	60.15	2480.00	41.19	0.046920	0.063526	0.622800	0.738600	1.967186	4.987051	0.372664	1423.92	0.904448	0.011800
58	0.102000	0.381000	0.07600	60.15	2480.00	41.19	0.046920	0.063658	0.624100	0.737061	1.975562	5.019408	0.373715	1423.92	0.909247	0.011935
59	0.102000	0.381000	0.07600	60.15	2480.00	41.19	0.046920	0.063791	0.625400	0.735529	1.984011	5.052100	0.374759	1423.92	0.914086	0.012072
60	0.102000	0.381000	0.07600	60.15	2480.00	41.19	0.046920	0.063923	0.626700	0.734004	1.992536	5.085133	0.375794	1423.92	0.918967	0.012209
61	0.102000	0.381000	0.07600	60.15	2480.00	41.19	0.046920	0.064056	0.628000	0.732484	2.001136	5.118510	0.376822	1423.92	0.923890	0.012349
62	0.102000	0.381000	0.07600	60.15	2480.00	41.19	0.046920	0.064189	0.629300	0.730971	2.009812	5.152237	0.377843	1423.92	0.928856	0.012490
63	0.102000	0.381000	0.07600	60.15	2480.00	41.19	0.046920	0.064321	0.630600	0.729464	2.018565	5.186319	0.378856	1423.92	0.933864	0.012632
64	0.102000	0.381000	0.07600	60.15	2480.00	41.19	0.046920	0.064454	0.631900	0.727963	2.027397	5.220759	0.379862	1423.92	0.938917	0.012776
65	0.102000	0.381000	0.07600	60.15	2480.00	41.19	0.046920	0.064586	0.633200	0.726469	2.036308	5.255565	0.380860	1423.92	0.944013	0.012921
66	0.102000	0.381000	0.07600	60.15	2480.00	41.19	0.046920	0.064719	0.634500	0.724980	2.045300	5.290740	0.381852	1423.92	0.949154	0.013069
67	0.102000	0.381000	0.07600	60.15	2480.00	41.19	0.046920	0.064852	0.635800	0.723498	2.054372	5.326290	0.382836	1423.92	0.954341	0.013217
68	0.102000	0.381000	0.07600	60.15	2480.00	41.19	0.046920	0.064984	0.637100	0.722022	2.063527	5.362220	0.383814	1423.92	0.959573	0.013368
69	0.102000	0.381000	0.07600	60.15	2480.00	41.19	0.046920	0.065117	0.638400	0.720551	2.072765	5.398536	0.384784	1423.92	0.964852	0.013520
70	0.102000	0.381000	0.07600	60.15	2480.00	41.19	0.046920	0.065249	0.639700	0.719087	2.082087	5.435244	0.385748	1423.92	0.970177	0.013674
71	0.102000	0.381000	0.07600	60.15	2480.00	41.19	0.046920	0.065382	0.641000	0.717629	2.091495	5.472348	0.386705	1423.92	0.975551	0.013829
72	0.102000	0.381000	0.07600	60.15	2480.00	41.19	0.046920	0.065515	0.642300	0.716176	2.100989	5.509855	0.387655	1423.92	0.980972	0.013986
73	0.102000	0.381000	0.07600	60.15	2480.00	41.19	0.046920	0.065647	0.643600	0.714730	2.110570	5.547771	0.388598	1423.92	0.986443	0.014146
74	0.102000	0.381000	0.07600	60.15	2480.00	41.19	0.046920	0.065780	0.644900	0.713289	2.120240	5.586101	0.389536	1423.92	0.991963	0.014307
75	0.102000	0.381000	0.07600	60.15	2480.00	41.19	0.046920	0.065912	0.646200	0.711854	2.130000	5.624852	0.390466	1423.92	0.997533	0.014469

76	0.102000	0.381000	0.07600	60.15	2480.00	41.19	0.046920	0.066045	0.647500	0.710425	2.139850	5.664030	0.391391	1423.92	1.003153	0.014634
77	0.102000	0.381000	0.07600	60.15	2480.00	41.19	0.046920	0.066178	0.648800	0.709001	2.149793	5.703641	0.392309	1423.92	1.008826	0.014800
78	0.102000	0.381000	0.07600	60.15	2480.00	41.19	0.046920	0.066310	0.650100	0.707583	2.159829	5.743692	0.393220	1423.92	1.014550	0.014969
79	0.102000	0.381000	0.07600	60.15	2480.00	41.19	0.046920	0.066443	0.651400	0.706171	2.169959	5.784188	0.394126	1423.92	1.020327	0.015139
80	0.102000	0.381000	0.07600	60.15	2480.00	41.19	0.046920	0.066575	0.652700	0.704765	2.180185	5.825138	0.395026	1423.92	1.026158	0.015312
81	0.102000	0.381000	0.07600	60.15	2480.00	41.19	0.046920	0.066708	0.654000	0.703364	2.190508	5.866547	0.395919	1423.92	1.032043	0.015486
82	0.102000	0.381000	0.07600	60.15	2480.00	41.19	0.046920	0.066841	0.655300	0.701969	2.200929	5.908422	0.396807	1423.92	1.037983	0.015663
83	0.102000	0.381000	0.07600	60.15	2480.00	41.19	0.046920	0.066973	0.656600	0.700579	2.211450	5.950772	0.397689	1423.92	1.043979	0.015842
84	0.102000	0.381000	0.07600	60.15	2480.00	41.19	0.046920	0.067106	0.657900	0.699194	2.222071	5.993602	0.398565	1423.92	1.050031	0.016023
85	0.102000	0.381000	0.07600	60.15	2480.00	41.19	0.046920	0.067238	0.659200	0.697816	2.232794	6.036920	0.399435	1423.92	1.056140	0.016206
86	0.102000	0.381000	0.07600	60.15	2480.00	41.19	0.046920	0.067371	0.660500	0.696442	2.243621	6.080733	0.400299	1423.92	1.062307	0.016391
87	0.102000	0.381000	0.07600	60.15	2480.00	41.19	0.046920	0.067504	0.661800	0.695074	2.254553	6.125050	0.401158	1423.92	1.068533	0.016578
88	0.102000	0.381000	0.07600	60.15	2480.00	41.19	0.046920	0.067636	0.663100	0.693711	2.265591	6.169878	0.402012	1423.92	1.074818	0.016768
89	0.102000	0.381000	0.07600	60.15	2480.00	41.19	0.046920	0.067769	0.664400	0.692354	2.276737	6.215224	0.402859	1423.92	1.081164	0.016960
90	0.102000	0.381000	0.07600	60.15	2480.00	41.19	0.046920	0.067901	0.665700	0.691002	2.287991	6.261098	0.403702	1423.92	1.087571	0.017154
91	0.102000	0.381000	0.07600	60.15	2480.00	41.19	0.046920	0.068034	0.667000	0.689655	2.299357	6.307507	0.404539	1423.92	1.094040	0.017351
92	0.102000	0.381000	0.07600	60.15	2480.00	41.19	0.046920	0.068167	0.668300	0.688314	2.310834	6.354459	0.405370	1423.92	1.100572	0.017550
93	0.102000	0.381000	0.07600	60.15	2480.00	41.19	0.046920	0.068299	0.669600	0.686977	2.322425	6.401963	0.406197	1423.92	1.107168	0.017752
94	0.102000	0.381000	0.07600	60.15	2480.00	41.19	0.046920	0.068432	0.670900	0.685646	2.334132	6.450029	0.407018	1423.92	1.113828	0.017956
95	0.102000	0.381000	0.07600	60.15	2480.00	41.19	0.046920	0.068564	0.672200	0.684320	2.345955	6.498664	0.407834	1423.92	1.120554	0.018163
96	0.102000	0.381000	0.07600	60.15	2480.00	41.19	0.046920	0.068697	0.673500	0.682999	2.357896	6.547877	0.408645	1423.92	1.127347	0.018373
97	0.102000	0.381000	0.07600	60.15	2480.00	41.19	0.046920	0.068830	0.674800	0.681683	2.369958	6.597679	0.409451	1423.92	1.134207	0.018585
98	0.102000	0.381000	0.07600	60.15	2480.00	41.19	0.046920	0.068962	0.676100	0.680373	2.382141	6.648079	0.410251	1423.92	1.141135	0.018799
99	0.102000	0.381000	0.07600	60.15	2480.00	41.19	0.046920	0.069095	0.677400	0.679067	2.394448	6.699085	0.411047	1423.92	1.148133	0.019017
100	0.102000	0.381000	0.07600	60.15	2480.00	41.19	0.046920	0.069227	0.678700	0.677766	2.406880	6.750709	0.411838	1423.92	1.155201	0.019237

Table 6.15: Fracture Parameters for Average CTOD and Variance (0% RHA)

S/N	K^s_{IC} (MPa)	SQ K^s_{IC} (MPa)	CTODc (Group 1)	CTODc (Group 2)	CTODc (Group 3)	CTODc Average	S^2
1	0.6700000	0.4489000	0.0005940	-0.0007120	0.0052940	0.0017253	0.997794533
2	0.6850000	0.4692250	0.0011670	-0.0001660	0.0057170	0.0022393	0.951484633
3	0.7000000	0.4900000	0.0017400	0.0003800	0.0061400	0.0027533	0.906453333
4	0.7150000	0.5112250	0.0023130	0.0009260	0.0065630	0.0032673	0.862700633
5	0.7300000	0.5329000	0.0028860	0.0014720	0.0069860	0.0037813	0.820226533
6	0.7450000	0.5550250	0.0034590	0.0020180	0.0074090	0.0042953	0.779031033
7	0.7600000	0.5776000	0.0040320	0.0025640	0.0078320	0.0048093	0.739114133
8	0.7750000	0.6006250	0.0046050	0.0031100	0.0082550	0.0053233	0.700475833
9	0.7900000	0.6241000	0.0051780	0.0036560	0.0086780	0.0058373	0.663116133
10	0.8050000	0.6480250	0.0057510	0.0042020	0.0091010	0.0063513	0.627035033
11	0.8200000	0.6724000	0.0063240	0.0047480	0.0095240	0.0068653	0.592232533
12	0.8350000	0.6972250	0.0068970	0.0052940	0.0099470	0.0073793	0.558708633
13	0.8500000	0.7225000	0.0074700	0.0058400	0.0103700	0.0078933	0.526463333
14	0.8650000	0.7482250	0.0080430	0.0063860	0.0107930	0.0084073	0.495496633
15	0.8800000	0.7744000	0.0086160	0.0069320	0.0112160	0.0089213	0.465808533
16	0.8950000	0.8010250	0.0091890	0.0074780	0.0116390	0.0094353	0.437399033

17	0.9100000	0.8281000	0.0097620	0.0080240	0.0120620	0.0099493	0.410268133
18	0.9250000	0.8556250	0.0103350	0.0085700	0.0124850	0.0104633	0.384415833
19	0.9400000	0.8836000	0.0109080	0.0091160	0.0129080	0.0109773	0.359842133
20	0.9550000	0.9120250	0.0114810	0.0096620	0.0133310	0.0114913	0.336547033
21	0.9700000	0.9409000	0.0120540	0.0102080	0.0137540	0.0120053	0.314530533
22	0.9850000	0.9702250	0.0126270	0.0107540	0.0141770	0.0125193	0.293792633
23	1.0000000	1.0000000	0.0132000	0.0113000	0.0146000	0.0130333	0.274333333
24	1.0150000	1.0302250	0.0137730	0.0118460	0.0150230	0.0135473	0.256152633
25	1.0300000	1.0609000	0.0143460	0.0123920	0.0154460	0.0140613	0.239250533
26	1.0450000	1.0920250	0.0149190	0.0129380	0.0158690	0.0145753	0.223627033
27	1.0600000	1.1236000	0.0154920	0.0134840	0.0162920	0.0150893	0.209282133
28	1.0750000	1.1556250	0.0160650	0.0140300	0.0167150	0.0156033	0.196215833
29	1.0900000	1.1881000	0.0166380	0.0145760	0.0171380	0.0161173	0.184428133
30	1.1050000	1.2210250	0.0172110	0.0151220	0.0175610	0.0166313	0.173919033
31	1.1200000	1.2544000	0.0177840	0.0156680	0.0179840	0.0171453	0.164688533
32	1.1350000	1.2882250	0.0183570	0.0162140	0.0184070	0.0176593	0.156736633
33	1.1500000	1.3225000	0.0189300	0.0167600	0.0188300	0.0181733	0.150063333
34	1.1650000	1.3572250	0.0195030	0.0173060	0.0192530	0.0186873	0.144668633
35	1.1800000	1.3924000	0.0200760	0.0178520	0.0196760	0.0192013	0.140552533
36	1.1950000	1.4280250	0.0206490	0.0183980	0.0200990	0.0197153	0.137715033
37	1.2100000	1.4641000	0.0212220	0.0189440	0.0205220	0.0202293	0.136156133

38	1.2250000	1.5006250	0.0217950	0.0194900	0.0209450	0.0207433	0.135875833
39	1.2400000	1.5376000	0.0223680	0.0200360	0.0213680	0.0212573	0.136874133
40	1.2550000	1.5750250	0.0229410	0.0205820	0.0217910	0.0217713	0.139151033
41	1.2700000	1.6129000	0.0235140	0.0211280	0.0222140	0.0222853	0.142706533
42	1.2850000	1.6512250	0.0240870	0.0216740	0.0226370	0.0227993	0.147540633
43	1.3000000	1.6900000	0.0246600	0.0222200	0.0230600	0.0233133	0.153653333
44	1.3150000	1.7292250	0.0252330	0.0227660	0.0234830	0.0238273	0.161044633
45	1.3300000	1.7689000	0.0258060	0.0233120	0.0239060	0.0243413	0.169714533
46	1.3450000	1.8090250	0.0263790	0.0238580	0.0243290	0.0248553	0.179663033
47	1.3600000	1.8496000	0.0269520	0.0244040	0.0247520	0.0253693	0.190890133
48	1.3750000	1.8906250	0.0275250	0.0249500	0.0251750	0.0258833	0.203395833
49	1.3900000	1.9321000	0.0280980	0.0254960	0.0255980	0.0263973	0.217180133
50	1.4050000	1.9740250	0.0286710	0.0260420	0.0260210	0.0269113	0.232243033
51	1.4200000	2.0164000	0.0292440	0.0265880	0.0264440	0.0274253	0.248584533
52	1.4350000	2.0592250	0.0298170	0.0271340	0.0268670	0.0279393	0.266204633
53	1.4500000	2.1025000	0.0303900	0.0276800	0.0272900	0.0284533	0.285103333
54	1.4650000	2.1462250	0.0309630	0.0282260	0.0277130	0.0289673	0.305280633
55	1.4800000	2.1904000	0.0315360	0.0287720	0.0281360	0.0294813	0.326736533
56	1.4950000	2.2350250	0.0321090	0.0293180	0.0285590	0.0299953	0.349471033
57	1.5100000	2.2801000	0.0326820	0.0298640	0.0289820	0.0305093	0.373484133
58	1.5250000	2.3256250	0.0332550	0.0304100	0.0294050	0.0310233	0.398775833

59	1.5400000	2.3716000	0.0338280	0.0309560	0.0298280	0.0315373	0.425346133
60	1.5550000	2.4180250	0.0344010	0.0315020	0.0302510	0.0320513	0.453195033
61	1.5700000	2.4649000	0.0349740	0.0320480	0.0306740	0.0325653	0.482322533
62	1.5850000	2.5122250	0.0355470	0.0325940	0.0310970	0.0330793	0.512728633
63	1.6000000	2.5600000	0.0361200	0.0331400	0.0315200	0.0335933	0.544413333
64	1.6150000	2.6082250	0.0366930	0.0336860	0.0319430	0.0341073	0.577376633
65	1.6300000	2.6569000	0.0372660	0.0342320	0.0323660	0.0346213	0.611618533
66	1.6450000	2.7060250	0.0378390	0.0347780	0.0327890	0.0351353	0.647139033
67	1.6600000	2.7556000	0.0384120	0.0353240	0.0332120	0.0356493	0.683938133
68	1.6750000	2.8056250	0.0389850	0.0358700	0.0336350	0.0361633	0.722015833
69	1.6900000	2.8561000	0.0395580	0.0364160	0.0340580	0.0366773	0.761372133
70	1.7050000	2.9070250	0.0401310	0.0369620	0.0344810	0.0371913	0.802007033
71	1.7200000	2.9584000	0.0407040	0.0375080	0.0349040	0.0377053	0.843920533
72	1.7350000	3.0102250	0.0412770	0.0380540	0.0353270	0.0382193	0.887112633
73	1.7500000	3.0625000	0.0418500	0.0386000	0.0357500	0.0387333	0.931583333
74	1.7650000	3.1152250	0.0424230	0.0391460	0.0361730	0.0392473	0.977332633
75	1.7800000	3.1684000	0.0429960	0.0396920	0.0365960	0.0397613	1.024360533
76	1.7950000	3.2220250	0.0435690	0.0402380	0.0370190	0.0402753	1.072667033
77	1.8100000	3.2761000	0.0441420	0.0407840	0.0374420	0.0407893	1.122252133
78	1.8250000	3.3306250	0.0447150	0.0413300	0.0378650	0.0413033	1.173115833
79	1.8400000	3.3856000	0.0452880	0.0418760	0.0382880	0.0418173	1.225258133

80	1.8550000	3.4410250	0.0458610	0.0424220	0.0387110	0.0423313	1.278679033
81	1.8700000	3.4969000	0.0464340	0.0429680	0.0391340	0.0428453	1.333378533
82	1.8850000	3.5532250	0.0470070	0.0435140	0.0395570	0.0433593	1.389356633
83	1.9000000	3.6100000	0.0475800	0.0440600	0.0399800	0.0438733	1.446613333
84	1.9150000	3.6672250	0.0481530	0.0446060	0.0404030	0.0443873	1.505148633
85	1.9300000	3.7249000	0.0487260	0.0451520	0.0408260	0.0449013	1.564962533
86	1.9450000	3.7830250	0.0492990	0.0456980	0.0412490	0.0454153	1.626055033
87	1.9600000	3.8416000	0.0498720	0.0462440	0.0416720	0.0459293	1.688426133
88	1.9750000	3.9006250	0.0504450	0.0467900	0.0420950	0.0464433	1.752075833
89	1.9900000	3.9601000	0.0510180	0.0473360	0.0425180	0.0469573	1.817004133
90	2.0050000	4.0200250	0.0515910	0.0478820	0.0429410	0.0474713	1.883211033
91	2.0200000	4.0804000	0.0521640	0.0484280	0.0433640	0.0479853	1.950696533
92	2.0350000	4.1412250	0.0527370	0.0489740	0.0437870	0.0484993	2.019460633
93	2.0500000	4.2025000	0.0533100	0.0495200	0.0442100	0.0490133	2.089503333
94	2.0650000	4.2642250	0.0538830	0.0500660	0.0446330	0.0495273	2.160824633
95	2.0800000	4.3264000	0.0544560	0.0506120	0.0450560	0.0500413	2.233424533
96	2.0950000	4.3890250	0.0550290	0.0511580	0.0454790	0.0505553	2.307303033
97	2.1100000	4.4521000	0.0556020	0.0517040	0.0459020	0.0510693	2.382460133
98	2.1250000	4.5156250	0.0561750	0.0522500	0.0463250	0.0515833	2.458895833
99	2.1400000	4.5796000	0.0567480	0.0527960	0.0467480	0.0520973	2.536610133
100	2.1550000	4.6440250	0.0573210	0.0533420	0.0471710	0.0526113	2.615603033

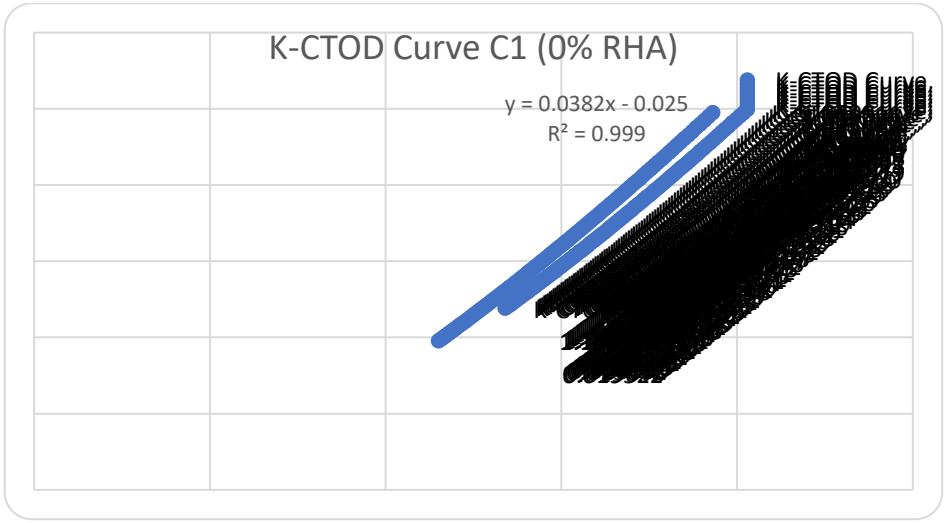
K-CTOD Curve C1 (0% RHA)
y = 0.0382x - 0.025
R² = 0.999
K-CTOD Curve

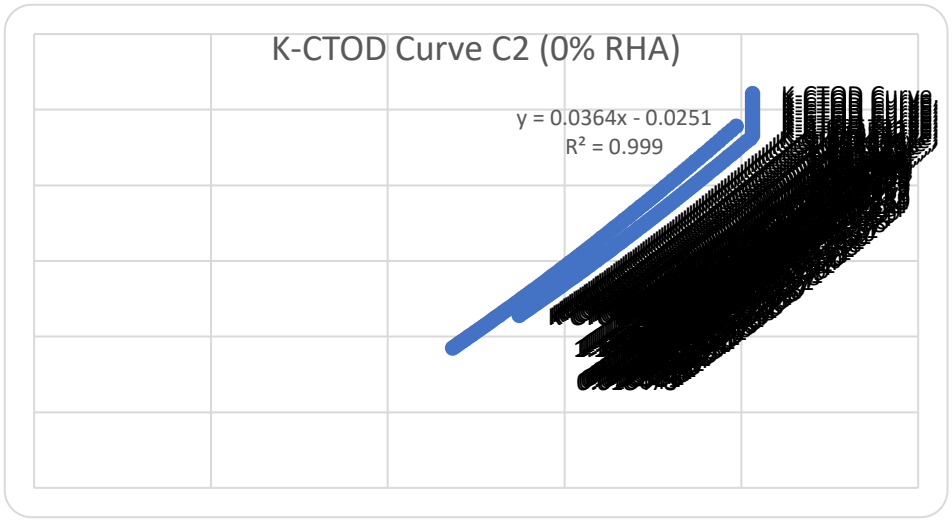
K-CTOD Curve C2 (0% RHA)
y = 0.0364x - 0.0251
R² = 0.999
K-CTOD Curve

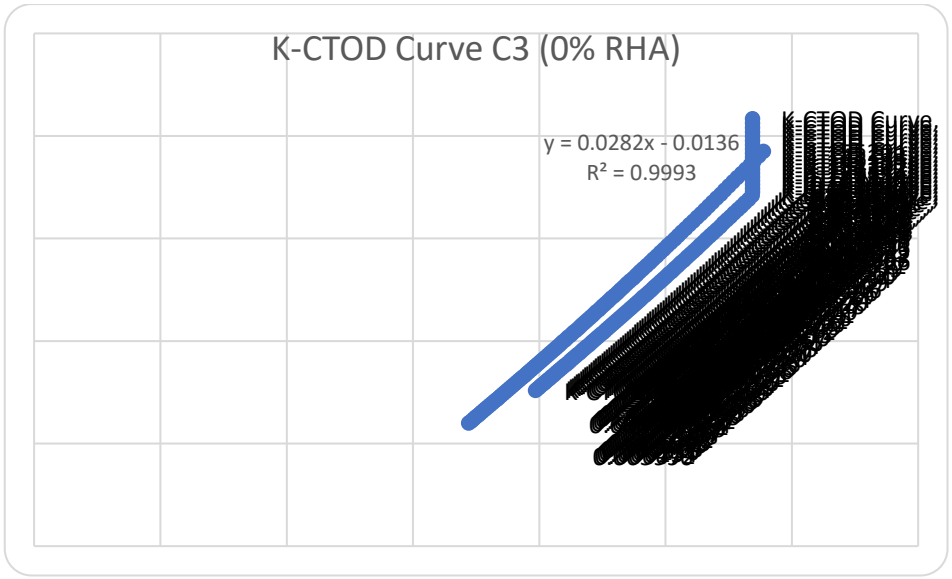
K-CTOD Curve C3 (0% RHA)
y = 0.0282x - 0.0136
R² = 0.9993
K-CTOD Curve

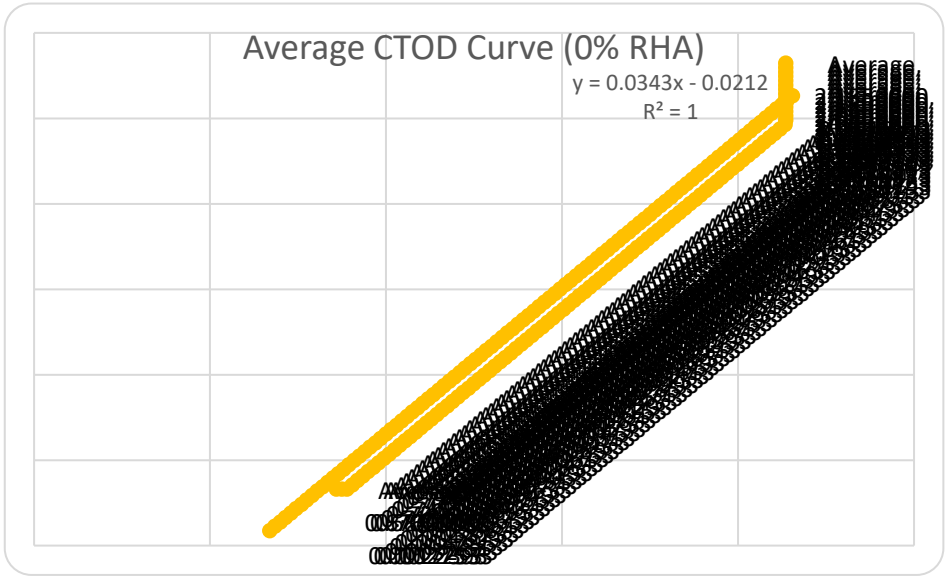
Average CTOD Curve (0% RHA)
y = 0.0343x - 0.0212
R² = 1
Average

Table 6.16: Fracture Parameters for A1 Peak Load

S/N	W(m)	S(m)	B(m)	f'_c (MPa)	W (kg/m^3)	E (GPa)	a_0 (m)	a_c (m)	α_c	β	$F(\alpha_c)$	$V(\alpha_c)$	N (α_c, β)	Pmax (N)Avg	K^s_{IC} (MPa)	$CTOD_C$ (mm)
1	0.102000	0.381000	0.07600	63.70	2343.70	38.94	0.029580	0.056100	0.550000	0.527273	1.593713	3.596529	0.579137	2538.01	1.227332	0.022019
2	0.102000	0.381000	0.07600	63.70	2343.70	38.94	0.029580	0.056233	0.551300	0.526029	1.599034	3.615607	0.579857	2538.01	1.232884	0.022215
3	0.102000	0.381000	0.07600	63.70	2343.70	38.94	0.029580	0.056365	0.552600	0.524792	1.604395	3.634851	0.580572	2538.01	1.238475	0.022414
4	0.102000	0.381000	0.07600	63.70	2343.70	38.94	0.029580	0.056498	0.553900	0.523560	1.609798	3.654264	0.581283	2538.01	1.244107	0.022614
5	0.102000	0.381000	0.07600	63.70	2343.70	38.94	0.029580	0.056630	0.555200	0.522334	1.615241	3.673847	0.581990	2538.01	1.249778	0.022817
6	0.102000	0.381000	0.07600	63.70	2343.70	38.94	0.029580	0.056763	0.556500	0.521114	1.620726	3.693603	0.582692	2538.01	1.255489	0.023021
7	0.102000	0.381000	0.07600	63.70	2343.70	38.94	0.029580	0.056896	0.557800	0.519900	1.626254	3.713534	0.583390	2538.01	1.261241	0.023227
8	0.102000	0.381000	0.07600	63.70	2343.70	38.94	0.029580	0.057028	0.559100	0.518691	1.631823	3.733641	0.584084	2538.01	1.267035	0.023435
9	0.102000	0.381000	0.07600	63.70	2343.70	38.94	0.029580	0.057161	0.560400	0.517488	1.637436	3.753927	0.584773	2538.01	1.272870	0.023645
10	0.102000	0.381000	0.07600	63.70	2343.70	38.94	0.029580	0.057293	0.561700	0.516290	1.643092	3.774394	0.585458	2538.01	1.278747	0.023857
11	0.102000	0.381000	0.07600	63.70	2343.70	38.94	0.029580	0.057426	0.563000	0.515098	1.648792	3.795043	0.586140	2538.01	1.284667	0.024071
12	0.102000	0.381000	0.07600	63.70	2343.70	38.94	0.029580	0.057559	0.564300	0.513911	1.654536	3.815877	0.586816	2538.01	1.290630	0.024287
13	0.102000	0.381000	0.07600	63.70	2343.70	38.94	0.029580	0.057691	0.565600	0.512730	1.660324	3.836899	0.587489	2538.01	1.296636	0.024505
14	0.102000	0.381000	0.07600	63.70	2343.70	38.94	0.029580	0.057824	0.566900	0.511554	1.666158	3.858110	0.588158	2538.01	1.302687	0.024725
15	0.102000	0.381000	0.07600	63.70	2343.70	38.94	0.029580	0.057956	0.568200	0.510384	1.672037	3.879512	0.588823	2538.01	1.308781	0.024947
16	0.102000	0.381000	0.07600	63.70	2343.70	38.94	0.029580	0.058089	0.569500	0.509219	1.677962	3.901108	0.589484	2538.01	1.314921	0.025172
17	0.102000	0.381000	0.07600	63.70	2343.70	38.94	0.029580	0.058222	0.570800	0.508059	1.683933	3.922900	0.590141	2538.01	1.321105	0.025399
18	0.102000	0.381000	0.07600	63.70	2343.70	38.94	0.029580	0.058354	0.572100	0.506904	1.689952	3.944891	0.590794	2538.01	1.327336	0.025628
19	0.102000	0.381000	0.07600	63.70	2343.70	38.94	0.029580	0.058487	0.573400	0.505755	1.696018	3.967083	0.591443	2538.01	1.333613	0.025859
20	0.102000	0.381000	0.07600	63.70	2343.70	38.94	0.029580	0.058619	0.574700	0.504611	1.702131	3.989478	0.592088	2538.01	1.339937	0.026092
21	0.102000	0.381000	0.07600	63.70	2343.70	38.94	0.029580	0.058752	0.576000	0.503472	1.708293	4.012078	0.592730	2538.01	1.346308	0.026328
22	0.102000	0.381000	0.07600	63.70	2343.70	38.94	0.029580	0.058885	0.577300	0.502338	1.714504	4.034887	0.593368	2538.01	1.352726	0.026566
23	0.102000	0.381000	0.07600	63.70	2343.70	38.94	0.029580	0.059017	0.578600	0.501210	1.720765	4.057907	0.594002	2538.01	1.359194	0.026806

24	0.102000	0.381000	0.07600	63.70	2343.70	38.94	0.029580	0.059150	0.579900	0.500086	1.727075	4.081140	0.594632	2538.01	1.365710	0.027049
25	0.102000	0.381000	0.07600	63.70	2343.70	38.94	0.029580	0.059282	0.581200	0.498968	1.733436	4.104589	0.595259	2538.01	1.372275	0.027294
26	0.102000	0.381000	0.07600	63.70	2343.70	38.94	0.029580	0.059415	0.582500	0.497854	1.739848	4.128257	0.595882	2538.01	1.378890	0.027541
27	0.102000	0.381000	0.07600	63.70	2343.70	38.94	0.029580	0.059548	0.583800	0.496745	1.746311	4.152146	0.596502	2538.01	1.385556	0.027791
28	0.102000	0.381000	0.07600	63.70	2343.70	38.94	0.029580	0.059680	0.585100	0.495642	1.752826	4.176259	0.597118	2538.01	1.392273	0.028044
29	0.102000	0.381000	0.07600	63.70	2343.70	38.94	0.029580	0.059813	0.586400	0.494543	1.759394	4.200598	0.597730	2538.01	1.399042	0.028299
30	0.102000	0.381000	0.07600	63.70	2343.70	38.94	0.029580	0.059945	0.587700	0.493449	1.766015	4.225168	0.598339	2538.01	1.405863	0.028557
31	0.102000	0.381000	0.07600	63.70	2343.70	38.94	0.029580	0.060078	0.589000	0.492360	1.772690	4.249970	0.598945	2538.01	1.412736	0.028817
32	0.102000	0.381000	0.07600	63.70	2343.70	38.94	0.029580	0.060211	0.590300	0.491276	1.779419	4.275007	0.599547	2538.01	1.419663	0.029080
33	0.102000	0.381000	0.07600	63.70	2343.70	38.94	0.029580	0.060343	0.591600	0.490196	1.786203	4.300283	0.600145	2538.01	1.426644	0.029346
34	0.102000	0.381000	0.07600	63.70	2343.70	38.94	0.029580	0.060476	0.592900	0.489121	1.793043	4.325800	0.600741	2538.01	1.433679	0.029614
35	0.102000	0.381000	0.07600	63.70	2343.70	38.94	0.029580	0.060608	0.594200	0.488051	1.799938	4.351562	0.601333	2538.01	1.440770	0.029885
36	0.102000	0.381000	0.07600	63.70	2343.70	38.94	0.029580	0.060741	0.595500	0.486986	1.806891	4.377571	0.601921	2538.01	1.447916	0.030159
37	0.102000	0.381000	0.07600	63.70	2343.70	38.94	0.029580	0.060874	0.596800	0.485925	1.813900	4.403831	0.602506	2538.01	1.455119	0.030436
38	0.102000	0.381000	0.07600	63.70	2343.70	38.94	0.029580	0.061006	0.598100	0.484869	1.820968	4.430345	0.603089	2538.01	1.462379	0.030715
39	0.102000	0.381000	0.07600	63.70	2343.70	38.94	0.029580	0.061139	0.599400	0.483817	1.828094	4.457116	0.603667	2538.01	1.469696	0.030998
40	0.102000	0.381000	0.07600	63.70	2343.70	38.94	0.029580	0.061271	0.600700	0.482770	1.835280	4.484148	0.604243	2538.01	1.477072	0.031283
41	0.102000	0.381000	0.07600	63.70	2343.70	38.94	0.029580	0.061404	0.602000	0.481728	1.842526	4.511444	0.604816	2538.01	1.484507	0.031572
42	0.102000	0.381000	0.07600	63.70	2343.70	38.94	0.029580	0.061537	0.603300	0.480690	1.849832	4.539007	0.605385	2538.01	1.492002	0.031863
43	0.102000	0.381000	0.07600	63.70	2343.70	38.94	0.029580	0.061669	0.604600	0.479656	1.857199	4.566841	0.605951	2538.01	1.499558	0.032158
44	0.102000	0.381000	0.07600	63.70	2343.70	38.94	0.029580	0.061802	0.605900	0.478627	1.864629	4.594949	0.606514	2538.01	1.507174	0.032455
45	0.102000	0.381000	0.07600	63.70	2343.70	38.94	0.029580	0.061934	0.607200	0.477602	1.872121	4.623335	0.607074	2538.01	1.514853	0.032756
46	0.102000	0.381000	0.07600	63.70	2343.70	38.94	0.029580	0.062067	0.608500	0.476582	1.879676	4.652003	0.607631	2538.01	1.522593	0.033060
47	0.102000	0.381000	0.07600	63.70	2343.70	38.94	0.029580	0.062200	0.609800	0.475566	1.887296	4.680956	0.608185	2538.01	1.530398	0.033367
48	0.102000	0.381000	0.07600	63.70	2343.70	38.94	0.029580	0.062332	0.611100	0.474554	1.894980	4.710199	0.608736	2538.01	1.538266	0.033678
49	0.102000	0.381000	0.07600	63.70	2343.70	38.94	0.029580	0.062465	0.612400	0.473547	1.902730	4.739734	0.609284	2538.01	1.546199	0.033992

50	0.102000	0.381000	0.07600	63.70	2343.70	38.94	0.029580	0.062597	0.613700	0.472544	1.910547	4.769567	0.609829	2538.01	1.554198	0.034309
51	0.102000	0.381000	0.07600	63.70	2343.70	38.94	0.029580	0.062730	0.615000	0.471545	1.918430	4.799700	0.610371	2538.01	1.562263	0.034630
52	0.102000	0.381000	0.07600	63.70	2343.70	38.94	0.029580	0.062863	0.616300	0.470550	1.926382	4.830138	0.610911	2538.01	1.570396	0.034954
53	0.102000	0.381000	0.07600	63.70	2343.70	38.94	0.029580	0.062995	0.617600	0.469560	1.934402	4.860885	0.611447	2538.01	1.578596	0.035281
54	0.102000	0.381000	0.07600	63.70	2343.70	38.94	0.029580	0.063128	0.618900	0.468573	1.942492	4.891946	0.611980	2538.01	1.586865	0.035613
55	0.102000	0.381000	0.07600	63.70	2343.70	38.94	0.029580	0.063260	0.620200	0.467591	1.950652	4.923324	0.612511	2538.01	1.595204	0.035947
56	0.102000	0.381000	0.07600	63.70	2343.70	38.94	0.029580	0.063393	0.621500	0.466613	1.958883	4.955024	0.613039	2538.01	1.603613	0.036286
57	0.102000	0.381000	0.07600	63.70	2343.70	38.94	0.029580	0.063526	0.622800	0.465639	1.967186	4.987051	0.613564	2538.01	1.612094	0.036628
58	0.102000	0.381000	0.07600	63.70	2343.70	38.94	0.029580	0.063658	0.624100	0.464669	1.975562	5.019408	0.614086	2538.01	1.620647	0.036974
59	0.102000	0.381000	0.07600	63.70	2343.70	38.94	0.029580	0.063791	0.625400	0.463703	1.984011	5.052100	0.614606	2538.01	1.629273	0.037324
60	0.102000	0.381000	0.07600	63.70	2343.70	38.94	0.029580	0.063923	0.626700	0.462741	1.992536	5.085133	0.615123	2538.01	1.637972	0.037678
61	0.102000	0.381000	0.07600	63.70	2343.70	38.94	0.029580	0.064056	0.628000	0.461783	2.001136	5.118510	0.615637	2538.01	1.646747	0.038036
62	0.102000	0.381000	0.07600	63.70	2343.70	38.94	0.029580	0.064189	0.629300	0.460829	2.009812	5.152237	0.616149	2538.01	1.655598	0.038397
63	0.102000	0.381000	0.07600	63.70	2343.70	38.94	0.029580	0.064321	0.630600	0.459879	2.018565	5.186319	0.616658	2538.01	1.664525	0.038763
64	0.102000	0.381000	0.07600	63.70	2343.70	38.94	0.029580	0.064454	0.631900	0.458933	2.027397	5.220759	0.617164	2538.01	1.673531	0.039133
65	0.102000	0.381000	0.07600	63.70	2343.70	38.94	0.029580	0.064586	0.633200	0.457991	2.036308	5.255565	0.617667	2538.01	1.682614	0.039507
66	0.102000	0.381000	0.07600	63.70	2343.70	38.94	0.029580	0.064719	0.634500	0.457053	2.045300	5.290740	0.618169	2538.01	1.691778	0.039886
67	0.102000	0.381000	0.07600	63.70	2343.70	38.94	0.029580	0.064852	0.635800	0.456118	2.054372	5.326290	0.618667	2538.01	1.701022	0.040269
68	0.102000	0.381000	0.07600	63.70	2343.70	38.94	0.029580	0.064984	0.637100	0.455188	2.063527	5.362220	0.619163	2538.01	1.710348	0.040656
69	0.102000	0.381000	0.07600	63.70	2343.70	38.94	0.029580	0.065117	0.638400	0.454261	2.072765	5.398536	0.619656	2538.01	1.719757	0.041047
70	0.102000	0.381000	0.07600	63.70	2343.70	38.94	0.029580	0.065249	0.639700	0.453338	2.082087	5.435244	0.620147	2538.01	1.729250	0.041443
71	0.102000	0.381000	0.07600	63.70	2343.70	38.94	0.029580	0.065382	0.641000	0.452418	2.091495	5.472348	0.620636	2538.01	1.738827	0.041844
72	0.102000	0.381000	0.07600	63.70	2343.70	38.94	0.029580	0.065515	0.642300	0.451502	2.100989	5.509855	0.621122	2538.01	1.748490	0.042249
73	0.102000	0.381000	0.07600	63.70	2343.70	38.94	0.029580	0.065647	0.643600	0.450590	2.110570	5.547771	0.621605	2538.01	1.758241	0.042659
74	0.102000	0.381000	0.07600	63.70	2343.70	38.94	0.029580	0.065780	0.644900	0.449682	2.120240	5.586101	0.622086	2538.01	1.768080	0.043074
75	0.102000	0.381000	0.07600	63.70	2343.70	38.94	0.029580	0.065912	0.646200	0.448777	2.130000	5.624852	0.622565	2538.01	1.778008	0.043494

76	0.102000	0.381000	0.07600	63.70	2343.70	38.94	0.029580	0.066045	0.647500	0.447876	2.139850	5.664030	0.623041	2538.01	1.788026	0.043918
77	0.102000	0.381000	0.07600	63.70	2343.70	38.94	0.029580	0.066178	0.648800	0.446979	2.149793	5.703641	0.623515	2538.01	1.798137	0.044348
78	0.102000	0.381000	0.07600	63.70	2343.70	38.94	0.029580	0.066310	0.650100	0.446085	2.159829	5.743692	0.623987	2538.01	1.808340	0.044783
79	0.102000	0.381000	0.07600	63.70	2343.70	38.94	0.029580	0.066443	0.651400	0.445195	2.169959	5.784188	0.624456	2538.01	1.818637	0.045223
80	0.102000	0.381000	0.07600	63.70	2343.70	38.94	0.029580	0.066575	0.652700	0.444308	2.180185	5.825138	0.624923	2538.01	1.829030	0.045668
81	0.102000	0.381000	0.07600	63.70	2343.70	38.94	0.029580	0.066708	0.654000	0.443425	2.190508	5.866547	0.625387	2538.01	1.839519	0.046118
82	0.102000	0.381000	0.07600	63.70	2343.70	38.94	0.029580	0.066841	0.655300	0.442545	2.200929	5.908422	0.625850	2538.01	1.850107	0.046574
83	0.102000	0.381000	0.07600	63.70	2343.70	38.94	0.029580	0.066973	0.656600	0.441669	2.211450	5.950772	0.626310	2538.01	1.860793	0.047036
84	0.102000	0.381000	0.07600	63.70	2343.70	38.94	0.029580	0.067106	0.657900	0.440796	2.222071	5.993602	0.626767	2538.01	1.871581	0.047503
85	0.102000	0.381000	0.07600	63.70	2343.70	38.94	0.029580	0.067238	0.659200	0.439927	2.232794	6.036920	0.627223	2538.01	1.882470	0.047975
86	0.102000	0.381000	0.07600	63.70	2343.70	38.94	0.029580	0.067371	0.660500	0.439061	2.243621	6.080733	0.627676	2538.01	1.893462	0.048454
87	0.102000	0.381000	0.07600	63.70	2343.70	38.94	0.029580	0.067504	0.661800	0.438199	2.254553	6.125050	0.628127	2538.01	1.904559	0.048938
88	0.102000	0.381000	0.07600	63.70	2343.70	38.94	0.029580	0.067636	0.663100	0.437340	2.265591	6.169878	0.628576	2538.01	1.915762	0.049428
89	0.102000	0.381000	0.07600	63.70	2343.70	38.94	0.029580	0.067769	0.664400	0.436484	2.276737	6.215224	0.629023	2538.01	1.927073	0.049925
90	0.102000	0.381000	0.07600	63.70	2343.70	38.94	0.029580	0.067901	0.665700	0.435632	2.287991	6.261098	0.629468	2538.01	1.938493	0.050427
91	0.102000	0.381000	0.07600	63.70	2343.70	38.94	0.029580	0.068034	0.667000	0.434783	2.299357	6.307507	0.629910	2538.01	1.950024	0.050936
92	0.102000	0.381000	0.07600	63.70	2343.70	38.94	0.029580	0.068167	0.668300	0.433937	2.310834	6.354459	0.630350	2538.01	1.961666	0.051451
93	0.102000	0.381000	0.07600	63.70	2343.70	38.94	0.029580	0.068299	0.669600	0.433094	2.322425	6.401963	0.630789	2538.01	1.973423	0.051973
94	0.102000	0.381000	0.07600	63.70	2343.70	38.94	0.029580	0.068432	0.670900	0.432255	2.334132	6.450029	0.631225	2538.01	1.985294	0.052501
95	0.102000	0.381000	0.07600	63.70	2343.70	38.94	0.029580	0.068564	0.672200	0.431419	2.345955	6.498664	0.631659	2538.01	1.997283	0.053036
96	0.102000	0.381000	0.07600	63.70	2343.70	38.94	0.029580	0.068697	0.673500	0.430586	2.357896	6.547877	0.632091	2538.01	2.009390	0.053577
97	0.102000	0.381000	0.07600	63.70	2343.70	38.94	0.029580	0.068830	0.674800	0.429757	2.369958	6.597679	0.632521	2538.01	2.021617	0.054126
98	0.102000	0.381000	0.07600	63.70	2343.70	38.94	0.029580	0.068962	0.676100	0.428931	2.382141	6.648079	0.632949	2538.01	2.033966	0.054681
99	0.102000	0.381000	0.07600	63.70	2343.70	38.94	0.029580	0.069095	0.677400	0.428107	2.394448	6.699085	0.633375	2538.01	2.046438	0.055244
100	0.102000	0.381000	0.07600	63.70	2343.70	38.94	0.029580	0.069227	0.678700	0.427287	2.406880	6.750709	0.633799	2538.01	2.059037	0.055814